THE REACTIVE AND DISSOCIATIVE BEHAVIOR OF SIZE-SELECTED CLUSTERS AND ION COMPLEXES IN THE GAS PHASE

APPROVED BY
DISSERTATION COMMITTEE:

THIS IS AN ORIGINAL MANUSCRIPT
IT MAY NOT BE COPIED WITHOUT
THE AUTHOR'S PERMISSION

THE REACTIVE AND DISSOCIATIVE BEHAVIOR OF SIZE-SELECTED CLUSTERS AND ION COMPLEXES IN THE GAS PHASE

by

SIMIN DOKHT MALEKNIA, B.S., M.S.

DISSERTATION

Presented to the Faculty of the Graduate School of

The University of Texas at Austin

in Partial Fulfilment

of the Requirements

for the Degree of

DOCTOR OF PHILOSOPHY

THE UNIVERSITY OF TEXAS AT AUSTIN

May, 1992

THE REACTIVE AND DISSOCIATIVE BEHAVIOR

OF SIZE-SELECTED CLUSTERS AND ION

COMPLEXES IN THE GAS PHASE

Publication No._____

Simin Dokht Maleknia, Ph.D.

The University of Texas at Austin, 1992

Supervisor : Jennifer Sue Brodbelt

Molecular complexation properties of several types of size-selected ions are examined in the gas phase by mass spectrometric techniques. Transition metal oxide clusters of $(MoO_3)_n^-$ where n = 2-12 and $(WO_3)_n^-$ extending to n = 8 are generated by field and laser desorption, and electron capture in the negative ionization mode. The structures of these clusters are characterized by low energy collision induced dissociation (CID). The clusters dissociate by the neutral loss of metal trioxide units. Reactions of ligands such as ethylene oxide and cyclohexene sulfide are examined to distinguish the structural variations of the clusters. The systematic evaluation of the size effect in molecular recognition processes is examined by association reactions of crown ether macrocyclic hosts with alkali metal ions and primary amine substrates. Ion complexes of crown ethers with two different alkali metals are formed by liquid secondary ion mass spectrometry. These complexes produce crown ether/alkali metal

adduct ions upon gas-phase isolation and high energy dissociation. The abundance ratios of product ions are correlated to the alkali metal ion selectivites of the crown ether. The selectivity of 18-crown-6 follows the order of $Na^+ \geq K^+ > Li^+ > Rb^+ > Cs^+$, and the concept of "maximum contact point" (MCP) describes this order. In contrast, the high energy activation of alkali metal ion adducts of crown ethers results in homolytic cleavages of C-C or C-O bonds. The metastable ion dissociation of hydrogen bonded complexes of crown ethers with ammonium or methyl-ammonium shows a stability order of 21-crown-7 > 18-crown-6 > 15-crown-5. High energy CID of the ion complexes proceeds by cavity size dependent intramolecular ring opening reactions of the host. Complexes of crown ethers with methyl- and tosyl-hydrazinium ions dissociate by covalent bond cleavages of the N-N or N-S bonds of the guest substrates. Finally, reactions of perfluorinated cyclic or bicyclic ether anions with O_2 are examined as models of oxygen transport by perfluorinated compounds. These complexes show binding strengths that reflect both the topological and chemical nature of the hosts.

Table of Contents

Chapter 1 - Aspects of Size-Selective Chemistry in the Gas Phase

Molecular association reactions for the formation of complexes (1-3) or clusters (4,5) are controlled by a wide variety of intermolecular and intramolecular interactions. Structural parameters, such as the geometry or size of the molecular units, as well as electronic properties direct the assembly process. The evaluation of changes in chemical interactions that occur as a function of an increase in the number of molecular units involved in the association reaction may be probed by size-selective chemistry. However, solvation of the molecular units influences the thermodynamics of reactions (6-9), and only gas-phase reactions provide information about the intrinsic properties of the associative interactions. Moreover, mass spectrometric techniques facilitate the formation and characterization of isolated clusters or complexes in the gas phase.

The present study demonstrates the application of tandem mass spectrometric techniques for the investigation of the size-selective chemistry of two kinds of molecular cluster systems. First, the reactivities of chalcogenide atom donors important in metal oxide catalyzed oxidation and hydrodesulfurization processes

(10,11), such as reactions of ethylene oxide with size selected cluster anions of molybdenum and tungsten trioxides, are examined. These systems are transition-metal based and represent assemblies in which the repeating units are bonded by non-covalent forces. The second type of size-selective association reactions is directed toward the evaluation of molecular recognition (1-3) processes in the gas phase. The primary objective for this study is to correlate the gas-phase complexation properties of macrocyclic hosts to their properties in the solution. Crown ethers (12) and their acyclic analogs are selected as host models and reactions with alkali metal ions are examined for the evaluation of gas-phase size selectivities of the macrocyclic hosts. Additionally, size-selective reactions with primary amines are investigated. These reactions are well-documented in solution and provide comparative fundamental information for host-guest binding interactions in the gas phase. Finally, the reactions of crown ethers and their perfluorinated analogs with O_2 are examined because perfluorinated compounds are used as blood substitutes (13) for the transport of oxygen.

Chapter 3 discusses the formation, reactivity and characterization of transition metal oxide clusters. Formation and structural elucidation of clusters reveal fundamental physical and chemical properties of matter as it evolves from its atomic or molecular state to the bulk. Cluster ion distributions are used as a measure of

stability order and related to the formation of a specific geometry or electronic structure (i.e. magic numbers (4)). Clusters are classified according to the nature of the binding forces, for example van der Waals clusters of rare gases and closed-shell molecules (14), hydrogen-bonded clusters of water (15), ionic clusters of metal halides (16), valence clusters of carbon (17), negative ion clusters of carbon dioxide (18), and metallic clusters (19).

Metal oxide cluster anions are composed of an assembly of molecular units which contain versatile topological and electronic structures. One important application of these clusters is based on the lability of their lattice oxygen atoms or their unique properties in electron transfer/storage in catalytic reactions (20). In the gas phase, first the assembly of metal oxide molecular units for the formation of cluster ions is investigated. Secondly, catalytic properties of the oxide clusters are examined by reactions with several ligands. Cluster anions of transition metal oxides of MoO_3 and WO_3 are generated by several ionization techniques including resistive heating of oxides in electron capture ionization mode or field desorption, and laser vaporization of oxides from surface. Abundant clusters are observed for $(WO_3)_n^-$, where n = 2 - 8, and for $(MoO_3)_n^-$ extending to n = 12. Structural elucidation of size-selected cluster anions by collision induced dissociation (CID) techniques show that certain fragmentation pathways which lead to especially stable clusters are favored.

Reactions of metal oxide clusters with chalcogenide atom donors are used to investigate chemical differences of the size-selected clusters. In reactions with ethylene oxide, exclusive adducts are formed with cluster sizes of $n \geq 4$. For example, abundant adduct ions are observed for $n = 4$ or 6, but the odd number cluster adduct ions are less abundant. These results suggest that odd size clusters are significantly different in reactivity due to electronic or geometric differences. Structural characterization of the adduct ions by CID show the loss of ethylene oxide or ethylene as fragments. The neutral loss of ethylene suggests that the epoxide oxygen is oriented toward a metal center in the cluster, and upon collisional activation the epoxide oxygen is abstracted by the cluster. These results show the utility of mass spectrometric techniques for the formation of cluster ions, and the investigation of catalytic processes in the gas phase.

Association reactions at the molecular level control many important biological processes, such as the transport of ions and amino acids across cell membranes, or enzyme/substrate interactions (3). Effective and selective complexation between host and guest molecules are directed by non-covalent interactions and highly influenced by size and conformational compatibilities of the substrate and molecular receptor (1,2). Macrocycles have been used as models to imitate enzyme catalyzed reactions and reveal important aspects of binding and transport of metal ions. Complexation

reactions that control biological processes by informational exchange at the molecular level depend on structural recognition of the host and guest. Progress in the understanding and applications of molecular recognition in solution has led to the design and synthesis of highly structured organic hosts that complex a specific site of the guest molecule with size-selective binding preferences (21-24). The stability and conformation of the host molecules are highly solvent dependent, and the solvophilicity of the binding sites influences their availability for complexation. These solvent effects plus the complexity factor of self-complexation of the hosts have influenced the syntheses of macrocyclic hosts with a rigid or fixed cavity (24) to maximize the host-guest binding interactions.

Some of the simplest structured macrocyclic host models are crown ethers and cryptates. The investigation of complexation reactions of these macrocyclic hosts provides the most fundamental understanding of binding properties of host-guest interactions. For example, the metal ion binding abilities of crown ethers serve as models that mimic the cation binding abilities of antibiotics. Crown ether macrocycles provide a unique host series with increasing cavity sizes and serve well as receptor models because of conformational flexibility and the presence of multiple binding sites (12).

The solution chemistry of crown ethers has been investigated in detail by spectrometric techniques of NMR (25), and ultrasonic absorption (26), and methods of potentiometric (27) and calorimetric titrations (6). Solvation plays an important role in complexation processes, and thus gas-phase reactions provide optimum conditions for the evaluation of the intrinsic role of non-covalent intermolecular forces involved in molecular recognition processes. Additionally, molecular modeling studies have been used to provide a theoretical estimation of the effects of solvation on the selectivity and direction of binding reactions of macrocyclic hosts (28). These results provide a basis for comparison to the gas-phase reactions. The reactivities of crown ethers in the gas phase are compared to their perfluorinated and in some cases acyclic analogs. Fluorine substitution changes the dimensions of the cavities and decreases the basicity of the hosts, however, an increase in electron affinities is expected. Acyclic analogs allow evaluation of the importance of the macrocyclic effect (29) on the intrinsic complexation reactions of polyether hosts.

The evaluation of host/guest interactions in the gas phase is initiated by selective complex ion formation between crown ether hosts and various substrates, followed by subsequent use of tandem mass spectrometric techniques for structural elucidation. Molecular structural characterization of the host molecules by CID is presented in Chapter 4. Additionally, a comparison is made to the fragmentation

behavior of acyclic and perfluorinated polyethers. For example, crown ethers and their perfluorinated analogs dissociate by similar pathways with the predominant neutral loss of ethylene oxide or C_2F_4O units, respectively. The loss of single ethylene oxide unit is not favored, and fragment ion abundances due to losses of two or three ethylene oxide units increase as the cavity size increases. The fragmentation patterns of the uncomplexed host molecules are used to contrast the changes in dissociation pathways that occur from interactions with the guest molecules.

One important factor that controls the complexation process is the complementary fit of the macrocyclic cavity size with guest molecules. In solution, this concept has been termed as "best fit" or "ion-cavity" (1) for crown ether complexes with alkali metal ions, and defines the preference for the cation whose ionic diameter best matches the cavity sizes determined by atomic models and crystal structures. However, examination of the formation constants reveals that the binding preferences of crown ethers for alkali metals are solvent dependent.

In order to examine the selectivity of crown ether macrocycles for alkali metal ion complexation in the absence of solvation effects, ion complexes of crown ethers with two different alkali metals are generated by liquid secondary ionization, and subsequently isolated in the gas phase and characterized by CID. The major

dissociation pathways are the formation of crown ether/alkali metal adducts which indicate that these complexes are held only by electrostatic or van der Waals forces. Abundances of product ions from CID of the ion complexes are then used to qualitatively correlate selectivities of crown ethers for alkali metal ion complexation in the gas phase. These results are presented in Section A of Chapter 5. For example, the selectivity order for 18-crown-6 is $Na^+ \geq K^+ > Li^+ > Rb^+ > Cs^+$. In the absence of solvation effects, the "maximum contact point" (MCP) concept is introduced to describe preferences of crown ethers for alkali metal ion complexation. The MCP concept predicts binding preferences for a slightly smaller cation than predicted by "best fit" because higher electric field-dipole interactions result within the cavity for a given conformer.

Another important factor that affects host-guest binding preferences is the molecular preorganization (30). In the solid state, organization of the complexes are controlled by crystal structures while in solution conformational equilibria exist which depend on the character of the solvent. Additionally, binding forces between solvent and host or solvent and guest may be on the same order as the binding forces between the host and guest. In the gas phase, the effect of preorganization on selectivities of crown ethers for alkali metal complexation is investigated and discussed in Section A of Chapter 5. For this purpose, ion complexes of crown ether dimers with two

different alkali metals are formed and examined by CID. The results show a shift for selectivities of crown ethers for alkali metal binding toward preferences observed in solution. This change in the gas-phase selectivity is likely due to the increase of structural complexity and steric effects of the precursor dimer ions undergoing unimolecular dissociation. Again, the CID results of the dimer complexes show mostly crown ether/alkali metal adduct ions, and these results restrict the important binding interactions to non-covalent types.

Structural characterization of the crown ether/alkali metal adduct ions by CID is presented in Section B of Chapter 5 as a comparison to the dissociation pathway of crown ether complexes with mixed alkali metal ions described in Section A of Chapter 5. In contrast to limited dissociation pathways of the ion complexes, the CID spectra of the alkali metal ion adducts show extensive fragmentation. Collisional activation of the closed-shell alkali metal ion adducts proceeds by homolytic cleavages of carbon-carbon or carbon-oxygen bonds which result in odd electron acyclic product ion structures. The strong interactions of alkali metal ions with the oxygen sites reflect the changes in the fragmentation pattern in comparison to dissociation pathways of the protonated ethers. These results show that upon CID the effective binding of the guest causes ring opening of the macrocyclic host.

Complexation of a molecular receptor to a specific site of the guest molecule demonstrates the unique exchange of intermolecular bond information. Molecular recognition for selective complex formation between crown ethers and primary amine substrates is discussed in Chapter 6. In the gas phase, the formation and stability of these complexes are directed by effective hydrogen-bonding interactions, and thus a variety of amine guests of different sizes were chosen to probe the means by which internal energy is distributed within the host-guest complexes and the strengths of the complexation interactions. For example, the stability order for the ion complexes of polyethers with ammonium or methylammonium is 21-crown-7 > 18-crown-6 > 15-crown-5 > hexaethylene glycol based on metastable ion dissociation results. The extent of these gas-phase intramolecular interactions is evaluated by CID of the ion complexes at two different collision energies. At low energy CID, the ion complexes are activated with less than 5 eV of internal energy. The predominant low energy dissociation reactions are the neutral loss of the amine guest with an intramolecular proton transfer to the polyether host and systematic losses of ethylene oxide units from the protonated macrocycle. The high energy activation deposits about 40 to 60 eV in the ion complexes. This magnitude of energy causes homolytic cleavages of carbon-carbon and carbon-oxygen bonds of the macrocyclic host resulting in acyclic, odd electron product ion structures. As the number of ion-dipole interactions increases, the extent of intramolecular ring opening dissociation reactions increases,

and relative abundances of the odd electron, acyclic product ions increase as compared to fragment ions resulting from the systematic losses of ethylene oxide units.

The preferential covalent bond activation of the host or guest molecules are also examined by CID analyses of the ion complexes of hydrazines and crown ethers. The dissociation energy of the nitrogen-nitrogen (31) or nitrogen-sulfur (32) bonds is on the same order as the association energy for complexation of primary amines to crown ethers which has been estimated as 46 kcal/mole from proton-transfer reactions in a high pressure mass spectrometer (33). Activation of the hydrazine ion complexes proceeds by intramolecular ring opening fragmentation of the polyether host. Ion complexes of methyl- and tosyl-hydrazines dissociate by cleavages of the nitrogen-nitrogen or nitrogen-sulfur bonds of the guest molecules. These results show that the higher order effect of multiple hydrogen-bonding survives the covalent bond activation of the guest molecules.

To demonstrate that host-guest chemistry in the gas phase is also useful for biologically relevant studies, a comparison of reactivities of crown ethers to their perfluorinated analogs is examined. Perfluorochemical compounds have been used as blood substitutes (13) because of their ability to transport oxygen across cell membranes. Since the mechanism of O_2 binding is not well understood, the reactions

with oxygen are investigated, and the results are presented in Section A of Chapter 7. Fluorine substitution increases the electron affinities of the macrocyclic host. Selective adducts are generated with the perfluorinated crown ethers in the electron capture ionization mode, whereas adducts with hydro crown ethers are not observed in the positive or negative ionization modes. Also, complexes with acyclic ethers and their perfluorinated analogs are not observed. These results show that perfluorinated cyclic structures are required for this complexation process. Results of CID of the perfluorinated crown/O_2 ion complexes show two parallel fragment ion series. The more abundant fragments are due to neutral losses of $(C_2F_4O)_n$ which indicate that the O_2 is retained, and its binding interaction is on the order of the carbon-carbon or carbon-oxygen bonds. A less abundant series corresponding to the loss of O_2 in conjunction with losses of ethylene oxide units is also observed.

For a more detailed analysis of the cavity size effect, the CID pathways of the anion complex of O_2 with a perfluorinated bicyclic ether is compared to crown ethers. The results are presented in Section B of Chapter 7. These CID results also show the parallel series observed for the perfluoro crown ether/O_2 complexes. The fragment ion series for the loss of oxygen is more abundant than the one for neutral losses of $(C_2F_4O)_n$ units which indicates that O_2 is less efficiently bound to the bicyclic host as compared to the monocyclic crown ethers. Additionally, the fluoride complex of the

perfluorinated bicyclic ether is analyzed by CID. In contrast to the CID fragmentation pattern of the O_2 adduct, fluorine is always retained by the fragment ions which suggest that fluorine binding interactions are favored over binding of molecular oxygen.

These examples of selective complex formation in the gas phase for macrocyclic polyether hosts or transition metal oxide clusters demonstrate the ability to examine intrinsic reactivities and molecular association processes. Structural elucidation by CID proves to be useful for estimation of the strengths of interactions of the ion complexes or clusters in the gas phase. The detailed studies described in the next six chapters provide the foundation for the future advanced investigations of aspects of host-guest chemistry in a solvent free environment.

References :

1. Vogtle, F.; Weber, E.; Eds. *Host Guest Complex Chemistry : Macrocycles*, Springer-Verlag : New York, 1985.

2. Atwood, J. L.; Ed. *Inclusion Phenomena and Molecular Recognition*, Plenum Press : New York, 1988.

3. Cram, D. J. in *Techniques of Chemistry*, Vol. 10, part 2, Jones, J. B.; Sih, C. J.; Perlman, D.; Eds. Wiley-Interscience: New York, 1976.

4. Russell, D. H.; Ed. *Gas Phase Inorganic Chemistry*, Plenum Press : New York, 1989.

5. Futrell, J. H.; Ed. *Gaseous Ion Chemistry and Mass Spectrometry*, Wiley-Interscience : New York, 1986.

6. Izatt, R. M.; Terry, R. E.; Haymore, B. L.; Hansen, L. D.; Dalley, N. K.; Avondet, A. G.; Christensen, J. J. *J. Am. Chem, Soc.* **1976**, *98*, 7621-7626.

7. Izatt, R. M.; Izatt, N. E.; Rossiter, B. E.; Christensen, J. J.; Haymore, B. L. *Science*, **1978**, *199*, 994- 996.

8. Dishong, D. M.; Gokel, G. W. *J. Org. Chem.*, **1982**, *47*, 147-148.

9. Takeda, Y.; Yano, H.; Ishibashi, M.; Isozumi, H. *Bull. Chem. Soc. Jpn.*, **1980**, *53*, 72-76.

10. Gates, B. C.; Guczi, L.; Knozinger, H. *Metal Clusters in Catalysis*, Elsevier: New York, 1986.

11. Parshall, G. W. *Homogeneous Catalysis: The Applications and Chemistry of Catalysis by Soluble Transition Metal Complexes,* Wiley-Interscience : New York, 1980.

12. Pedersen, C. J. *J. Am. Chem, Soc.* **1967**, *89*, 7017-7036.

13. Weiss, R. *Science*, **1987**, *132*, 200-202.

14. Knickelbein, M. B.; Menezes, W. J. C. *Chem. Phys. Lett.*, **1991**, *184*, 433-438.

15. Castleman, A. W.; Tzeng, W. B.; Wei, S.; Morgan, S. *J. Chem. Soc. Faraday Trans*, **1990**, *86*, 2417-2426.

16. Campana, J. E.; Dunlap, B. I. *Int. J. Mass Spectrom. Ion Proc.* **1984**, *57*, 103-123.

17. Heath, J. R.; O'Brien, S. C.; Zhang, Q.; Liu, Y.; Curl, R. F.; Kroto, H. W.; Tittel, F. K.; Smalley, R. E. *J. Am. Chem, Soc.* **1985**, *107*, 7779-7780.

18. Klotz, C. E.; Compton, R. E. *J. Chem. Phys.* **1978**, *69*, 1636.

19. Gord, J. R.; Buckner, S. W.; Freiser, B. S. *Chem. Phys. Lett.*, **1988**, *153*, 577-582.

20. Pope, M. T. *Heteropoly and Isopolyoxometalates*, Springer : New York, 1983.

21. Helgeson, R. C.; Tarnowski, T. L.; Timko, J. M.; Cram, D. J. *J. Am. Chem, Soc.* **1977**, *99*, 6411.

22. Bryant, J. A.; Blanda, M. T.; Vincenti, M.; Cram, D. J. *J. Am. Chem, Soc.*

1991, *113*, 2167-2172.

23. Tsukube, H.; Yamashita, K.; Iwachido, T.; Zenki, M. *J. Org. Chem.*, **1991**, *56*, 268-272.

24. Takemura, H.; Shinmyozu, T.; Inazu, T. *J. Am. Chem, Soc.* **1991**, *113*, 1323-1331.

25. (A) Wu, G.; Jiang, W.; Lamb, J. D.; Bradshaw, J. S.; Izatt, R. M. *J. Am. Chem, Soc.* **1991**, *113*, 6538. (b) Schmidt, E.; Popov, A. I. *J. Am. Chem, Soc.* **1983**, *105*, 1873.

26. Liesegang, G. W.; Farrow, M. M.; Vazquez, F. A.; Purdie, N.; Eyring, E. M. *J. Am. Chem, Soc.* **1977**, *99*, 3240.

27. (a) Frensdorff, H. K. *J. Am. Chem, Soc.* **1971**, *93*, 600. (b) Michaux, G.; Reisse, J. *J. Am. Chem, Soc.* **1982**, *104*, 6895.

28. (a) Wipff, G.; Weiner, P.; Kollman, P. *J. Am. Chem, Soc.* **1982**, *104*, 3249. (b) Howard, A. E.; Singh, U. C.; Billeter, M.; Kollman, P. A. *J. Am. Chem,*

Soc. **1988**, *110*, 6984.

29. Hancock, R. D.; McDougall, G. J. *J. Am. Chem, Soc.* **1980**, *102*, 6551-6553.

30. (a) Cram, D. J. *Angew. Chem. Int.*, **1986**, *25*, 1039-1057. (b) Reinhoudt, D. N.; Dijkstra, P. J. *Pure and Appl. Chem.*, **1988**, *60*, 477-482.

31. Schmidt, E. W. *Hydrazine and its Derivatives*, Wiley : New York, 1984.

32. Fleig, V. H.; Becke-Goehring, M. *Zeit. Anorg. Chemie,* **1970**, *375*, 8-14.

33. Moet-Ner, M. *J. Am. Chem, Soc.* **1983**, *105*, 4912-4915.

Chapter 2 - **Experimental Techniques and Methods**

A variety of different types of mass spectrometers and tandem experimental designs have been applied to the study of gas-phase reaction processes (1,2). The basic concept in these experiments is the measurement of mass-to-charge ratios of ions before and after reactions. The reactions involved may be associative, such as ion/molecule complexation (3), or dissociative for structural characterization (4,5). Complexation processes proceed either with initial formation of ions and subsequent reactions with neutral molecules or with simultaneous introduction of the substrates into the ionization chamber. Structural elucidation of the ion complexes formed in the gas phase is established by application of mass spectrometry/mass spectrometry (MS/MS) techniques of collision induced dissociation (CID) (4,5) or metastable dissociation (MD) (6). The following methods are used for the formation of ion/molecule complexes or clusters: chemical ionization (CI) (7), field desorption (8) (FD) (8), laser desorption (LD) (9), and secondary ion mass spectrometry (SIMS) (10), and each is described separately.

2.1 Ionization Processes

Methods of ionization were selected to control the formation of ion/molecule complexes or clusters, and to complement the physical properties of the compounds of interest. The following techniques are classified as soft ionization techniques which generate ions with low internal energies and cause minimum fragmentation. These conditions favor the formation of clusters and ion/molecule complexes that are held by non-covalent interactions. A common feature of three of these ionization methods is the low pressure (approximately $< 10^{-6}$ torr) for FD, LD, and SIMS, whereas in the case of CI a high pressure (1 to 4 torr) is used.

Chemical Ionization (CI) : A primary beam of electrons from an electrically heated filament is accelerated to several hundred volts through the source chamber which is designed to contain high pressures of a reagent gas and the analyte molecules. The pressure of the reagent gas is generally several orders of magnitude higher than the analyte. The ionization process is systematically explained as a two-step reaction mechanism that initiates with ionization of the reagent gas and follows by a charge-exchange or cation exchange reaction between reagent ions and the

analyte molecules. However, stabilized adducts may form between reagent gas ions and the analyte molecules instead of a simple cation or charge-exchange process. Both positive and negative ions are formed by these processes. Additionally, negative ions are formed by electron capture processes which require thermal electrons with less than 0.1 eV energy. A large flux of low energy electrons including thermal electrons is produced at high pressure conditions which promote a large number of collisions in the source.

Reagent gases used included argon and methane at typically 2 torr. These gases were used to assist in the production of thermal electrons for negative ionization, or for proton transfer experiments. Typically, the source temperature was maintained at 80°C. For the formation of ion/molecule complexes a dual metering valve was used to allow the introduction of the reagent gas and reactive gases or liquids. The samples were introduced by the use of a direct probe, a gas probe for volatiles, or a direct evaporation probe. The latter probe incorporates a platinum or rhenium wire tip, and the samples coated on the wire are vaporized by resistive heating. The use of direct evaporation probe was required for the production of metal oxide clusters in the CI mode.

Field Desorption (FD) : In this technique, the analyte is applied on an emitter which is typically a 10 μm tungstun wire covered with carbon microneedles, and placed in a high electric field (on the order of 10^8 to 10^{10} V/cm) generated in the source of the mass spectrometer. This high electric field distorts the potential well and consequently the energy levels of the analyte molecule. Positive ions are generated by the loss of an electron to the emitter by electron tunneling processes. Other mechanisms that generate both positive and negative ions are desolvation and thermal ionization. In addition, a current is passed through the emitter to assist in the vaporization process. The FD method was used for the metal oxide cluster formation as a comparison to the thermal desorption process of CI. The source temperature was 80°C. Metal oxides were loaded on benzonitrile activated carbon emitters from a methanol suspension by the dipping technique.

Laser Desorption (LD) : In this case the source of energy for desorption is in the form of pulsed photons. Both ions and neutrals are formed by the desorption process. Mechanisms of ion formation are by thermal evaporation of ions from the solid, or thermal evaporation of neutral molecules followed by ionization in the gas phase. Direct emission of ions under non-thermal equilibrium conditions is also possible. Laser desorption was applied to the cluster ion formation of metal oxides.

Secondary Ion Mass Spectrometry (SIMS) : The energy for desorption and ionization of the analyte is supplied by the momentum transfer from a flux of high energy ions, such as cesium ions generated from a cesium gun. This primary ion beam is accelerated to about 20 or 30 kV and upon collisions with the sample surface, a secondary ion beam consisting of analyte and matrix ions is generated which is extracted and focussed by the ion optics. A combination of neutrals with positive and negative ions are formed by the impact of the primary beam. Analyses of non-volatile samples is possible either directly from solids, or from a solution containing the analyte suspended in a liquid matrix. In the latter case the ionization method is termed liquid SIMS.

The SIMS technique was used for the production of metal oxide clusters and for the formation of ion/molecule complexes of crown ethers.

2.2 Tandem Mass Spectrometry

Structural details of ion/molecule complexes or clusters were elucidated by applications of CID and MD, both of which are common tandem mass spectrometric techniques. Two types of mass spectrometers were employed for these experiments. The instruments included a triple-quadrupole mass spectrometer (Finnigan TSQ-70, located at the University of Texas) and a four-sector magnetic analyzer mass spectrometer (JEOL HX110/HX110, located at Massachusetts Institute of Technology). Details of each instrument are described separately below.

Principles of CID processes (4,5) for both instruments include first mass-selection of an ion of interest (precursor ion) by the first mass analyzer, followed by acceleration into the collision cell where dissociation into fragment ions occurs after conversion of the initial kinetic energy of the precursor ion into internal energy by collisions with neutral gas molecules. A second mass analyzer is used to determine the resulting product ions. This sequence gives detailed structural information about the precursor ions because fragmentation patterns are obtained. The major distinction between the CID processes in quadrupole and sector instruments is the energetics of the collisions due to the operating voltages of the two instruments. Collisions in a

quadrupole instrument occur in electron-volt (low energy) regimes whereas the conditions of a sector instrument provide kiloelectron-volt (high energy) collisions. The energy imparted in the ions for dissociation depends on the masses of the target gas and the ion involved in the collision and is defined as the energy in the center-of-mass frame (E_{cm}) by :

$$E_{cm} = (E_{lab} \times M_t) / (M_t + M_p)$$

where E_{lab} is the collision energy in the laboratory frame, M_t is the mass of the target gas, and M_p is the mass of the precursor ion.

Another difference between high and low energy CID processes is the residence time of ions in the collision cell or the periodicity of collisions which is affected by the pressure of the collision gas, the length of collision cell, and the velocity of ions. The experiments performed at low energy on the quadrupole instrument favored multiple collisions due to the high target gas pressure and slow velocity of ions. Single collision conditions were favored in high energy CID experiments with the sector instrument due to the large velocity of ions.

Metastable ion dissociation (6) experiments were used to determine the relative

binding strengths of the ion/molecule complexes. For these types of experiments, precursor ions are not collisionally activated because of the absence of the target gas, and dissociations occur spontaneously due only to the excess internal energy of precursor ions which is typically estimated at 0-1 eV. Therefore, only product ions from the lowest energy dissociation mechanisms are expected, and metastable dissociations are useful for evaluating threshold behavior. These experiments were performed on the sector instrument.

2.3 Instrumentation

Triple-Quadrupole Mass Spectrometer : The formation and reactivity of metal oxide clusters in the CI mode discussed in Chapter 3 was carried out with the Finnigan TSQ-70 instrument. Structural characterization of cyclic ethers discussed in Chapter 4 was performed with the TSQ-70. This instrument was also used for the formation and characterization of ion/molecule complexes of perfluorinated ethers discussed in Chapter 7.

A schematic diagram of this instrument is shown in Figure 2.1. The manifold consists of source and analyzer compartments that are differentially pumped to allow

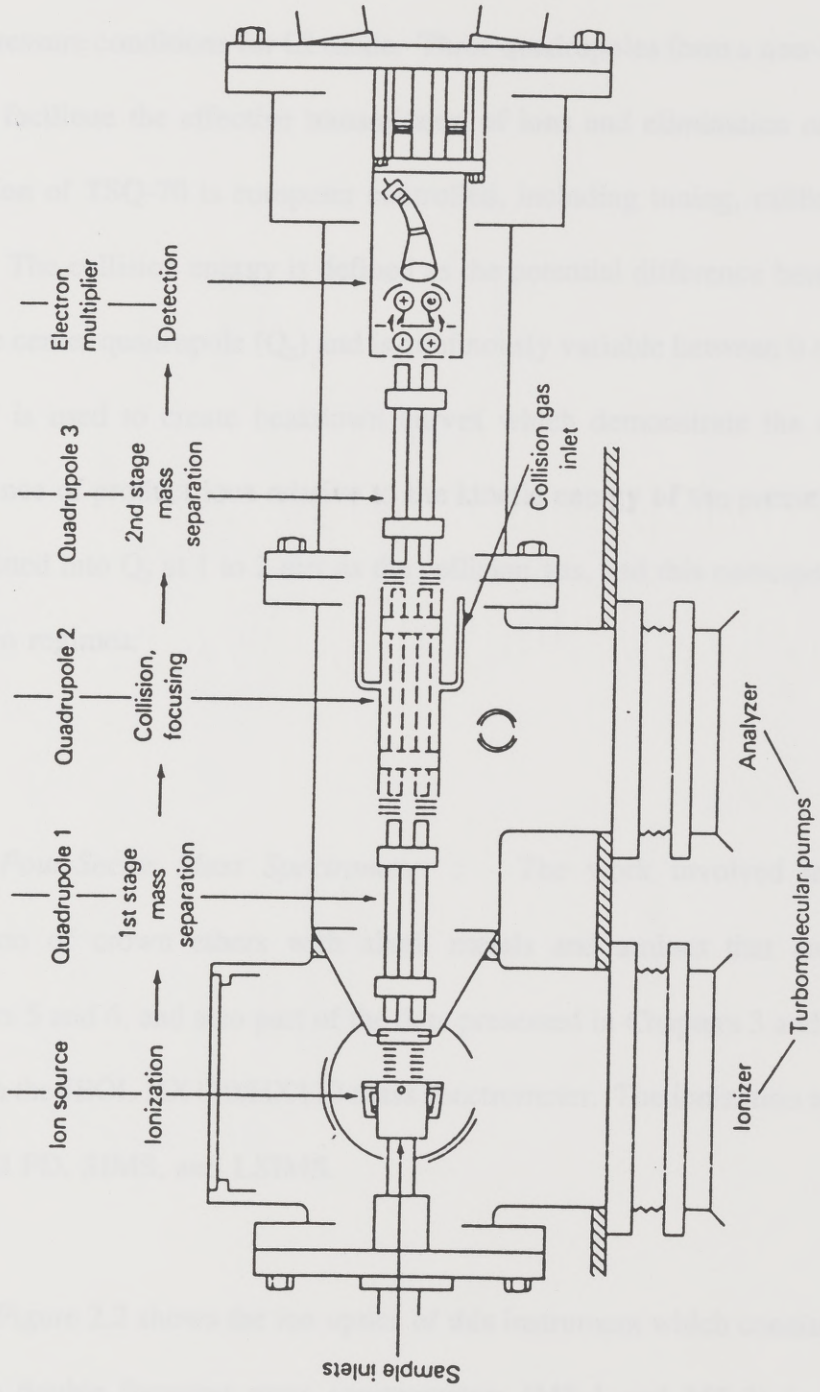

Figure 2.1 : Schematic of the Finnigan TSQ-70 triple quadrupole mass spectrometer.

high pressure conditions for CI mode. Three quadrupoles form a non-linear ion optics which facilitate the effective transmission of ions and elimination of neutrals. The operation of TSQ-70 is computer controlled, including tuning, calibration, and CID scans. The collision energy is defined as the potential difference between the source and the center quadrupole (Q_2) and is continously variable between 0 to 200 eV. This feature is used to create beakdown curves which demonstrate the appearance and abundance of product ions relative to the kinetic energy of the precursor ion. Argon is admitted into Q_2 at 1 to 2 torr as the collision gas, and this corresponds to multiple collision regimes.

Four-Sector Mass Spectrometer : The work involved in complex ion formation of crown ethers with alkali metals and amines that are discussed in Chapters 5 and 6, and also part of the data presented in Chapters 3 and 7 were carried out with the JEOL HX110/HX110 mass spectrometer. The ionization techniques used included FD, SIMS, and LSIMS.

Figure 2.2 shows the ion optics of this instrument which consists of two Nier-Johnson double focusing mass spectrometers (MS-1 and MS-2) in the E_1B_1/E_2B_2 configuration with a collision cell in the third field-free region. Both MS-1 and MS-2

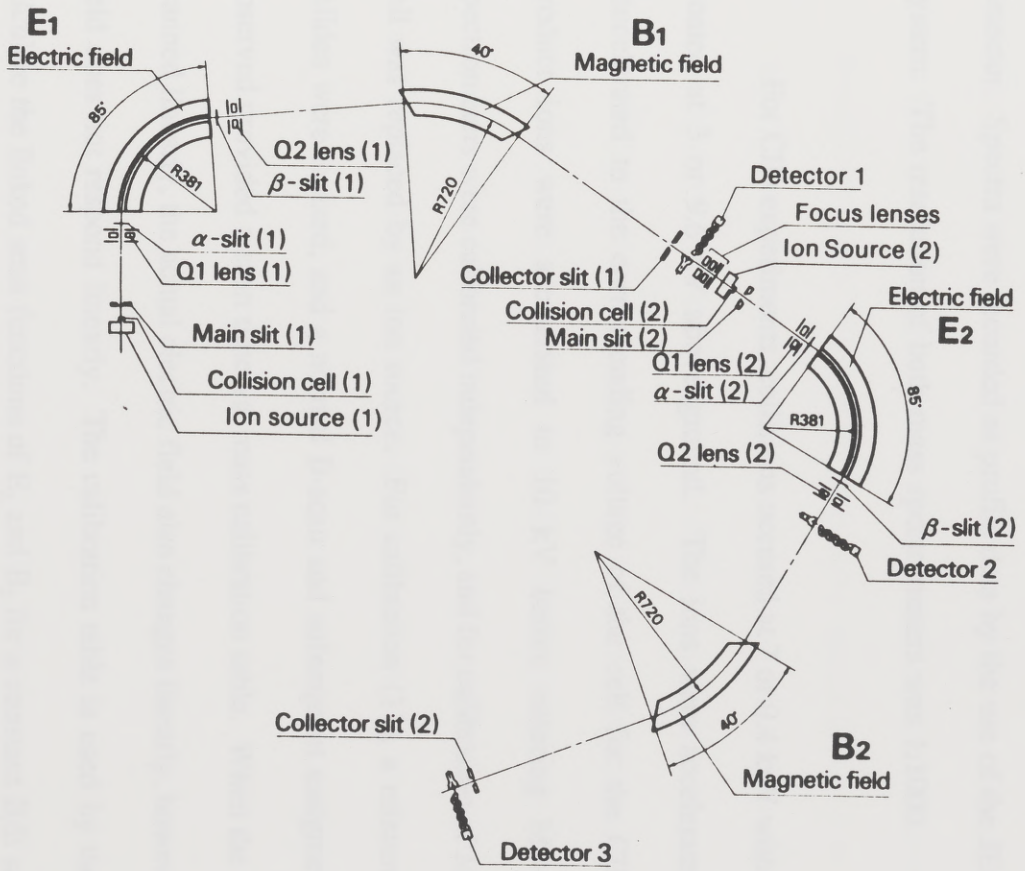

Figure 2.2 : Ion optics of the JEOL HX110/HX110 tandem mass spectrometer.

have a mass range of 14500 Da at 10 kV accelerating voltage. Detectors are located off axis after the collector slits of MS-1 and MS-2 with an additional detector located after the electric sector of MS-2. A 20 kV post-accelerating electrode preceeds each detector. Spectra were recorded as profile data by the use of the JEOL DA5000 data system. The resolution of both mass spectrometers was 1:1000.

For CID experiments, collisions occured at 7 or 0.4 keV with the collision cell floated at 3 or 9.6 kV above ground. The ions were accelerated at 10 kV and deccelerated to the corresponding voltage of the cell for the CID process. The product ions were accelerated to 10 kV before entering MS-2. Both mass spectrometers were calibrated independently, and for calibration of MS-2 the collision cell was replaced by an ion source. For calibration (11), a mixture of alkali metal halides were ionized, and a normal B-scan and subsequent assigment of the masses observed provided a scan time vs. mass calibration table. When the electric sector is scanned linearly, the actual electric field also changes linearly, however, the magnetic field does not respond linearly. The calibration table is used by the data system to calculate the linked scan functions of E_2 and B_2 for a constant B/E scan in CID (11). The helium collision gas was metered to cause 30% attenuation of the precursor ion beam which results in single collision conditions.

Time-of-Flight Mass Spectrometer : Laser desorption experiments were performed on a Vestec VT-2000 time-of-flight instrument located at Massachusetts Institute of Technology. This ionization technique was used for the formation of metal oxide clusters discussed in Chapter 3. Metal oxides were dried on the steel probe tip from a methanol suspension. The lasers included a Lumonics Nd:YAG operated at the third harmonic of 355 nm in the Q-switch mode or a Laser Science, Inc. VSL-337ND nitrogen laser operated at 337 nm. Spectra were recorded at an acceleration voltage of - 20 kV by accumulation of 50 laser shots at an output frequency of 5 Hz with the use of a LeCroy 8013A transient recorder. The calibration and data processing were performed on a Micro VAX-3600 computer. The resolving power of this instrument is 1:350 with mass assignment accuracies of 0.01%.

2.4 Materials :

The perfluorinated compounds were provided by Professor R. J. Lagow and synthesized by the direct fluorination technique of LaMar (12). These compounds include perfluorinated 12-crown-4, 15-crown-5, 18-crown-6, dicyclohexano-24-crown-8, and 4,7,13,16,21,24-hexaoxa-1,10-diazabicyclo[8.8.8] hexacosane (cryptand). Examples of structures of these compounds are presented in Scheme 2.1. The commercial source of polyethers of 12-crown-4, 15-crown-5, and 18-crown-6, tetraethylene dimethylether, hexaethylene glycol was Aldrich Chemical Company (Milwaukee, WI), and 21-crown-7 was purchased from Parish Chemical Company (Vineyard, UT). Metal oxides of MoO_3 and WO_3 were purchased from Aldrich. Additionally, compounds of ethylene sulfide, cyclohexene sulfide, 2,3-butanedione, 2,4-pentanedione (acetylacetone) were purchased from Aldrich. The commercial source of ethylene oxide was Wilson Oxygen (Austin, TX).

Scheme 2.1 : Chemical structures of macrocyclic compounds.

15-crown-5

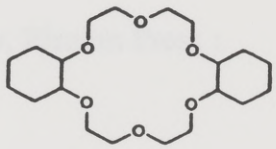

dicyclohexyl-18-crown-6

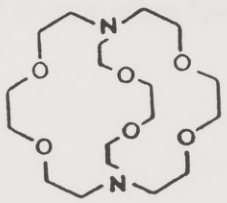

4, 7, 13, 16, 21, 24-hexaoxa-1, 10-

diazabicyclo [8.8.8] hexacosane (cryptand)

References :

1. Bowers, M. T.; Ed. *Gas Phase Ion Chemistry*, Vol. 2, Academic Press : New York, 1979.

2. Russell, D. H.; Ed. *Gas Phase Inorganic Chemistry*, Plenum Press : New York, 1989.

3. Futrell, J. H.; *Gaseous Ion Chemistry and Mass Spectrometry*, Wiley : New York, 1986.

4. McLafferty, F. W.; Ed. *Tandem Mass Spectromety*, Wiley Interscience : New York, 1983.

5. Bush, K. L.; Glish, G. L.; McLuckey, S. A.; Eds. *Mass spectromerty/Mass spectrometry Techniques and Applications*, VCH : New York, 1988.

6. Cooks, R. G.; Beynon, J. H.; Caprioli, R. M.; Lester, G. R. *Metastable Ions*, Elsevier: New York, 1973.

7. Harrison A. G.; *Chemical Ionization Mass Spectrometry*, CRC Press : Florida, 1983.

8. Pròkai, L. *Field Desorption Mass Spectrometry*, Brame, E. G.; Ed. Practical Spectroscopy Series, Vol. 9, Marcel Dekker : New York, 1990.

9. Hillenkamp, F.; Karas, M.; Rosmarinowsky, J.; in *Desorption Mass Spectrometry*, Lyon, P. A.; Ed. ACS Symposium Series 291, 1985.

10. Benninghoven, A.; Okano, J.; Shimizu, R.; Werner, H. W.; Eds. *Secondary Ion Mass Spectrometry SIMS IV*, Springer-Verlag, NewYork, 1984.

11. Sato, K.; Asada, T.; Ishihara, M.; Kunihiro, F.; Kammei, Y.; Kubota, E.; Costello, C. E.; Matin, S. A.; Scoble, H. A.; Biemann, K. *Anal. Chem.* **1987**, *59*, 1652-1659.

12. Lin, W. H.; Bailey, W. I.; Lagow, R. J. *J. Am. Chem. Soc. Chem. Commun.* **1985**, 1385.

Chapter 3 - A. **Reactions of Size-Selected Metal Oxide Clusters**

3.1 Introduction :

The increasing interest in gas phase studies of transition metal oxides stems in part from their use as catalysts in various oxidation processes (1,2). For example, molybdenum containing catalysts have been used in ammoxidation of hydrocarbons (3), demetalation (4), selective oxidation of olefins (5), various photooxidation reactions (6,7), and hydrotreating processes such as hydrodesulfurization and hydrodenitrogenation (8-12). The latter two processes are particularly important in the oil industry because there is an increasing trend towards large scale refining of heavy crude oils containing high percentages of sulfur and nitrogen. Such oxide catalysts are also useful for epoxidation of olefins (13). Additionally, it has been demonstrated that methanol is oxidized to formaldehyde over MoO_3 in a process in which any Mo that is not coordinatively saturated may act as an active site (14). The mechanisms of these oxidation reactions often involve oxygen atom transfer from the oxides with participation by oxometal groups (15).

The factors that most greatly influence the catalytic properties of the oxides include structural coordination and oxidation state. One example highlighting the importance of the latter involves the homologation and metathesis of ethylene by MoO_3 (16). The active sites for homologation require a more reduced MoO_x species (like Mo^{4+}) than for metathesis, the latter proceeding via metal alkylidene and metallacyclobutane intermediates. Moreover, it was recently proven that it is the lattice oxygen ions of MoO_3, the most active catalyst for propene oxidation to acrolein, that are inserted into the organics undergoing oxidation, and not the oxygen atoms that may adsorb on the catalyst surface (17).

Another interest in transition metal oxides has developed from their use as dielectric or insulating materials in electronic applications (18). Some oxides, such as WO_3, are intrinsically semiconducting and are being used in new solid state device and sensor technology. For example, thin films of semiconducting material have shown remarkable sensitivities as gas sensors for propane, NH_3, H_2, H_2S, and for reducing agents (19,20). In many cases, the mechanism of activity depends on the extraction and infusion of carriers from the oxide by oxygen adsorbed and/or organic species oxidized at the surface.

There have been numerous studies of metal clusters, and more recently metal

oxide clusters, using various mass spectrometric techniques (21,22). Increasingly, attention has been focussed on the characterization of the reactive behavior of these clusters in the gas phase. For example, alkene oxidation by transition metal oxides was studied (23), ion/molecule reactions of Co/oxygen cluster ions were investigated (24), and the reactivities of a range of bare metal clusters including Al_n^+ (25), Pt_n^+ (26), Fe_n^+ (27), Nb_n^+ (28), $CuFe^+$ (29), and Ni_n^+ (30) with neutral substrates such as CO, N_2, O_2, CH_4, C_2H_4 and NH_3 were examined. Correlations of ion abundances with structural configuration have also been drawn: the cluster ion distributions for selected metal oxides was shown to be dependent on the electron configuration of the metal in the oxide (31). Further studies of gas-phase metal oxide clusters are of interest not only because they can yield information of intrinsic heterogeneous catalytic mechanisms but also because clusters afford a natural array of size-selected related structures.

The aims of the study described in this chapter are to: 1) demonstrate the viability of producing an array of clusters by using a simple, inexpensive thermal desorption method, and 2) present a survey of the interesting reactive behavior of two size-selected series of metal oxide clusters. Our initial work led to the production of molybdenum and tungsten oxide cluster ions by using a simple thermal desorption method to generate clusters in the gas-phase and the determination of their

dissociative behavior by using low energy collision activated dissociation techniques (32). These results are followed with an investigation of the reactive behavior of the oxides. The ion/molecule reaction chemistry of these oxides was examined for two reasons. First, certain neutral reagents were chosen to probe the intrinsic reactive behavior and product formation of the size-selected clusters. Second, both structural and energy differences of ions can be distinguished on the basis of their reactive behavior with selected compounds (33). The reactive species of particular interest are ethylene oxide, cyclohexene oxide, ethylene sulfide, cyclohexene sulfide, 2,3-butanedione, and 2,4-pentanedione (acetylacetone). Low energy collision activation is used to compare the relative dissociative behavior of the product ions. Since no suitable compounds with known structures exist, the reactive and dissociative behavior of the cluster ions cannot be compared to the behavior of model compounds. However, collisional activation is still valuable as a tool for comparing relative differences in dissociative behavior within a related series of ions.

3.2 Results and Disscusion :

Negative Ionization Mass Spectra and Collision Induced Dissociation

The clusters were generated by using a thermal desorption probe. This is a remarkably simple method for producing an array of clusters, and does not involve the use of a laser for desorption and/or ionization, nor does it involve the use of a super-sonic expansion. Negative electron capture mass spectra of the metal oxide clusters, $(MoO_3)_n^-$ and $(WO_3)_n^-$, are shown in Figure 3.1, respectively. The $(MoO_3)_n^-$ clusters were observed up to a range of 2000 u, where n = 13, and the $(WO_3)_n^-$ clusters were observed up to n = 8. The monomer, MO_3, was not observed for either metal, and the dimer gave a relatively weak signal, although the relative abundances of the higher mass cluster ions decreased essentially monotonically with increasing n. Typically, trimer and hexamer species have the greatest abundances.

Often collisional activation experiments are used to compare the dissociative behavior of one ion having an unknown structure to the dissociative behavior of model compounds. This allows general structural correlations to be made. However, collisional activation experiments may also be used to compare the dissociative

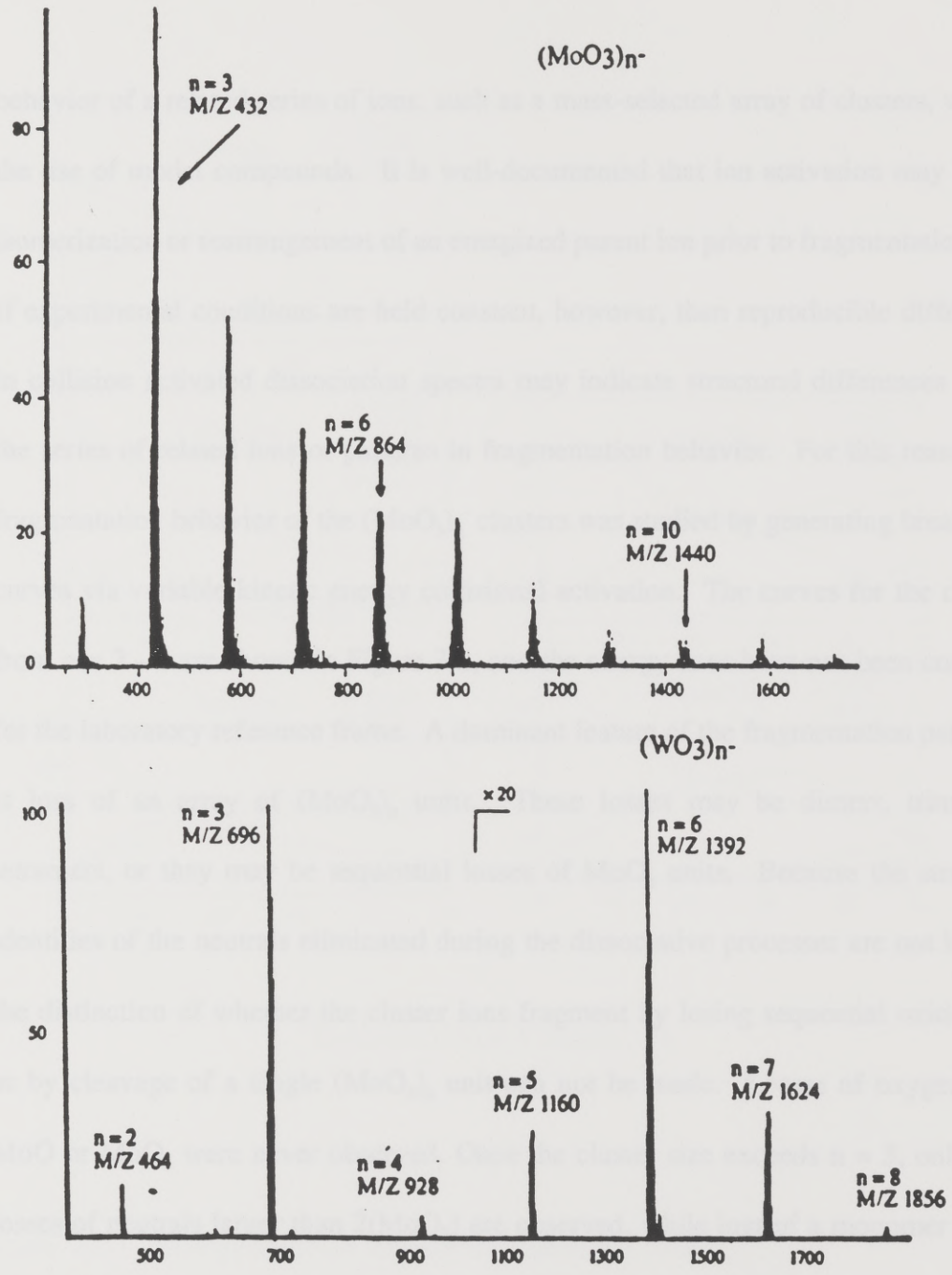

Figure 3.1 : Electron capture negative ionization mass spectra of $(MoO_3)_n^-$ and $(WO_3)_n^-$ clusters recorded on Finnigan TSQ-70.

behavior of a related series of ions, such as a mass-selected array of clusters, without the use of model compounds. It is well-documented that ion activation may induce isomerization or rearrangement of an energized parent ion prior to fragmentation [34]. If experimental conditions are held constant, however, then reproducible differences in collision activated dissociation spectra may indicate structural differences within the series of related ions or patterns in fragmentation behavior. For this reason, the fragmentation behavior of the $(MoO_3)_n^-$ clusters was studied by generating breakdown curves via variable kinetic energy collisional activation. The curves for the clusters from n = 3 - 7 are shown in Figure 3.2, and the energy axes have not been corrected for the laboratory reference frame. A dominant feature of the fragmentation pathways is loss of an array of $(MoO_3)_n$ units. These losses may be dimers, trimers or tetramers, or they may be sequential losses of MoO_3 units. Because the structural identities of the neutrals eliminated during the dissociative processes are not known, the distinction of whether the cluster ions fragment by losing sequential oxide units or by cleavage of a single $(MoO_3)_n$ unit can not be made. Losses of oxygen, Mo, MoO or MoO_2 were never observed. Once the cluster size exceeds n = 5, only total losses of neutrals larger than $2(MoO_3)$ are observed, while loss of a monomer unit is only observed for the smaller (n = 3,4) clusters. For the cluster sizes n = 4 - 7, the favored dissociative pathways result in formation of $(MoO_3)_2^-$ and $(MoO_3)_3^-$, suggesting that the dimer and trimer species have special stabilities. The $(WO_3)_n$

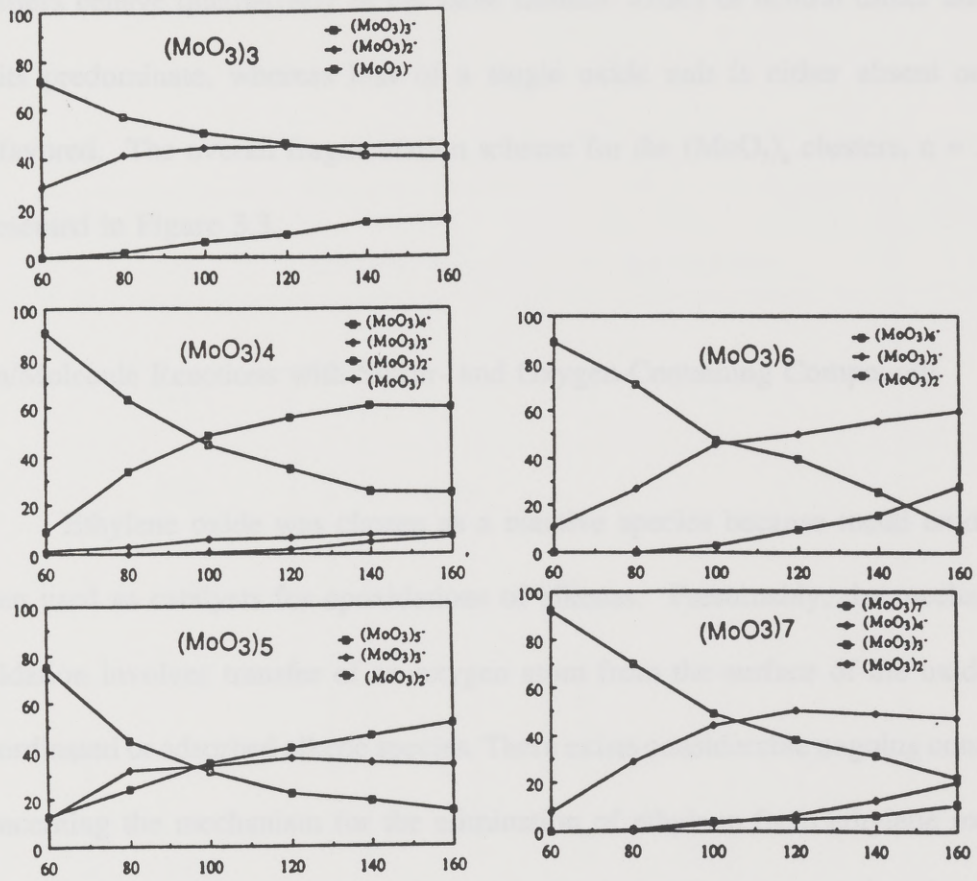

Figure 3.2 : Energy-resolved breakdown curves for $(MoO_3)_n^-$.

clusters behave qualitatively in the same fashion: losses of neutral dimer and trimer units predominate, whereas loss of a single oxide unit is either absent or highly unfavored. The overall fragmentation scheme for the $(MoO_3)_n$ clusters, n = 3 - 7, is presented in Figure 3.3.

Ion/Molecule Reactions with Sulfur- and Oxygen-Containing Compounds

Ethylene oxide was chosen as a reactive species because metal oxides have been used as catalysts for epoxidations of alkenes. Presumably, the mechanism of oxidation involves transfer of an oxygen atom from the surface of the oxide to the coordinated or adsorbed alkene species. There exists considerable ongoing controversy concerning the mechanism for the elimination of ethylene from ethylene oxide and from ethylene sulfide on metals. For example, it has been shown that the complex Li_2WCl_6 reacts with substituted ethylene oxide via epoxide ring opening to form an oxametallacyclobutane (35). The oxametallacyclobutane presumably then undergoes C-W and C-O bond cleavages, producing an alkene and a tungsten-oxygen complex. Alternatively, the reaction may occur by a concerted process. The latter was proposed for the reaction of ethylene sulfide on molybdenum (36). Calculations for ethylene sulfide reactions on both complexes and at surfaces, however, suggest that the concerted mechanism is more energetically favorable at a surface than for a complex

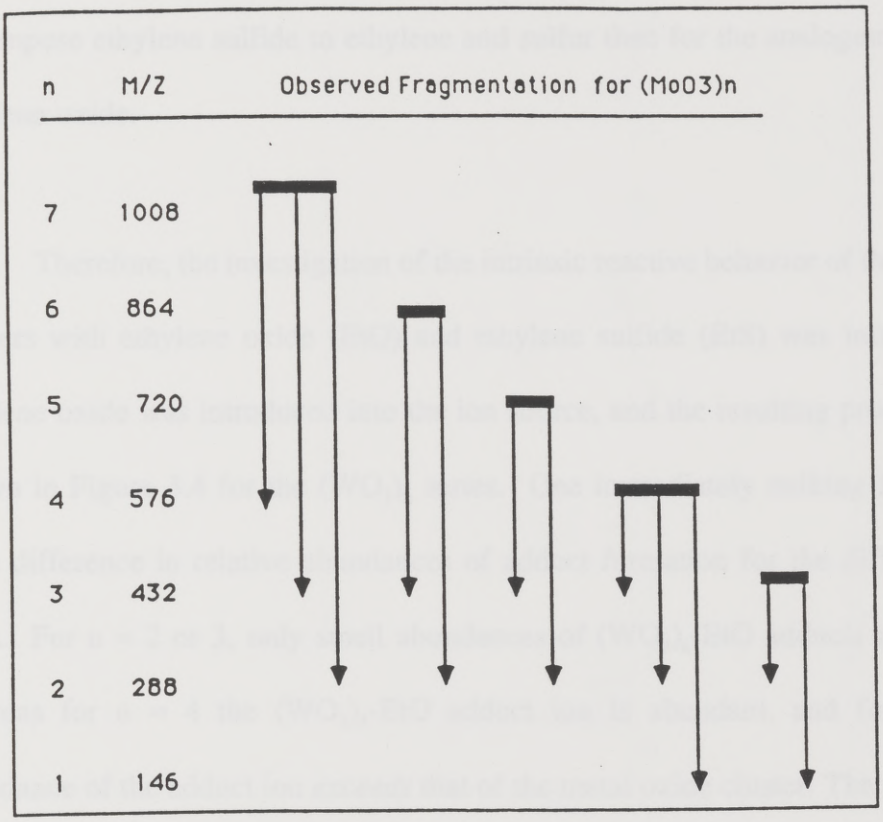

Figure 3.3 : Fragmentation pathways for dissociation of $(MoO_3)_n^-$ clusters.

(36). Additionally, different reactivities of ethylene oxide and ethylene sulfide on metals were observed, due in part to the different strengths of C-O and C-S bonds (37). The C-O bond in ethylene oxide is stronger, and less energy is required to decompose ethylene sulfide to ethylene and sulfur than for the analogous process for ethylene oxide.

Therefore, the investigation of the intrinsic reactive behavior of the ionic oxide clusters with ethylene oxide (EtO) and ethylene sulfide (EtS) was initiated. First, ethylene oxide was introduced into the ion source, and the resulting product ions are shown in Figure 3.4 for the $(WO_3)_n$ series. One immediately striking feature is the huge difference in relative abundances of adduct formation for the different cluster sizes. For n = 2 or 3, only small abundances of $(WO_3)_n$-EtO adducts are observed, whereas for n = 4 the $(WO_3)_4$-EtO adduct ion is abundant, and for n = 6 the abundance of the adduct ion *exceeds* that of the metal oxide cluster. The odd-n cluster adduct ions (n = 5 and n = 7) are of small abundances. Only for n = 4 is the oxygen addition adduct more abundant than the ethylene oxide adduct, perhaps indicating that the geometry of the n = 4 cluster in some way assists in the elimination of ethylene, unlike the n = 6 cluster in which expulsion of ethylene is clearly disfavored.

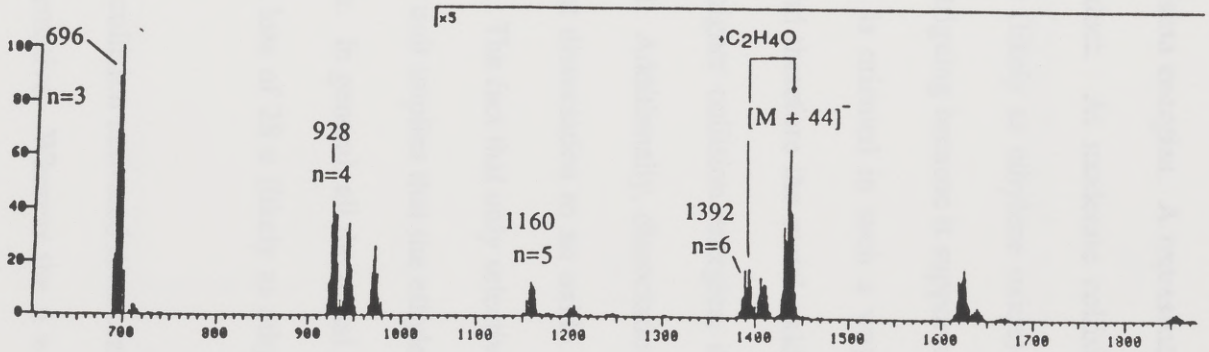

Figure 3.4 : Mass spectrum of the products of the reaction between ethylene oxide and $(WO_3)_n$.

Structural characterization of the adducts was done by using collisional activation at a range of collision energies. A representative case is shown in Figure 3.5 for the $(WO_3)_4$/EtO adduct. At moderate collision energies, the adduct ion fragments by loss of C_2H_4O (likely as ethylene oxide) or by loss of ethylene. The latter result is particularly intriguing because it supports the suggestion that the metal oxide/ethylene oxide adduct is oriented in such a way that the epoxide oxygen is bonded to a metal center, and therefore the metal oxide is capable of abstracting a solitary oxygen atom. At higher collision energies, dissociation by loss of oxide cluster units is also observed. Additionally, dissociation to an oxide dimer with one extra oxygen is observed, but dissociation to an oxide trimer or monomer with one extra oxygen is not observed. The fact that only selective dissociation channels occur with retention of the oxygen unit implies that the ethylene oxide addition may occur at a specific site of the cluster. In general, all the metal oxide/ethylene oxide adducts dissociate predominantly via loss of 28 u (likely as ethylene).

A comparison of the collision activated dissociation behavior of $(WO_3)_4$-EtO and $(WO_3)_6$-EtO is also informative. Whereas the n = 4 cluster adduct dissociates predominantly by either loss of EtO or ethylene, the n = 6 cluster dissociates *only* by loss of ethylene to form the $(WO_3)_6$-O species. Bare $(WO_3)_6$ product ions are never observed even at higher collision energies. This clearly indicates a distinction

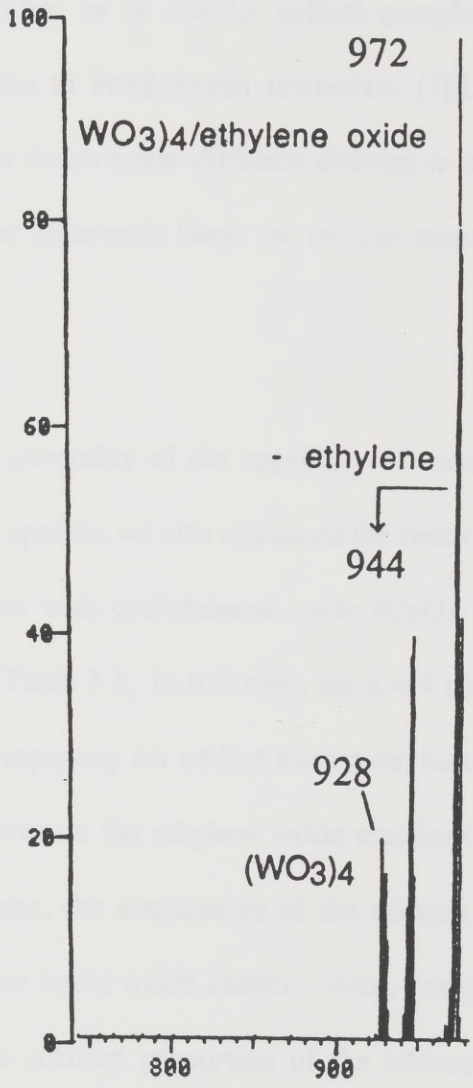

Figure 3.5 : CID mass spectrum of $(WO_3)_4$/ethylene oxide at 60 eV collision energy.

between the cluster sizes, possibly due to the differences in cluster structures, in electronic state densities or in frontier orbital energies (38), or the more subtle structural changes due to bond-stretch isomerism (39). The outcome is that the different cluster sizes demonstrate different abilities to bind oxygen. In the present case, the n = 6 cluster apparently binds the oxygen atom more strongly than the n = 4 cluster.

To probe the generality of the capability of metal oxide clusters to abstract oxygen from epoxide species, we also examined the reactive and dissociative behavior of the $(WO_3)_n$ clusters with cyclohexene oxide (CyO). The mass spectrum of the products is shown in Table 3.1. In this case, the n = 4 and n = 6 clusters again show the greatest relative propensity for adduct formation; however, the n = 3 cluster does form adducts (in contrast to the ethylene oxide reactions). With cyclohexene oxide as the reactive substrate, the abundances of the adducts for both n = 4 and n = 6 exceed that of the bare metal oxide cluster. Also, compared to the ethylene oxide adduct data, a greater relative proportion of the adducts exist as oxygen addition species (via loss of neutral cyclohexene) than as cyclohexene oxide adducts. This latter observation presumably reflects the reduced strength of the C-O bonds in cyclohexene oxide as compared to ethylene oxide. Collision activation of the $(WO_3)_4$/cyclohexene oxide cluster indicates that this adduct ion dissociates

Table 3.1 : Relative Product Distribution of Reactions of Cyclohexene Oxide and $(WO_3)_n$[a]

n	Scaling Factor	$(WO_3)_n$	$(WO_3)_n$/O	$(WO_3)_n$/CyO
3	1	0.85	0.01	0.15
4	5	0.15	0.35	0.50
5	10	0.80	0.05	0.15
6	10	0.10	0.65	0.25

[a] For each cluster size, the product abundances are expressed as the fraction of the total ion current for that size.

[b] The scaling factor indicates the overall distribution of cluster sizes.

predominantly to $(WO_3)_4^-$ (85% of the ion current) via loss of cyclohexene oxide and to $(WO_3)_4/O^-$ (15% of the ion current) by elimination of cyclohexene. Thus, oxygen atom abstraction from more bulky epoxide ligands by the metal oxide clusters is possible.

Similar studies were performed by using ethylene sulfide and cyclohexene sulfide instead of ethylene oxide and cyclohexene oxide as the reactive gases. A representative spectrum for the adducts produced in the source from $(WO_3)_n$ and ethylene sulfide is shown in Figure 3.6. One striking difference is obvious. Unlike the ethylene oxide reactions in which adducts of entire EtO units with $(WO_3)_n$ were formed, adducts due to the addition of ethylene sulfide (EtS) units are not observed. Instead, clusters with addition of one or in some cases two sulfur atoms are formed. The abundances of the n = 5,7 cluster adducts are small, as is the case for the ethylene oxide results, and the abundances of the n = 4,6 adducts are large. Interestingly, the n = 4 cluster shows predominant addition of *two* sulfur atoms whereas the n = 6 cluster shows only significant addition of one sulfur atom. This absence of ethylene sulfide adducts and presence of sulfur atom adducts (as compared to the ethylene oxide reactions) is consistent with the assumption that the lower C-S bond energy than the C-O bond energy (estimated as 20 kcal/mole difference (37)) is an important factor in determining the efficiencies of catalytic transformations. This

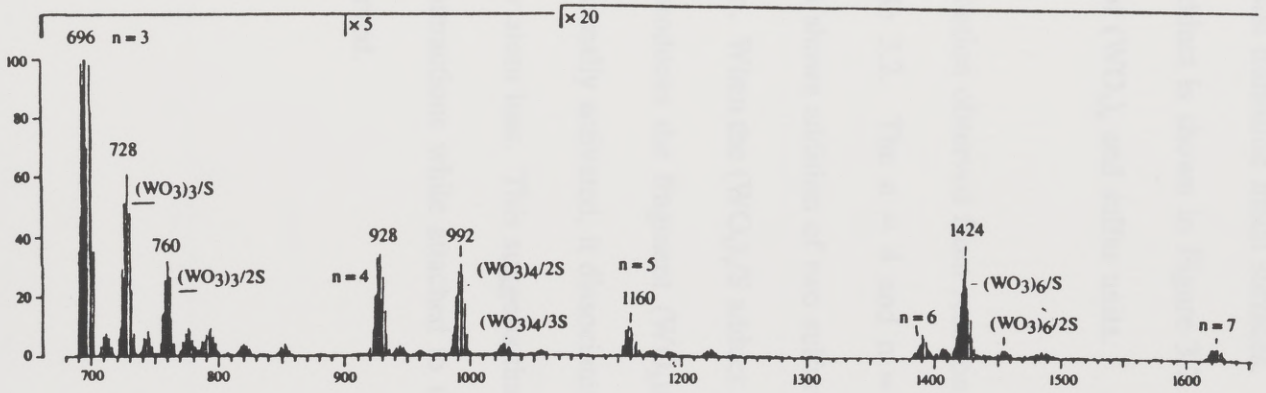

Figure 3.6 : Mass spectrum of the products of the reaction between ethylene sulfide and $(WO_3)_n$.

mimics the tendency for desulfurization of ethylene sulfide via intramolecular elimination on single crystal transition metal surfaces. The dissociation behavior of the n = 3 cluster/sulfur adduct is shown in Figure 3.7. This adduct dissociates via loss of any combination of $(WO_3)_n$ and sulfur units.

The product distribution observed from reaction of cyclohexene sulfide with $(WO_3)_n$ is shown in Table 3.2. The n = 4 and n = 6 cluster adducts are most abundant, and again n = 4 shows addition of two sulfur atoms whereas n = 6 favors addition of one sulfur atom. When the $(WO_3)_3$/S adduct is activated, it dissociates via loss of sulfur, and also produces the fragment (WO_3)/S. Alternatively, when the $(WO_3)_3$/2S adduct is collisionally activated, it dissociates only via loss of both sulfur atoms, not by single sulfur atom loss. This suggests that the sulfur atoms are linked by interatomic bonding interactions while attached to the oxide cluster. Losses of (WO_3) units are also observed.

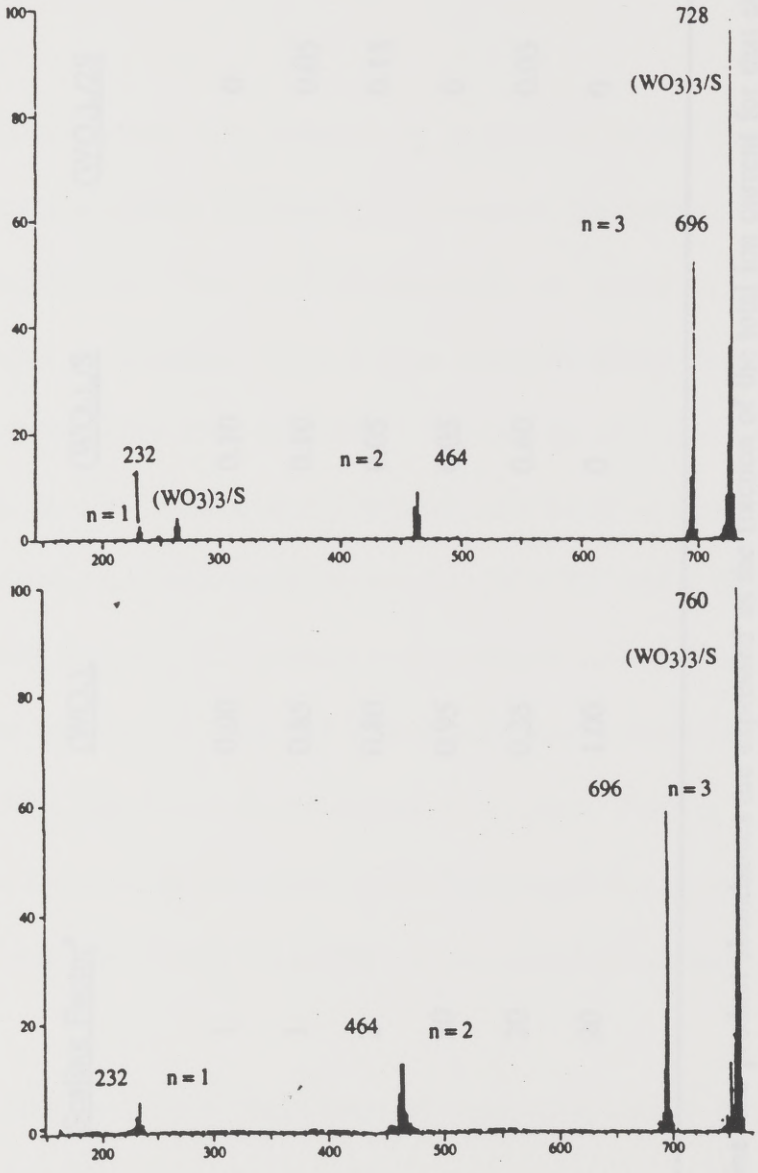

Figure 3.7 : CID mass spectra of $(WO_3)_3/S$ and $(WO_3)_3/2S$.

Table 3.2 : Relative Product Distribution from Reactions of Cyclohexene Sulfide and $(WO_3)_n$[a]

n	Scaling Factor[b]	$(WO_3)_n$	$(WO_3)_n/S$	$(WO_3)_n/2S$
2	1	0.90	0.10	0
3	1	0.85	0.10	0.05
4	2	0.80	0.05	0.15
5	20	0.95	0.05	0
6	20	0.35	0.60	0.05
7	20	1.00	0	0

[a] For each cluster size, the product abundances are expressed as the fraction of the total ion current for that size.

[b] The scaling factor indicates the overall distribution of cluster sizes.

Ion/Molecule Reactions with Diones

Acetylacetone was selected as a reactive probe because of its well-characterized properties as a metal chelating agent. The product distribution resulting from reactions of $(WO_3)_n$ with acetylacetone are shown in Table 3.3. Several observations are apparent. First, to some extent all of the sizes of the metal oxide clusters demonstrate some reactivity. Second, the size selectivity toward adduct formation does not obey a clearly defined trend based on odd or even cluster size. Third, products are consistently observed at $(M + 82)^-$, $(M + 100)^-$, and $(M + 182)^-$. Presumably the $(M + 82)^-$ product is an acetylacetone/metal oxide adduct that has undergone dehydration, while $(M + 182)^-$ represents a metal oxide cluster with two acetylacetone ligands that has undergone dehydration. For $n \geq 3$, the abundances of the adducts exceed the abundances of the bare cluster in all cases. Additionally, if $n = 3$ or $n = 6$, a propensity for addition of two acetylacetone units is observed.

Collision induced dissociation of these three adduct species reveals some further structural information (see Table 3.4). In the case of $(M + 100)^-$ or $(M + 182)^-$, loss of neutral acetylacetone is favored, whereas for the $(M + 82)^-$ ion, dissociation to produce the bare metal cluster is predominant. Furthermore, the $(WO_3)_3$/acetylacetone adduct ion also dissociates via loss of water. All the cluster

Table 3.3 : Relative Product Distribution for Reactions of $(WO_3)_n$ and 2,4-pentanedione[a]

n	Scale[b]	$(WO_3)_n$	$(WO_3)_n + 82$	$(WO_3)_n + 100$	$(WO_3)_n + 182$
2	1	0.65	0.05	0.15	0.15
3	1	0.15	0.10	0.20	0.55
4	1	0.01	0.05	0.80	0.15
5	10	0.05	0.05	0.45	0.45
6	10	0.10	0.05	0.30	0.55
7	10	0.25	0.05	0.45	0.25

[a] For each cluster size, the product abundances are expressed as the fraction of the total ion current for that size.

[b] The scaling factor indicates the overall distribution of cluster sizes.

Table 3.4 : Distribution of fragment ions from collisionally activated $(WO_3)_3$/2,4-pentanedione adducts[a]

Precursor Ion	Fragment Ions				
	$(WO_3)_2$	$(WO_3)_2/O$	$(WO_3)_3$	$(WO_3)_3/O$	$(WO_3)_3/82$
$[(WO_3)_3/(acac)_2$ - $H_2O]$ $(M + 182)^-$	0.10	0.30	0.15	0	0.45
$[(WO_3)_3/acac]$ $(M + 100)^-$	0.05	0.05	0.80	0.01	0.10
$[(WO_3)_3/acac$ - $H_2O]$ $(M + 82)^-$	0.10	0.10	0.80	0	0

[a] collision energy of 100 eV.

adducts dissociate to some extent to $(WO_3)_2/O^-$. The $(MoO_3)_n$ ions also formed $[M + 82]^-$, $[M + 100]^-$ and $[M + 182]^-$ adducts, and the fragmentation behavior of these species is analogous to the tungsten cluster behavior.

A comparison of the chelating capabilities of acetylacetone and 2,3-butanedione was also done. Similar to the reactive trends shown for acetylacetone/metal oxide clusters, the greatest relative abundances of adduct ions are produced for $(WO_3)_3$/butanedione and for $(WO_3)_6$/butanedione (Table 3.5). Without exception, the major dissociative channel of the adducts is loss of butanedione. In no case does any dehydration occur; this is attributed to the limited source of alpha-hydrogens available for migration to the oxygen for formation of a water molecule.

Table 3.5 : Product distribution from reactions of 2,3-butanedione and $(WO_3)_n$[a]

n	Scaling Factor	$(WO_3)_n$	$(WO_3)_n$/butanedione
3	1	0.25	0.75
4	1	0.50	0.50
5	1	0.70	0.30
6	10	0.15	0.85
7	10	0.95	0.05

[a] For each cluster size, the product abundances are expressed as the fraction of the total ion current for that size.

[b] The scaling factor indicates the overall distribution of cluster sizes.

3.3 Conclusion :

Both $(MoO_3)_n^-$ and $(WO_3)_n^-$ clusters dissociate predominantly via losses of small cluster units, resulting in stable dimers or trimers. The clusters react with ethylene oxide via addition of ethylene oxide or addition of oxygen. Collisional activation of these adducts indicates that dissociation by loss of ethylene oxide or ethylene is favored, and this suggests that the ethylene oxide is bonded to the cluster is such a way that the cluster-oxygen interaction is stronger than the C-O bonds in ethylene oxide. Analogous behavior in which oxygen abstraction may occur is observed for cluster reactions with cyclohexene oxide. Ion/molecule reactions with sulfur-containing substrates reveal that addition of one or two sulfur atoms to the clusters is possible, yet adducts of the clusters with entire cyclohexene sulfide or ethylene sulfide are never observed. Possibly this absence is because the C-S bonds are weaker than the C-O bonds, and therefore the elimination of an unsaturated hydrocarbon neutral (such as ethylene or cyclohexene) via cleavage of the C-S bonds is more facile. For these sulfide and oxide reactions, both n = 4 and n = 6 cluster sizes show greater relative product ion abundances than the other cluster sizes. Reactions with 2,3-butanedione and 2,4-pentanedione produce a much more complex array of product ions, including various additions and dehydrations. In general, the $(MoO_3)_n$ clusters produce smaller abundances of adducts than the $(WO_3)_n$ clusters.

The differences in the reactive behavior of the various sizes of cluster ions may indicate either a structural or energy difference in the clusters, and this will be discussed in Section B, in which alternative methods of forming the cluster ions prior to reactions are examined.

References :

1. Gates, B. C.; Guczi, L.; Knozinger, H. *Metal Clusters in Catalysis*; Elsevier, New York , 1986.

2. Grasselli, R. K.; Burrington, J. D. *Advances in Catalysis*, Eds. Eley, D. D.; Pines, H.; Weisz, P. B.; Academic Press: New York, **1981**, *30*, 131.

3. Reddy, B. M.; Narsimha, K.; Sivaraj, Ch.; Roa, P. K. *Applied Catalysis* **1989**, 55, L1.

4. Bielanski, A.; Haber, *J. Catal. Rev. Sci.* **1979**, *19*, 1.

5. Fierro, J.; Garcia De La Banda, J. F.; *Catal. Rev.-Sci. Eng.* **1986**, *28*, 265.

6. Awad, M. K.; Anderson, A. B. *J. Am. Chem. Soc.* **1990**, *112*, 1603.

7. Renneke, R. F.; Hill, C. L. *J. Am. Chem. Soc.* **1989**, *110*, 5461.

8. Grange, P. *Catal. Rev.-Sci. Eng.* **1980**, *21*, 135.

9. Laine, R. M. *Catal. Rev.-Sci. Eng.* **1983**, *25*, 459.

10. Chianelli, R. R. *Catal. Rev.-Sci. Eng.* **1984**, *26*, 361.

11. Prins, R.; DeBeer, V. H. J.; Somorjai, G. A. *Catal. Rev. Sci.* **1989**, *31*, 1.

12. Furimsky, E.; *Catal. Rev.-Sci. Eng.* **1980**, *22*, 371.

13. Parshall, G. W. Homogeneous Catalysis. *The Applications and Chemistry of Catalysis by Soluble Transition Metal Complexes*; Wiley-Interscience: New York, 1980.

14. Cheng, W.; Chowdhry, U.; Ferretti, A.; Firment, L.; Groff, P.; Machiels, C.; Mc Carron, E.; Ohuchi, F.; Staley, R.; Sleight, A. *Heterogenous Catalysis*; Ed. Shapiro, B.; Texas A & M Univ. Press, 1984; P 165.

15. Sheldon, R.; Kochi, J.; *Metal Catalyzed Oxidation of Organic Compounds*; Academic Press, New York, 1981.

16. Suzuki, T.; Gotoh, H. *Applied Catalysis* **1989**, *50*, 15.

17. Lopez Nieto, J. M.; Kremenic, G.; Martinez-Alonoso, A.; Tascon, J. M. D. *J. Mat. Science* **1990**, *25*, 289.

18. Madou, M. J.; Morrison, S. R. *Chemical Sensing with Solid State Devices*; Academic Press: CA, 1989.

19. Treitinger, L.; Voit, H. *NTG Fachberichte 79*, **1982**, *3*, 24.

20. Shaver, P. J., *Appl. Phys. Lett.* **1967**, *11*, 255.

21. Wheeler, R. G.; Laihing, K.; Wilson, W. L.; Duncan, M. A. *Chem. Phys. Lett.* **1986**, *131*, 8.

22. Nieman, G. C.; Parks, E. K.; Richtsmeier, S. C.; Liu, K.; Pobo, L.G.; Riley, S. J. *High Temp. Science* **1986**, *22*, 115.

23. Kang, H.; Beauchamp, J. L. *J. Am. Chem. Soc.* **1986**, *108*, 5663.

24. Freas, R. B.; Dunlap, B. I.; Waite, B. A.; Campana, J. E. *J. Chem. Phys.* **1987**, *86*, 1276.

25. Jarrold, M. F.; Bower, J. E. *J. Am. Chem. Soc.* **1988**, *110*, 6706.

26. Trevor, D. J.; Whetten, R. L.; Cox, D. M.; Kaldor, A. *J. Am. Chem. Soc.* **1985**, *107*, 518.

27. Parks, E. K.; Weiller, B. H.; Bechthold, P. S.; Hoffman, W. F.; Nieman, G. C.; Pobo, L. G.; Riley, S. J. *J. Chem. Phys.* **1988**, *88*, 1622.

28. Zakin, M. R.; Brickman, R. O.; Cox, D. M.; Kaldor, A. *J. Chem. Soc.* **1988**, *88*, 5943.

29. Tews, E. C.; Freiser, B. S. *J. Am. Chem. Soc.* **1987**, *109*, 4433.

30. Magnera, T.; David, D.; Michl, J. *J. Am. Chem. Soc.* **1987**, *109*, 936.

31. Michiels, E.; Gijbels, R. *Anal. Chem.* **1984**, *56*, 1115.

32. Proceedings at the 37th ASMS Conference on Mass Spectrometry and Allied Topics, May 1989, Miami Beach, FL.

33. Franklin J. (Ed.) Ion-Molecule Reactions Plenum: New York, 1979.

34. Busch, K. ; Glish, G., McLuckey, S. *Mass Spectrometry/Mass Spectrometry: Techniques and Applications of Tandem Mass Spectrometry*, VCH Publishers, New York, 1988.

35. Sharpless, K. B.; Teranishi, A. Y.; Backvall, Jan-E. *J. Am. Chem. Soc.* **1977**, *99*, 3120.

36. Serafin, J. G.; Friend, C. M. *J. Am. Chem. Soc.* **1989**, *111*, 6019.

37. Roberts, J. T.; Friend, C. M. *Surface Science* **1988**, *202*, 405.

38. Cotton, A.; Wilkinson, G.; *Advanced Inorganic Chemistry, Fifth Edition;* John Wiley and Sons, New York, 1988.

39. Jean, Y.; Lledos, A; Burdett,J.; Hoffmann,R.; *J. Am. Chem. Soc.* **1988**, *110*, 4506.

B. Comparison of Cluster Ion Formation by Using Different Ionization Methods

3.4 Introduction :

The existing methods for transition metal cluster ion formation include adiabatic expansion of vapors, laser vaporization of solids followed by flow condensation, and surface desorption of solids with trapped ion cooling (1,2). These techniques are in active use, and independent of the cost factor, methods selection is based on the physical properties of the substrates and the preference for production of a specific charge state of clusters. Relative abundances of cluster ions have been used as the measure of stability order of cluster ion sizes. The term "magic number" is used to denote the more abundant and presumably especially stable cluster ions (1). Cluster ion distributions are strongly dependent on the concentration and temperature of the clustering units in the gas phase. Another important factor is the conditions of the expansion or cooling process, such as the number of collisions the developing clusters encounter with background gases.

In Section A of this chapter, the reactivity and formation of transition metal oxide cluster ions of MoO_3 and WO_3 were discussed. The clusters were generated by resistive heating of oxides in the electron capture ionization mode. Mass spectra showed abundant trimer anions and the absence of monomers. These oxides show high electron affinities, for example a value of 2.58 eV has been estimated for molybdenum oxide (3). The chemistry of molybdenum (VI) and tungsten (VI) oxides is dominated by the formation of polyoxoanions in solution (4). The present study focuses on the formation of metal oxide cluster anions of MoO_3 and WO_3 in the gas phase. Recently, a fragment ion series for $(WO_3)_n^-$ extending to n = 9 was reported by liquid SIMS ionization of a technetium derivative of polyoxotungstates (5). Formation of metal oxide clusters from MoO_3 or WO_3 and the presence of analogous cluster series from ionization of a synthetic complex suggest that there are many kinetic pathways that result in formation of these clusters. The aim of this follow-up study is to correlate relative abundances of metal oxide cluster ions generated by different ionization techniques with their stabilities. Methods used include field desorption (FD), laser desorption (LD), and secondary ion mass spectrometry (SIMS).

3.5 Results and Discussion :

Mass spectra of MoO_3 and WO_3 in the electron capture ionization mode is presented in Section A of this chapter as Figure 3.1. In this mode, the source contained a high pressure of a reagent gas which assisted in the production of thermal electrons, and the oxides were volatilized by thermal desorption. The highest abundances of clusters were observed in the negative ionization mode for $(MoO_3)_n^-$, where n = 2 to 12, with a monotonic ion intensity decay after n = 3. The absence of the monomer and relatively low abundance of dimer suggest a special stability for the trimer. The stability of positive ion trimers formed by vaporization of metal oxides in a high temperature oven (Knudsen cell) (6,7) was reported previously. The closed ion source design required for the high pressure electron capture ionization technique may provide optimum conditions for formation of these sizes of clusters. Another important factor is the fast heating rate which provided a high oxide vapor concentration in the source.

The field desorption technique was selected as a comparison to the thermal ionization process used in electron capture ionization, however, in contrast to high pressure conditions of the electron capture technique, the source pressure in the FD

mode was < 10^{-6} torr. This ionization technique uses direct heating of the sample from an emitter in the presence of a high electric field which should provide the potential necessary for desorption and ionization of a wide range of clusters. The field desorption mass spectrum of MoO_3 (Figure 3.8) shows clusters from trimers to octamers with a fast ion decay after the hexamer. The absence of monomers and dimers with the presence of hexamers as the base peak in the spectrum suggest a special stability for trimers and hexamers.

Figure 3.9 shows the SIMS spectrum of WO_3 in which a 6 kV continuous neutral beam of xenon was used for sample desorption. An abundant ion for the monomer is observed. Also many oxygen deficient cluster ions are observed using the SIMS technique. The presence of these clusters suggest chemical modifications that occur during the ionization process. A very fast cluster ion decay after the trimer and the domination of reduced forms of clusters for the tetramer are among other characteristic features of this ionization process. The SIMS technique is also a low pressure method, therefore large cluster sizes are not observed. The probability for the presence of the reduced cluster increases with the cluster size. As the cluster mass increases, the ion signal for the oxygen deficient clusters becomes spread over an increasing mass range, effectively reducing the signal-to-noise ratio for any given peak in the cluster.

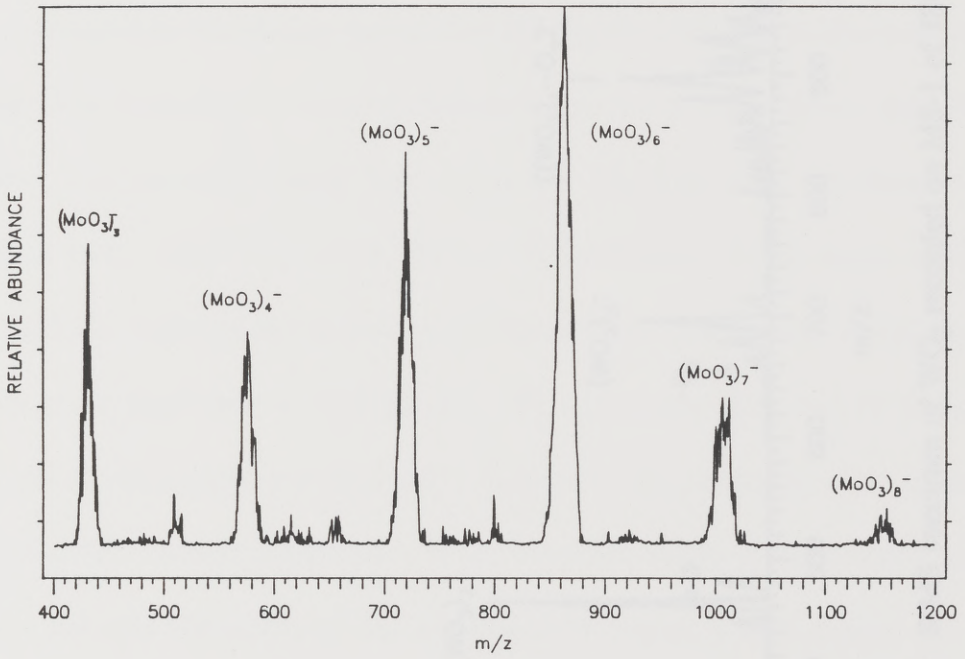

Figure 3.8 : Field desorption mass spectrum of MoO_3 recorded on MS-1 of JEOL HX110/HX110.

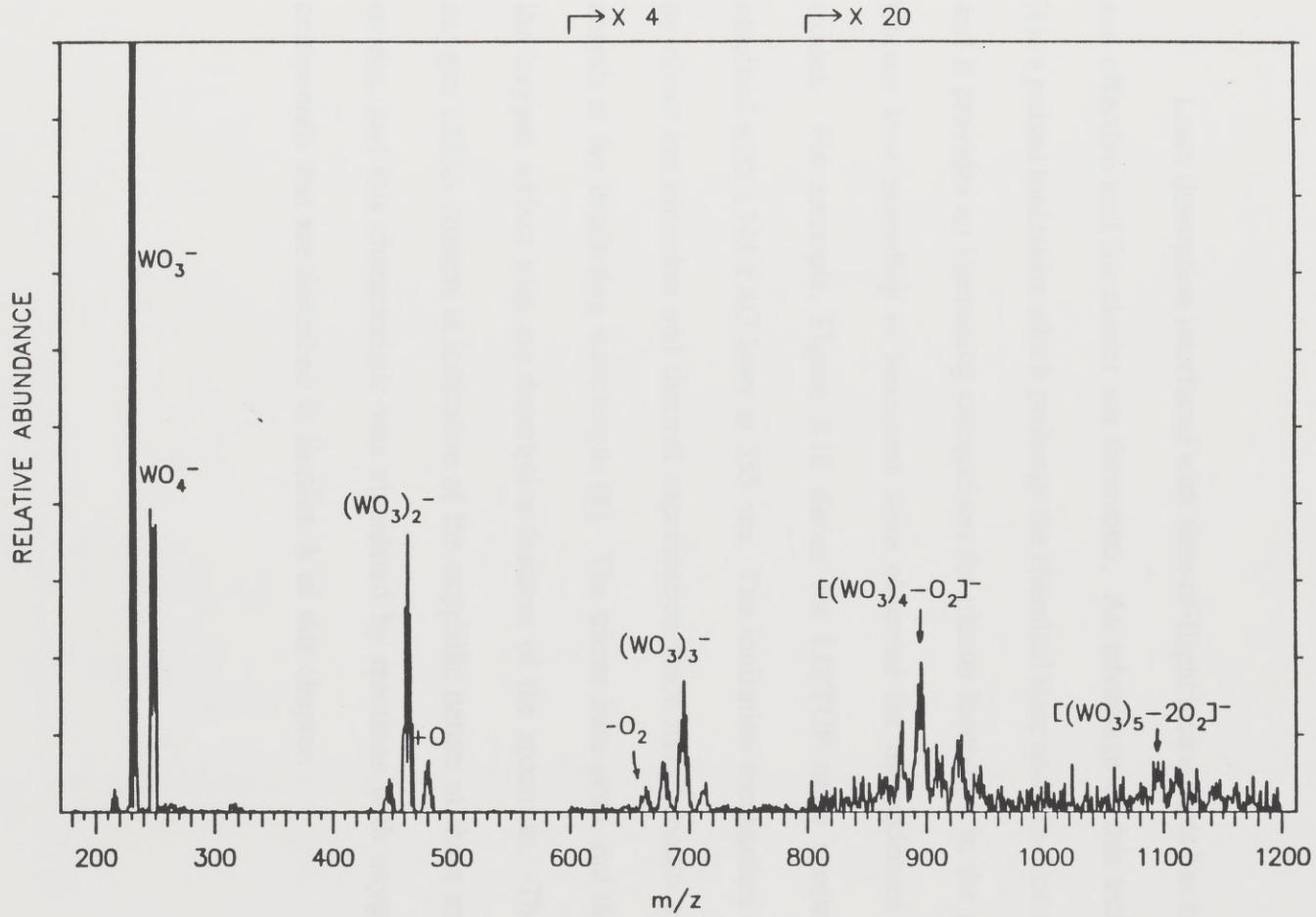

Figure 3.9 : SIMS spectrum of WO_3 recorded on MS-1 of JEOL HX110/HX110.

Laser desorption interfaced with time-of-flight instruments has been a popular and effective tool for cluster ion formation. An advantage of this technique is that it is a pulsed ionization which prolongs the chemical state and life-time of the sample, and it provides an interesting comparison for cluster formation in the present study. Cluster ions extending to hexamers were observed for molybdenum and tungsten oxides. For example, Figure 3.10 shows the LD/TOF mass spectrum of MoO_3 obtained with a Nd:YAG laser at 355 nm. The ionization mechanism is most likely by direct ion emission and thermal vaporization since molybdenum oxide does not absorb at the irradiating wavelength (8). The trimer base peak and the presence of the oxygen adduct ions are descriptive features of the spectrum. The presence of oxygen adduct clusters is indicative of the oxyphilic nature of these transition metal oxides, and this characteristic was elucidated by reactions with oxygen containing compounds that are described in Section A of this chapter.

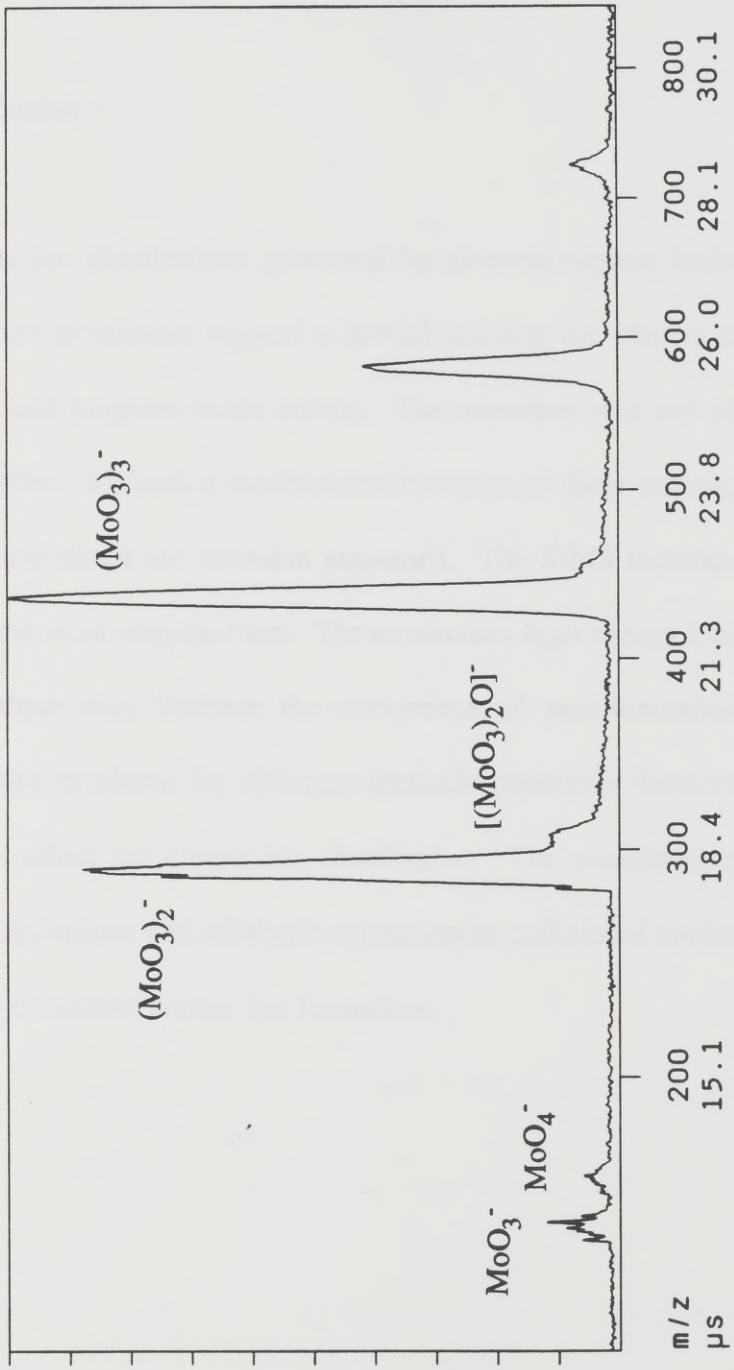

Figure 3.10 : Laser desorption mass spectrum of MoO_3 recorded on VESTEC 2000 time-of-flight mass spectrometer.

3.6 Conclusion :

Cluster ion distributions generated by electron capture ionization, field and laser desorption techniques suggest a special stability for trimers and hexamers of molybdenum and tungsten oxide anions. The monomer was not observed in these ionization modes. Ionization mechanisms common to these techniques are thermal vaporization and direct ion emission processes. The SIMS technique generated the monomer as the most abundant ion. The continuous high energy ionizing beam used in this technique may increase the occurrence of post-ionization fragmentation processes. Ions produced by different methods possess a distribution of internal energy which affect the cluster ion distribution. The metastability of ions alters cluster ion distributions and adiabatic expansion or collisional cooling processes are necessary for consistent cluster ion formation.

REFERENCES :

1. Russell, D. H.; Ed. *Gas Phase Ionorganic Chemistry*, Plenum Press : New York, 1989.

2. Futrell, J. H.; Ed. *Gaseous Ion Chemistry and Mass Spectrometry*, Wiley: New York, 1986.

3. Lias, S. G.; Bartmess, J. E.; Liebman, J. F.; Holmes, J. L.; Levin, R. D.; Mallard, W. G. *J. Phys. Chem. Ref. Data* **1988**, *17*, Supplement 1.

4. Pope, M. T.; *Heteropoly and Isopolyoxometalates*, Springer: New York, 1983.

5. Abrams, M. J.; Costello, C. E.; Shaikh, S. N.; Zubieta, J. *Inorg. Chimica Acta* **1991**, *180*, 9-11.

6. Berkowitz, J.; Inghram, M. G.; Chupka, W. A. *J. Chem. Phys.* **1956**, *26*, 842-846.

7. Burns, R. P.; DeMaria, G.; Drowart, J.; Grimley, R. T. *J. Chem. Phys.* **1959**, *32*, 1363-1366.

8. Hewett, W. D.; Newton, J. H.; Weltner Jr., W. *J. Phys. Chem.* **1975**, *79*, 2640-2649.

Chapter 4 - Structural Characterization of Polyethers by Collision Induced Dissociation Techniques

4.1 Introduction :

In recent years the role of macrocycles has become increasingly important in understanding principles of host-guest chemistry in molecular recognition (1,2). Crown ethers and their complexes are particularly important in biologically relevant transport and catalytic processes. There has been much interest in characterizing the structures of crown ether complexes and evaluating the thermodynamics of cation-ligand interactions (1-10). The reactive behavior and properties of crown ethers can be altered by many factors, including cavity size, and the nature of the donor atoms and substituents. For example, perfluorination of crown ethers results in compounds that have lower basicities and increased volatilities.

Various mass spectrometric characterizations of crown ethers, their structurally altered analogs, and complexes have been reported (11-19). The electron ionization mass spectra of various crown ethers have been recorded (12-16), and it was proposed that the ethers fragmented via formation of recyclized structures from linear intermediates. The chemical ionization and fast atom bombardment mass spectra of

some crown ethers have been reported by several groups (17-19). This comparative investigation of structural elucidation of crown ethers and their acyclic and perfluorinated analogs by collision induced dissociation (CID) was initiated to provide a basis for understanding the CID behavior of gas-phase ion complexes of these macrocyles.

4.2 Results and Discussion :

Collision Induced Dissociation of Crown Ethers

Positive chemical ionization of the series of crown ethers indicates that substantial abundances of both $(M - H)^+$ and $(M + H)^+$ ions are formed. The collision induced dissociation mass spectra of the protonated crown ethers: 12-crown-4, 15-crown-5, and 18-crown-6 are shown in Table 4.1. For each crown ether, the fragmentation pattern consists of a series of losses of $(C_2H_4O)_n$ units (44 amu). Thus, the fragment ions consistently observed include *m/z* 45, 89, 133, 177,..., depending on the size of the initial precursor ion. The loss of a single (C_2H_4O) unit is evidently disfavored, whereas the losses of $(C_2H_4O)_n$ where n = 2 or 3 are favored. The relative loss of $(C_2H_4O)_4$ increases by an order of magnitude as the macrocyclic ring size increases from 15-crown-5 to 18-crown-6.

Table 4.1 : CID of protonated crown ethers ions.[a]

	Percent of Total Fragment Ion Current for Loss of $(C_2H_4O)_n$			
Crown	n=1	n=2	n=3	n=4
12-4	2	38	62	--
15-5	1	46	51	2
18-6	<1	42	26	31

[a] at 10 eV lab collision energy

Upon protonation in the source, the crown ethers show extensive fragmentation; this is also found in electron ionization mass spectra. For example, protonated 18-crown-6 dissociates in the source to *m/z* 221, 177, 133, and 89, via losses of (C_2H_4O)n units. The CID spectra were recorded for each of these fragment ions extracted from the source. The series is shown in Figure 4.1, along with the CAD spectra of protonated 18-crown-6 (*m/z* 265). In each case, the selected ion dissociates via losses of $(C_2H_4O)_n$ units. Dissociation to *m/z* 89 or 45 are the predominant channels for this series of ions. Additionally, the CID spectra of these fragment ions produced from protonated 18-crown-6 closely resemble the CID spectra generated directly from protonated crown ethers of smaller ring size (15-crown-5 (*m/z* 221), 12-crown-4 (*m/z* 177), 9-crown-3 (*m/z* 133) see Table 4.1). This suggests that fragmentation in the ion source can result in structures that maintain their cyclic nature.

After collisional activation, the $(M - H)^+$ ions fragment in analogous ways to the $(M + H)^+$ ions, i.e. via losses of $(C_2H_4O)_n$ units. This results in an array of fragment ions of *m/z* 43, 87, 131, 175..., with the series extending up to the mass of the precursor ion. Negative ionization of the crown ethers results in moderate abundances of deprotonated $(M - H)^-$ ions. The CID results are listed in Table 4.2. These ions dissociate via many more routes than the $(M + H)^+$ or $(M - H)^+$ positive

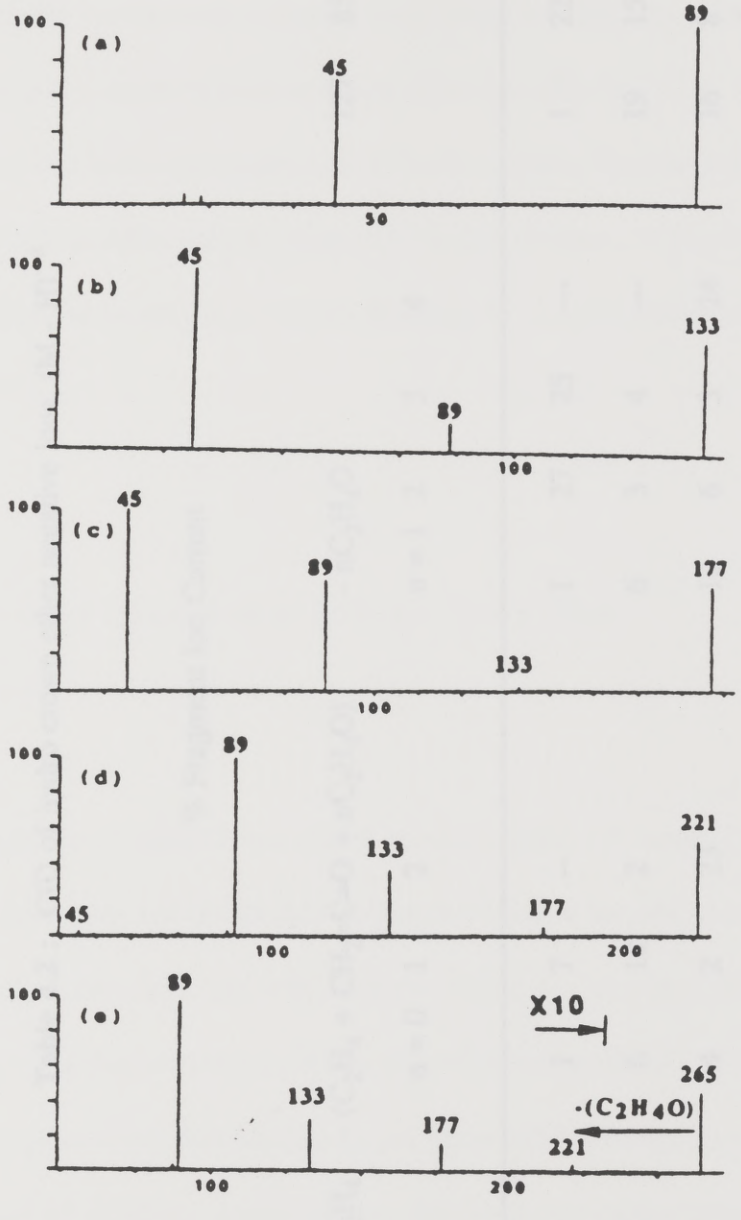

Figure 4.1 : CID mass spectra at 30 eV collision energy for E) 18-crown-6 (*m/z* 265), and its fragments at A) *m/z* 89, B) *m/z* 133, C) *m/z* 177, and D) *m/z* 221.

Table 4.2 : CID of hydro crown ether negative ions, $(M - H)^-$ [a]

Crown	% Fragment Ion Current									
	$-C_2H_4$	$-(C_2H_4 + CH_2=C=O + nC_2H_4O)$			$-nC_2H_4O$				127^-	85^-
		n = 0	1	2	n = 1	2	3	4		
12-4	17	1	7	--	1	27	25	---	1	22
15-5	24	6	18	2	6	3	4	---	19	15
18-6	1	4	2	23	12	6	3	24	16	8

[a] at 15 eV laboratory collision energy.

ions. All of the crown ether negative ions dissociate by loss of sequential C_2H_4O units, resulting in a series of fragment ions of *m/z* 43, 87, 131, 175... (again dependent on the size of the initial precursor ion). Simple ethylene loss from each negative ion is also observed, and this may be coupled with loss of ketene (CH_2=C=O). Sequential losses of C_2H_4O units may then occur, resulting in another series of ions at *m/z* 61, 105, 149, 193...

Collision Induced Dissociation of Perfluoro Crown Ethers

The perfluorinated crown ethers produce $(M - F)^+$ under positive chemical ionization conditions, but the simple protonated species are not observed. The $(M - F)^+$ ions likely result from $(M + H - FH)^+$. These positive ions dissociate via two routes upon collisional activation. They may eliminate units of C_2F_4O, a process that appears analogous to the dissociation routes observed for the hydro crown ethers that expelled units of C_2H_4O. Alternatively, the perfluoro crown ether ions eliminate $C_2F_2O_2$, and this abundant loss may occur in conjunction with the losses of C_2F_4O units.

The perfluoro crown ethers produce abundant anions, $M^{-\cdot}$, in the negative ion mode. The CAD mass spectra of the negative molecular ions of perfluorinated 18-crown-6, 15-crown-5, and 12-crown-4 ethers are shown in Table 4.3. These ethers dissociate via pathways analogous to the hydrogenated crown ethers. The major losses are a series of $(C_2F_4O)_n$ units. For the same relative collision energies and activation conditions, the perfluoro crown ethers show much less extensive fragmentation than do the hydro crown ethers, an expected result for fluorine substitution.

ERMS of Crown Ethers and Perfluoro Crown Ethers

Energy-resolved breakdown curves were acquired by varying the collision energy (the potential difference between the ion source and cental quadrupole) of a selected precursor ion. Energy resolved mass spectra are shown in Figure 4.2 for the hydro and perfluoro 18-crown-6 ethers. The relative ion abundances are plotted as a function of the relative collision energy to compensate for the large disparity in the mass-to-charge ratios of the selected precursor ions. For the protonated 18-crown-6 ether, loss of $(C_2H_4O)_4$ is the predominant dissociation channel at all energies, and the contribution increases relative to loss of $(C_2H_4O)_3$ and $(C_2H_4O)_2$ at higher kinetic energies.

Table 4.3 : CID of perfluoro crown ether negative molecular ions.

Percent Fragment Ion Current due to Loss of $(C_2F_4O)_n$[a]

Crown	n=1	n=2	n=3	n=4
12-4	47	47	6	--
15-5	60	30	10	--
18-6	32	41	27	0

[a] 10 eV lab collision energy

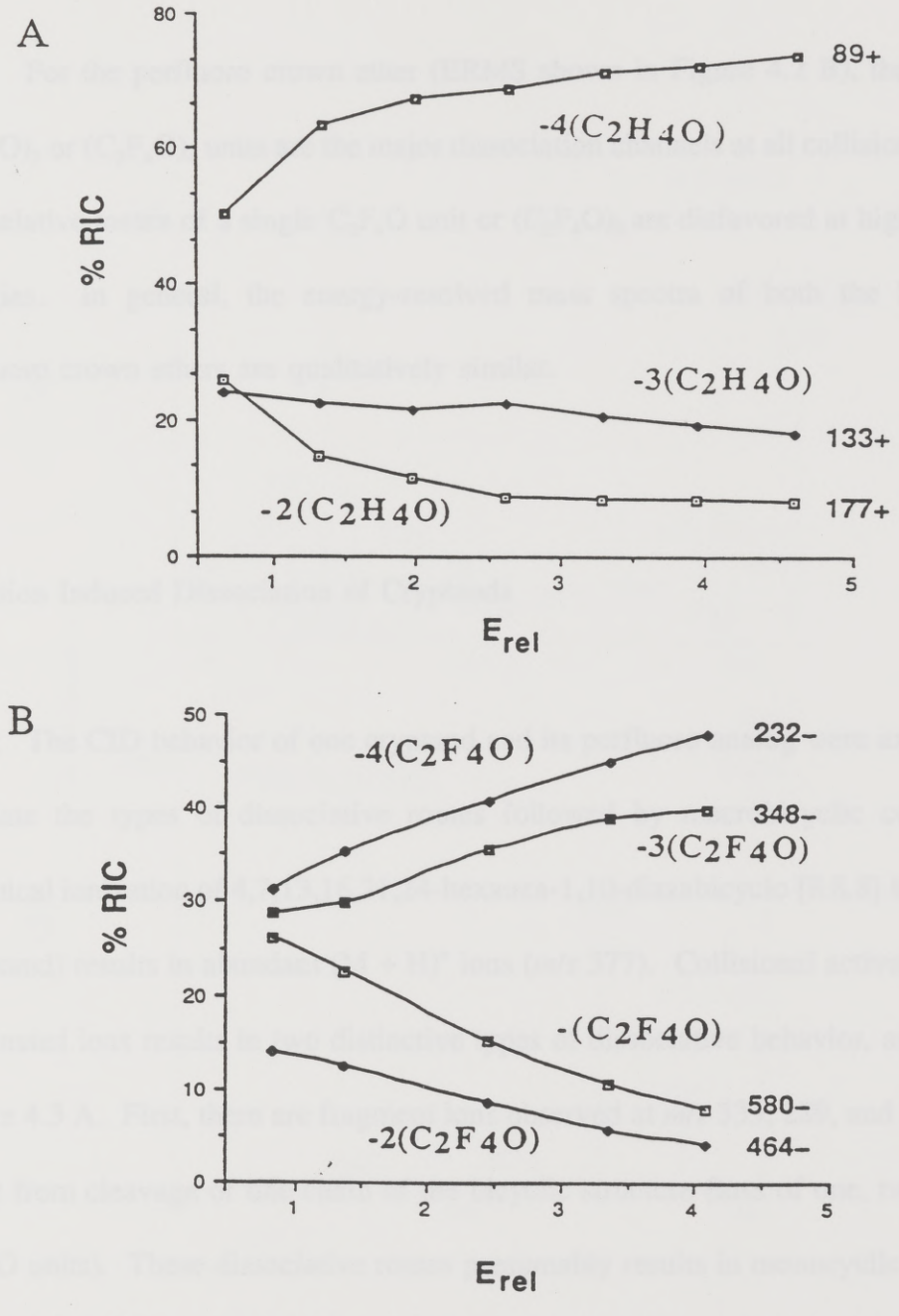

Figure 4.2 : Energy-resolved breakdown curves for A) protonated 18-crown-6, B) negative molecular ion of perfluoro 18-crown-6.

For the perfluoro crown ether (ERMS shown in Figure 4.2 B), the losses of $(C_2F_4O)_3$ or $(C_2F_4O)_4$ units are the major dissociation channels at all collision energies. The relative losses of a single C_2F_4O unit or $(C_2F_4O)_2$ are disfavored at higher kinetic energies. In general, the energy-resolved mass spectra of both the hydro and perfluoro crown ethers are qualitatively similar.

Collision Induced Dissociation of Cryptands

The CID behavior of one cryptand and its perfluoro analog were examined to evaluate the types of dissociative routes followed by macrobicyclic compounds. Chemical ionization of 4,7,13,16,21,24-hexaoxa-1,10-diazabicyclo [8.8.8] hexacosane (cryptand) results in abundant $(M + H)^+$ ions (*m/z* 377). Collisional activation of the protonated ions results in two distinctive types of dissociative behavior, as shown in Figure 4.3 A. First, there are fragment ions observed at *m/z* 333, 289, and 245 which result from cleavage of one chain of the bicyclic structure (loss of one, two or three C_2H_4O units). These dissociative routes presumably results in monocyclic ether ions with retention of both nitrogen atoms. Alternatively, cleavage involving the nitrogen bridge positions occur, and these dissociative pathways result in two predominant series of fragment ions: at *m/z* 70, 114, and 158, and at *m/z* 86, 130, and 174. Note

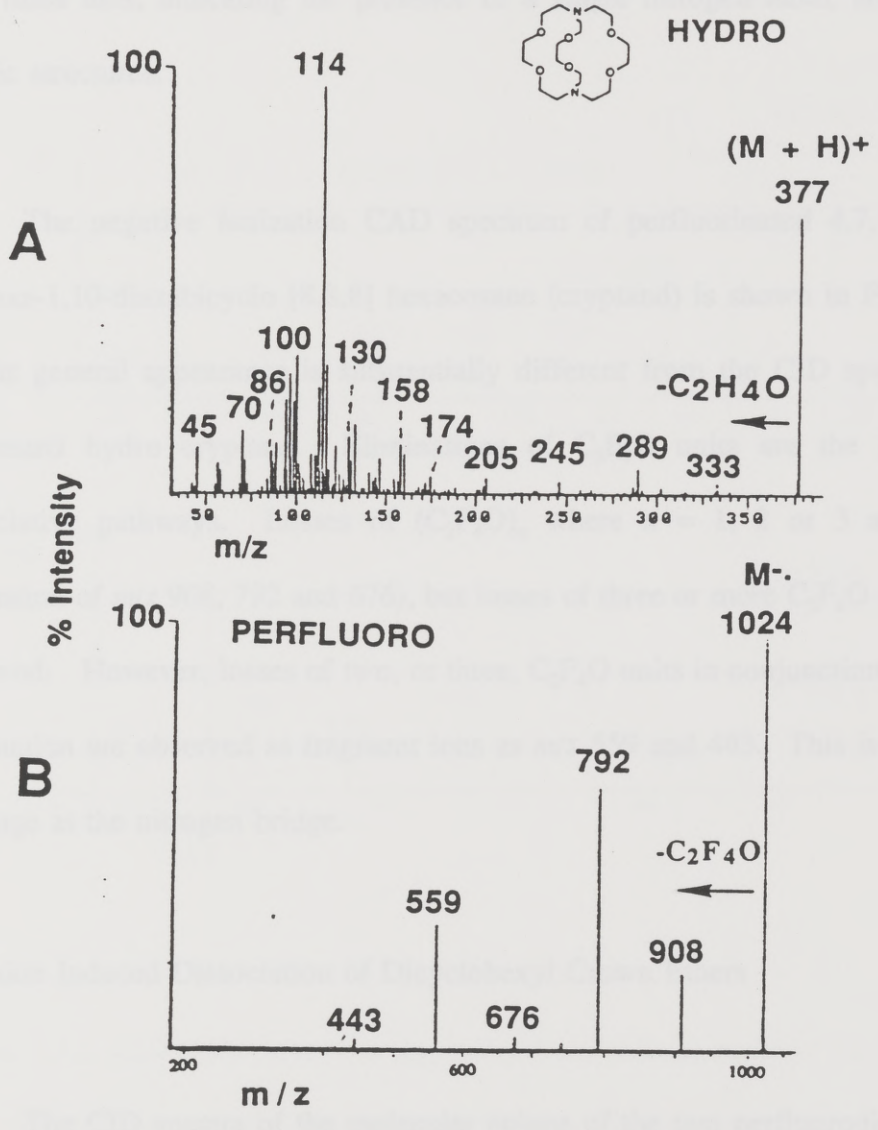

Figure 4.3 : CID mass spectra at E_{cm} = 3 eV for A) protonated cryptand, B) the negative ion of perfluorinated cryptand.

that each fragment in these series is separated by 44 u (C_2H_4O). These ions are all even mass ions, indicating the presence of a single nitrogen atom, and are likely acyclic structures.

The negative ionization CAD spectrum of perfluorinated 4,7,13,16,21,24-hexaoxa-1,10-diazabicyclo [8.8.8] hexacosane (cryptand) is shown in Figure 4.3 B, and its general appearance is substantially different from the CID spectra for the protonated hydro cryptand. Eliminations of C_2F_4O units are the predominant dissociative pathways. Losses of $(C_2F_4O)_n$ where n = 1, 2 or 3 are observed (formation of *m/z* 908, 792 and 676), but losses of three or more C_2F_4O units are not observed. However, losses of two, or three, C_2F_4O units in conjunction with C_4F_9N elimination are observed as fragment ions as *m/z* 559 and 443. This is evidence of cleavage at the nitrogen bridge.

Collision Induced Dissociation of Dicyclohexyl Crown Ethers

The CID spectra of the molecular anions of the two perfluorodicyclohexano crown ethers, 24-crown-8 and 18-crown-6, and the protonated hydro crown ethers were acquired. The spectrum for the first one is shown in Figure 4.4 A. These substituted perfluoro crown ethers do not dissociate via simple loss of C_2F_4O.

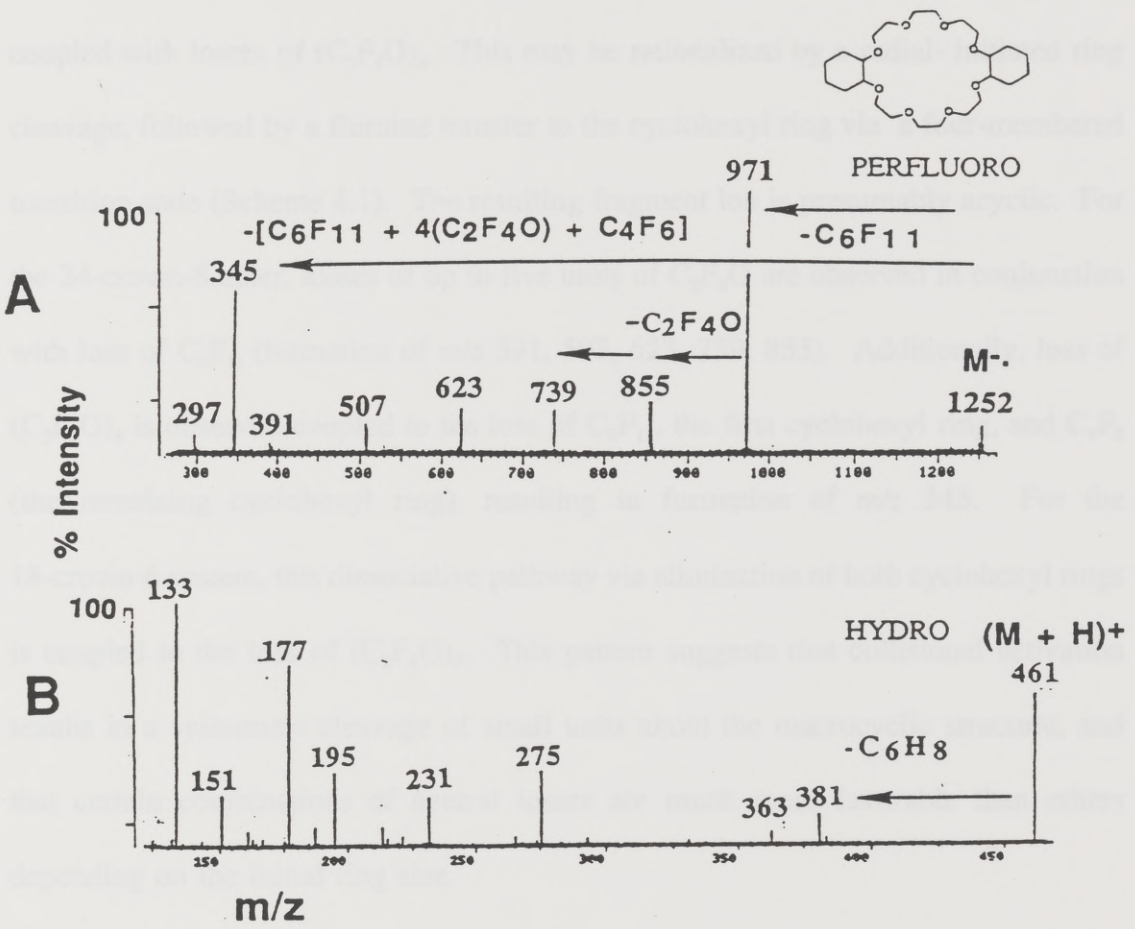

Figure 4.4 : CID mass spectra at E_{cm} = 2 eV for A) the negative ion of perfluoro dicyclohexano-24-crown-8, B) protonated hydro dicyclohexano-24-crown-8.

Instead, cleavage of C_6F_{11} (cyclohexyl ring) is a predominant process, and may be coupled with losses of $(C_2F_4O)_n$. This may be rationalized by a radial- initiated ring cleavage, followed by a fluroine transfer to the cyclohexyl ring via a four-membered transition state (Scheme 4.1). The resulting fragment ion is presumably acyclic. For the 24-crown-8 ether, losses of up to five units of C_2F_4O are observed in conjunction with loss of C_6F_{11} (formation of *m/z* 391, 507, 623, 739, 855). Additionally, loss of $(C_2F_4O)_4$ is observed coupled to the loss of C_6F_{11}, the first cyclohexyl ring, and C_4F_6 (the remaining cyclohexyl ring), resulting in formation of *m/z* 345. For the 18-crown-6 system, this dissociative pathway via elimination of both cyclohexyl rings is coupled to the loss of $(C_2F_4O)_3$. This pattern suggests that collisional activation results in a systematic cleavage of small units about the macrocyclic structure, and that certain combinations of neutral losses are much more favorable than others depending on the initial ring size.

Comparison of the CID spectra for perfluorodicyclohexano-24-crown-8 to the CID spectra of hydro-dicyclohexano-24-crown-8 (shown in Figure 4.4 B) reveals similarities. For the hydro crown, elimination of C_6H_8 (one cyclohexyl ring) or C_6H_8 + H_2O are observed as the smallest neutral losses from the protonated precursor ion. These dissociation routes result in the fragment ions observed at m/z 381 and m/z 363, respectively. The loss of C_6H_8 is rationalized by the mechanism suggested

Scheme 4.1 : Mechanisms of dissociation pathways of perfluorinated substituted crown ethers.

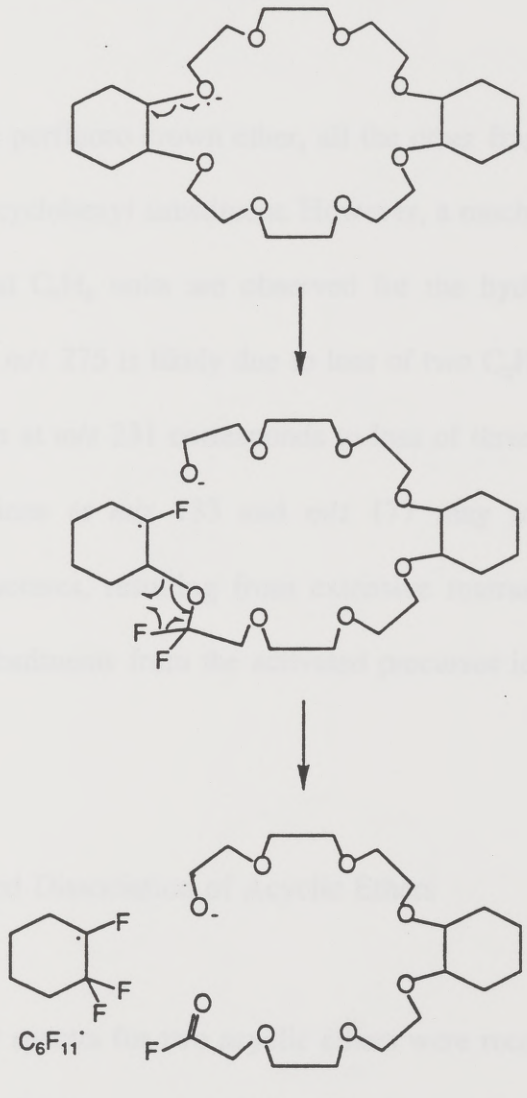

in Scheme 4.2. Macrocyclic ring opening initially occurs via a hydrogen transfer to the protonated oxygen site through a four-membered ring transition state. The cyclohexyl ring is cleaved upon proton abstraction by the other ether oxygen, via a second four-membered transition state.

Like the perfluoro crown ether, all the other fragmentation paths incorporate this loss of the cyclohexyl substituent. However, a much more diverse array of losses of $(C_2H_4O)_n$ and C_6H_8 units are observed for the hydro ether. For example, the fragment ion at *m/z* 275 is likely due to loss of two C_2H_4O units from the ion at *m/z* 363, and the ion at *m/z* 231 corresponds to loss of three C_2H_4O units from *m/z* 363. The fragment ions at *m/z* 133 and *m/z* 177 may represent the 9-crown-3 and 12-crown-4 structures, resulting from extensive rearrangment and cleavage of the cyclohexano substituents from the activated precursor ion.

Collision Induced Dissociation of Acyclic Ethers

The CID spectra for two acyclic ethers were recorded as a comparison to the CID behavior of the crown ethers. Both triethylene glycol dimethyl ether (TrEG-DME), an acyclic analog of 12-crown-4, and tetraethylene glycol dimethyl

Scheme 4.2 : Mechanisms of dissociation pathways of substituted crown ethers.

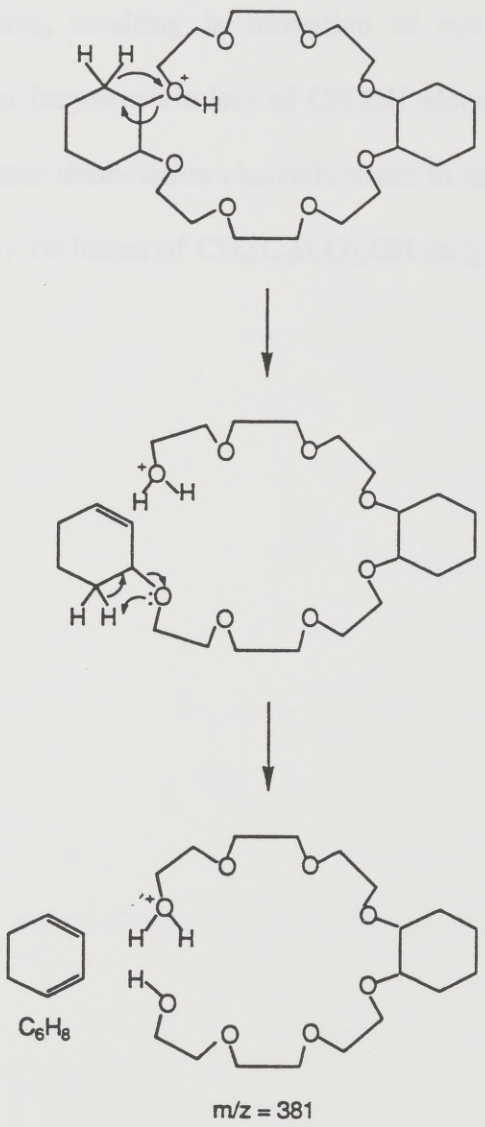

ether (TeEG-DME), an acyclic analog of 15-crown-5, were protonated and collisionally activated. The CID spectra are listed in Table 4.4. Protonated TrEG-DME loses methanol to form *m/z* 147, which may occur in conjunction with losses of C_2H_4O units, resulting in formation of *m/z* 103 and 59. Protonated TeEG-DME does not fragment via loss of CH_3OH alone, but by loss of $[CH_3OH + (C_2H_4O)_n]$. These latter dissociation channels result in ions at m/z 133, 103, 89, 59, and may alternatively be losses of $CH_3(C_2H_4O)_nOH$ ($n \geq 1$).

Table 4.4 : CID of protonated acyclic ether ions.

	Percent Total Fragment Ion Current[a,b]			
Ether	$-CH_3OH$	$-(C_3H_8O_2)$	$-(C_5H_{12}O_3)$	$-(C_7H_{16}O_4)$
TrEG-DME	2	44	54	0
TeEG-DME	0	5	48	47

[a] 10 eV lab collision energy

[b] small fragment ion abundances (<2%) at *m/z* 89 and 133 were also observed

4.3 Conclusions:

Upon collisional activation, crown ether and related perfluoro macrocyclic ions dissociate via similar routes. That is, systematic and sequential cleavages of the macrocyclic skeleton occur, and these cleavages may be in conjunction with elimination of substituents. Comparison of the CID spectra of the crown ethers with the CID spectra of acyclic analogs and crown ether fragment ions suggests that the cyclic structures are largely retained during the dissociation processes. Whereas both the hydro and perfluoro crown ethers showed very similar fragmentation patterns, the hydro and perfluoro cryptands showed very distinctive CID spectra. The perfluoro cryptand dissociates via four or five pathways, all easily rationalized. Incontrast, the hydro cryptand dissociates via complex pathways with extensive fragmentation of the macrocyclic structure. Upon collisional activation, the dicyclohexano crown ethers dissociate via neutral losses that suggest the macrocyclic structure is not retained unless the cyclohexano substituents are eliminated.

References :

1. D. Cram, *Science* **1988**, *240*, 760.

2. J. Lehn, *Angew Chem. Int. Ed. Engl.* **1988**, *27*, 89.

3. D. Cram, J. Cram, *Acc. Chem. Res* **1978**, *11*, 8.

4. R. Haward, *Chem. Soc. Rev.* **1983**, *12*, 285.

5. C. Pederson, *J. Am. Chem. Soc.* **1967**, *89*, 7017.

6. E. Graf, J. Lehn, J. *Am. Chem. Soc.* **1976**, *98*, 6403.

7. W. Farnham, D. Roe, D. Dixon, J. Calabrese, R. Harlow, *J. Am. Chem. Soc*, **1990**, *112*, 7707.

8. B. Dietrich, M. Hosseini, J. Lehn, R. Sessions, *J. Am. Chem. Soc.*, **1981**, *103*, 1282.

9. J. De Boer, D. Reinhoudt, S. Harkema, G. Van Hummel, F. De Jong, *J. Am. Chem. Soc.* **1982**, *104*, 4073.

10. A. Popov, *Pure Appl. Chem.* **1979**, *51*, 101.

11. A. K. Bose, O. Prakash, Y.H. Geng, J. Edasery, J. Org. Chem. **1983**, *48*, 1780.

12. Y. Lee, A. Popov, J. Allison, *Int. J. Mass Spectrom. Ion Phys.*, **1983**, *51*, 267.

13. P. Vouros, K. Biemann, *Org. Mass Spectrom.* **1970**, *3*, 1317.

14. A. Gomes, C. Oliveira, *Org. Mass Spectrom.***1977**, *12*, 407.

15. R. Gray, D. Reinhoudt, K. Spaargaren, J. De Bruijn, *J. Chem. Soc, Perkin II*, **1977**, 206.

16. D. Jaeger, R. Whitney, *J. Org. Chem.* **1975**, *40*, 92.

17. R. Hancock, R. Walder, H. Weigel, V. Gold, C. Sghibairz, *Org. Mass Spectrom.* **1983**, *18*, 402.

18. J. Miller, K. Balasanmugam, A. Fulcher, *Org. Mass Spectrom.* **1989**, *24*, 497.

19. G. Bonas, C. Bosso, M. Vignon, *J. Incl. Phenom. Mol. Recog. in Chem.*, **1989**, *7*, 637.

20. K.L. Busch, G.L. Glish, S.A. McLuckey, *Mass Spectrometry/Mass Spectrometry: Techniques and Applications of Tandem Mass Spectrometry*, VCH: New York, 1988.

Chapter 5 - A. Selectivities of Crown Ethers for Alkali Metal Ion Complexation

5.1 Introduction :

The principles of understanding many biological phenomena, such as enzyme binding and signal transmission across cell membranes, are based on molecular recognition and host-guest binding interactions (1). The selective binding involved in host-guest complexation requires an optimum or "preorganized" structure for each substrate prior to possible electrostatic or hydrogen bonding interactions (2). These processes are highly influenced by solvation effects (3). Macrocycles such as cage cryptands which have isolated cavities (4), and substituted lipophilic crown ethers (5) have been designed to study the factors of preorganization and solvation energy in recognition and complexation. However, controversy remains concerning the importance of solvent effects on host-guest selectivities. Gas-phase media provide an optimum environment to study the intrinsic behaviors of host-guest interactions.

Previously, alkali metal/crown ether binding has been investigated in detail in solution by several experimental techniques including calorimetric titration (6), potentiometry with ion selective electrodes (7), NMR (8), and ultrasonic absorption

kinetic methods (9). These studies provide a comparison when the solvation energy and ion pairing effects dominate selectivities. The investigation of gas-phase encapsulation of alkali metals by crown ethers provides a systematic model for understanding the direct influence of electronic properties of the enclosing cavity on selective electrostatic interactions. Recent theoretical studies of solvation effects (10) and solvent-induced preorganization (11) of ligands have been reported, and provide an interesting comparison of selective interactions of crown ethers with alkali metals to present gas-phase results.

Mass spectrometric techniques have been used previously to establish facile methods for measurements of thermodynamic stability constants of crown ether complexation with alkali metal ions (12). Also, selective complex formation has been observed by fast atom bombardment ionization of a solution of crown ethers and alkali metal halides (13). However, these studies report similar selectivities to solution results obtained by other techniques, since the measurements were directly based on abundances of desorbed ions from a *liquid* matrix. The host-guest chemistry of macrocycles *formed* and *evaluated* in a purely gas-phase environment was first reported for selective reactions of crown ethers and their perfluorinated analogs with molecular oxygen and fluoride ions (14). These studies suggested possible size selectivities between different substrates, and indicated that both topological and

chemical interactions affected the complexation reactions.

More recently, gas-phase reactions of crown ethers and alkali metal ions were examined by ligand exchange experiments (15). It was reported that alkali metal ions bound to a smaller crown ether exchanged to any crown ether with a larger cavity size. Additionally, crown ether dimers bound by alkali metal ions were generated only when the metal was not completely encapsulated by the ether. In this chapter, the kinetic method (16) is applied to the dissociation of complexes of ethers with two different alkali metals. This study qualitatively determines size selectivities of crown ethers in a solvent-free environment, and also evaluates pseudo-solvent effects on selectivities.

5.2 Alkali Metal/Ether Complex Ion Formation

Solutions of alkali metal halides (1M) and ethers (1M) in water were combined with an equal volume of the matrix, and approximately 0.5 µl was applied to the probe tip for analysis. Alkali metal/ether adduct ions were generated by the LSIMS

technique (17), and ions corresponding to alkali metal adducts of polyethers were also observed. A combination of solution and gas-phase reactions resulted in metal adduct ion formation in LSIMS mode (18). Table 5.1 provides a list of the ions observed from ionization of crown ethers (C), and alkali metal halides (MX). Generally, crown ether/alkali metal halide complexes of $(C + M.M.X)^+$ type were present in 1% abundance relative to the crown ether alkali metal adduct ion, $(C + M)^+$. Ionization of 21-crown-7 in an equimolar solution of potassium and rubidium chloride without O-benzyl glycerol was investigated to establish a basis for relative abundances of possible complex ions generated without the presence of a matrix which competes for alkali metal binding. Complex ions of $(C + M.M.X)^+$ or $(C_2 + M.M.X)^+$ were more abundant than ions of the type $(C + M + C)^+$, especially when metal ion diameters and cavity sizes were compatible, Table 5.2. Gas-phase selectivities of crown ethers for alkali metals were studied by formation of mixed crown ether/alkali metal halide complexes and subsequent CID experiments. The relative ratios of the fragment ions formed by CID of a selected complex are *not* dependent on the concentrations of the salts, matrix, and crown ethers in the source. This supports the idea that the selectivities measured by the kinetic method are not simply a reflection of concentration-dependent cluster formation, but instead represent actual competitive binding interactions.

Table 5.1 : Ion complexes observed from ionization of crown ethers (C) and alkali metal halides (MX).

$(C + M)^+$	crown ether/alkali metal
$(C + M + C)^+$	crown ether dimer/alkali metal
$(C + M.M.X)^+$	crown ether/alkali metal dimer
$(C + M.M'.X)^+$	crown ether/mixed-alkali metal dimer
$(C_2 + M.M'.X)^+$	crown ether dimer/mixed-alkali metal dimer

Table 5.2 : Ionic diameters and cavity sizes (7a).

Cation	Ionic Diameter, Å	Polyether Ring	Cavity Size, Å
Li^+	1.36	12-crown-4	1.2 - 1.5
Na^+	1.94	15-crown-5	1.7 - 2.2
K^+	2.66	18-crown-6	2.6 - 3.2
Rb^+	2.94	21-crown-7	3.4 - 4.3
Cs^+	3.34		

The kinetic method has been applied to other complex systems in which multiple binding interactions are operative (16c,d). These systems include deoxynucleosides (16c) and amino acids (16d). For these other studies and the present one, it is assumed that the frequency factors for cleavages of the multiple binding interactions are similar, and the multiple collision environment for adduct formation (i.e. in the ion source) approaches thermal equilibrium. Therefore, it is emphasized that the values reported in this study are estimates, and are derived from a method which involves several substantial approximations. However, based on the reproducibility of the dissociation spectra under a variety of conditions, the relative binding selectivities can be extracted from the data.

5.3 Results and Discussion :

Selectivities of cyclic ethers for alkali metal complexation in the gas phase have been examined by the application of the kinetic method. This method has been employed to quantitate relative gas-phase basicities using reactions that have similar frequency factors and negligible reverse activation barriers (16). These assumptions are not clearly delineated for crown ether/alkali metal ion complexes. However, under the experimental conditions of this study, the relative peak intensities of the product ions from collisional activation still give a qualitative measure of relative affinities of

crown ethers for alkali metal ions. Complexes of crown ethers with two different alkali metals were formed by the LSIMS technique. These complexes were isolated in the gas phase and activated by high energy collisions. Upon dissociation, mostly fragment ions such as crown ether/alkali metal adducts, i.e. $(C + M)^+$, were observed. This dissociation pattern suggests that complexes held only by electrostatic or van der Waals forces are formed, and was the basis for application of the kinetic method. Clearly, the two alkali metals in a complex such as $((18\text{-crown-6}) + K.Na.Cl)^+$ may qualitatively experience different interactions with the crown ether; however, alkali metal solvation effects are completely absent in these experiments, and most importantly, the dissociation patterns are independent of the initial metal salt concentrations used to form the complexes. Figure 5.1 illustrates the selectivity pattern for 18-crown-6 from dissociation of the $((18\text{-crown-6}) + K.Na.Cl)^+$ complex.

The process of alkali metal complexation by crown ethers has been described in solution by concepts of "preorganization" (2), "macrocyclic effect" (19), and "best fit" (6, 20). The results of collision induced dissociation experiments are partly described with these concepts in mind. The "macrocyclic effect" which accounts for the disparity of complexation selectivities and binding affinities between cyclic and acyclic ether analogs has been investigated in a parallel study by application of the

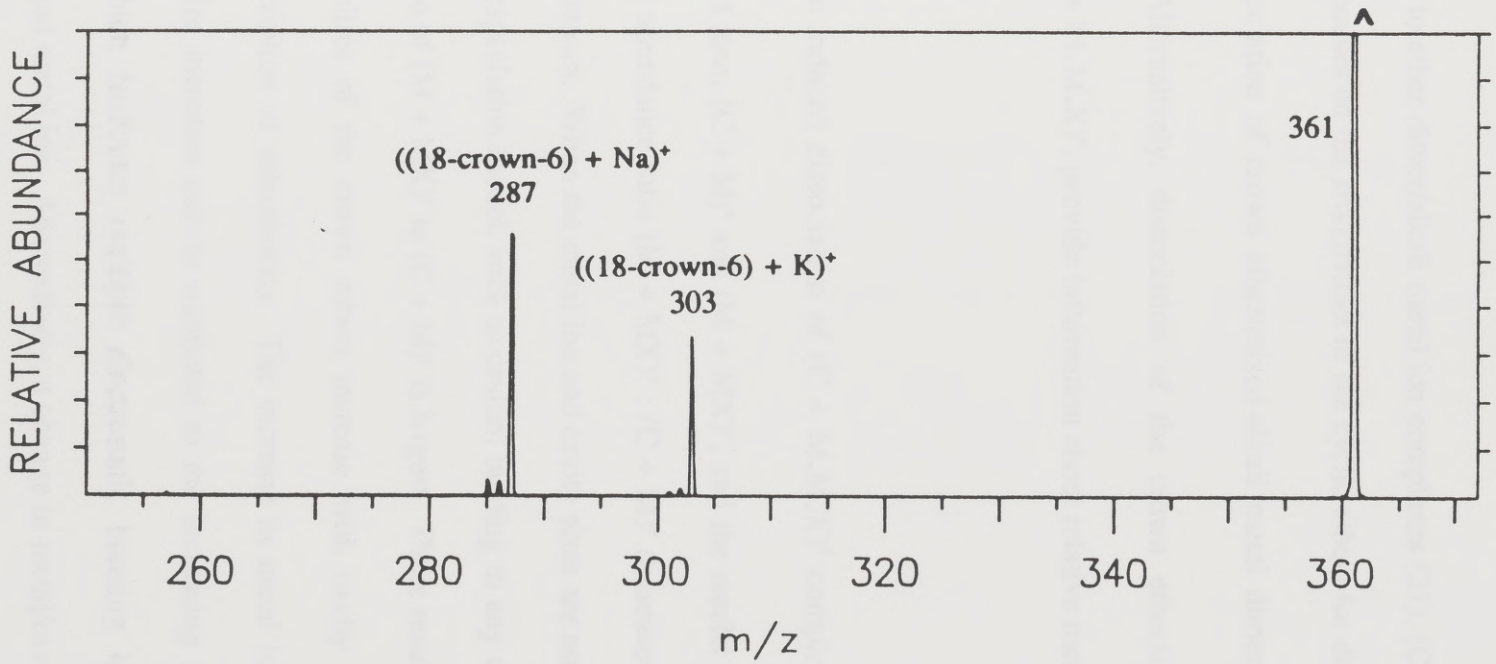

Figure 5.1 : CID mass spectrum of ((18-crown-6) + K.Na.Cl)$^+$ complex at 7 keV.

kinetic method to ether dimer/alkali metal ion complexes (21), $(C_1 + M + C_2)^+$. The present study focuses on the *selectivities* of the cyclic ethers for different alkali metal ions from dissociation of crown ether/mixed-alkali metal dimer, $(C + M.M'.X)^+$, complexes. Alternatively, dissociation of the crown ether/alkali metal dimer complexes, $(C + M.M.X)^+$, provide information about relative metal ion affinities vs. cavity sizes.

Collision induced dissociation of $(C + M.M.X)^+$ complexes generated two types of product ions, $(C + M)^+$ and $(M + MX)^+$, and the results are summarized in Table 5.3. The abundance ratio $(M + MX)^+ : (C + M)^+$ decreases as the size of the crown ether increases. When the metal ion and cavity sizes are not compatible based on a simple encapsulation model, such as cesium binding to any of the crown ethers studied, the ratio of $(M + MX)^+$ to $(C + M)^+$ is largest. These results indicate that the metal ion affinities of the crown ethers increase with cavity size, but give no qualitative description of selectivities. The increase in metal ion affinities as the crown cavity size increases can be attributed to the increasing number of oxygen donor sites which facilitates multiple electrostatic bonding interactions to the positively charged metal ion. Alternatively, a change in metal/cavity size ratio could also lead to a change in the frequency factor for the metal-ether dissociation reaction.

Table 5.3 : Percent abundances of crown ether/alkali metal complex to di-alkali metal halide product ions.

$$(C + M.M.X)^+ \xrightarrow{CID} (C + M)^+ + (M + MX)^+$$

Alkali Metal	12-Crown-4	15-Crown-5	18-Crown-6
	$(M+MX)^+ : (C+M)^+$	$(M+MX)^+ : (C+M)^+$	$(M+MX)^+ : (C+M)^+$
Li	5:95	1:99	1:99
K	84:16	36:64	21:79
Cs	94: 6	66:34	53:47

The ratios were calculated from CID spectra that contained an average of three to five accumulated scans.

For evaluation of selectivities, the crown ether/mixed-alkali metal dimers, (C + M.M'.X)$^+$, were examined. Collision induced dissociation of these complexes result predominantly in the formation of two fragments: (C + M)$^+$ and (C + M')$^+$. The results of this dimer study are shown in Table 5.4. Under the present experimental conditions, it is assumed that the crown ether/metal ion complex of greater abundance represents the preferred host-guest binding. Selectivities or preferences of crown ethers for alkali metals in the gas phase is perhaps best described by a "maximum contact point" (MCP) concept rather than the "best fit" (6,20) concept. The "best fit" is defined so that the predicted preference in *solution* will be for the cation whose ionic radius best matches the cavity sizes determined from atomic models and crystal structures. However, "Maximum Contact Point" predicts that in the absence of solvation effects, the preferences of the ethers will be for a slightly smaller cation because this achieves a higher electric field-dipole interaction within the cavity for a given conformation of the ether. The MCP concept emphasizes the importance of the structural flexibility of the crown ether and its ability to maximize crown-cation interactions, and this serves as a basis for derivation of energy-optimized structures of complexes in molecular mechanics studies (10). For example, in the present gas-phase studies the selectivity of 15-crown-5 for alkali metal ions is $Li^+ >> Na^+ > K^+ > Cs^+$. The trend for 18-crown-6 follows $Na^+ \geq K^+ > Li^+ > Rb^+ > Cs^+$, and the selectivity of 21-crown-7 is $K^+ > Na^+ \geq Rb^+ > Li^+ > Cs^+$.

Table 5.4 : Selectivities of crown ethers for alkali metal ion complexation based on product ion ratios of $(C + M)^+$ to $(C + M')^+$.

$$(C + M.M'.X)^+ \xrightarrow{CID} (C + M)^+ + (C + M')^+ + (M + M'X)^+$$

15-Crown-5 :							
Li > Na	Li > K		Li > Cs	Na > K		Na > Cs	K > Cs
100:10	100:2		100:1	100:10		100:3	100:15
18-Crown-6 :							
Na > Li	K > Li	Li > Rb	Li > Cs	Na > K		Na > Cs	K > Cs
100:40	100:40	100:40	100:10	100:60		100:3	100:15
21-Crown-7 :							
		Rb > Li	Li > Cs	K > Na	Na > Rb	Na > Cs	K > Rb
		100:50	100:60	100:85	100:80	100:85	100:60

The numbers were calculated from CID spectra that contained an average of three to five accumulated scans. Alkali metal halides of chlorides and iodides were examined in several cases, and the general selectivity trend remained the same.

Although the cavity size of 15-crown-5 fits optimally with the Na^+ ion, the preference of 15-crown-5 is for the Li^+ ion. The preferences of 15-crown-5 for Li^+, 18-crown-6 for Na^+, and 21-crown-7 for K^+ suggest that the selectivity of each cyclic ether is for the next smaller metal diameter than what is predicted by the concept "best fit".

In all cases, the formation of Cs^+/crown ether ions is disfavored following collisional activation of the crown ether/mixed alkali metal adducts. This is presumably because it is difficult for the macrocycle to maximize the Cs^+/crown interaction while also minimizing Cs^+/crown van der Waals repulsion (10). Even though cesium ion has a relatively good fit in the 21-crown-7 cavity, the repulsive terms remain significant. Moreover, crystal structures of crown ethers with various alkali metal ions have shown that the out-of-plane distance from the metal ion to the crown ether molecule increases as the size of the alkali metal ion increases (22). On the other hand, the retention of the lithium ion is favored only in the case of 15-crown-5, whereby lithium ion can simultaneously interact with all cavity oxygens. Lithium ion appears to be bound only relatively loosely to 18-crown-6 and 21-crown-7. For these latter two macrocycles, only the cesium ion interactions are even more strongly disfavored. Steric effects or electronic properties of enclosing cavity also influence structural preferences for complexation. Comparison of the binding of lithium and rubidium ions to 18-crown-6 and 21-crown-7 provides a unique example

of molecular size recognition; whereas 18-crown-6 selects lithium ion by a factor of two, the 21-crown-7 prefers rubidium ion.

From a comparison of the present gas-phase results to solution studies, the gas-phase selectivity trend of 15-crown-5 is most similar to the trend observed in less polar solvents where solvation effects are minimum (23a). It has been pointed out that metal ion solvation effects are a dominant contribution to observed equilibria in solution. For example, in propylene carbonate (23a), the log equilibrium constants measured by conductivity methods for complexation of 15-crown-5 were 4.26 for Li^+, 3.7 for Na^+, 3.41 for K^+, 3.04 for Rb^+, and 2.69 for Cs^+. In an aprotic solvent such as acetonitrile, the values (23b) measured were 3.60 for Li^+, 5.28 for Na^+, and 2.98 for K^+, all the latter values adhered to the "best fit" concept. In fact, in one comprehensive study (23c) of solvation effects on the interactions of Na^+ with 15-crown-5, the log equilibrium constants ranged from 1.49 in 20% methanol to 2.97 in 90% methanol. Numerous other solution studies report equilibrium constants that vary with the nature of the solvent, but few report results for the entire array of alkali metal ions. Moreover, theoretical treatment of 18-crown-6 predicts that the sodium ion complex is thermodynamically more stable than the potassium ion complex in the absence of solvation effects (10a,c). More comprehensive theoretical treatments of macrocyclic binding are not yet available, however, this first-case agreement with the

present gas-phase results suggests that the intrinsic selectivities of macrocycles can be evaluated *experimentally* by application of mass spectrometric techniques.

It was suggested earlier that structural factors such as "preorganization" of the precursor dimer ion may influence selectivities. For investigation of this hypothesis and to evaluate steric and/or pseudo-solvation effects on selectivities, complexes of $(C_2 + M.M'.X)^+$ were examined. In this context, "pseudo-solvation" refers to increased complexity of or increased steric/structural constraints within the selected adduct undergoing unimolecular dissociation. In solution solvation effects result from equilibrium intermolecular processes; in the gas-phase the observed changes in cation binding selectivity result from the intramolecular interaction within the different combination of cations, ethers, and associated anion. Because gas-phase selectivities from table 5.4 did not follow the best fit concept, dimer complexes of 15-crown-5 with sodium and lithium ions, 18-crown-6 with sodium and potassium ions, and 21-crown-7 with potassium and rubidium ions were generated as pseudo-solvated clusters and re-examined for this additional study. The complexes were produced from the same LSIMS mode described earlier, but this time the adducts formed with incorporation of two (rather than one) crown ether molecules were selected for CID experiments. The second crown ether molecule serves as a simple model of a competitive binding force, such as might be derived from a solvent shell. In all three

cases, selectivities of the crown ethers were shifted more toward the larger metal ion. For example, dissociation of $((18\text{-crown-6})_2 + K.Na.Cl)^+$ results in a fragment ion, $(18\text{-crown-6} + K)^+$ that is more abundant than $(18\text{-crown-6} + Na)^+$. Presumably the additional crown molecule effectively shields or solvates the salt molecule, and the resulting alterations in selectivity more closely mimic trends observed in solution. Likewise, these effects increase the selectivity of 15-crown-5 for sodium ions from 10% to 70% relative to lithium ions. The effects of the additional ether molecule also resulted in an equal preference for potassium and rubidium ions by 21-crown-7, as compared to the preferred selectivity for potassium ions by 21-crown-7 in the non-solvated case.

5.4 Conclusion :

The selectivities of crown ethers for alkali metal ion complexation have been studied in a solvent-free condition. The kinetic method was used to estimate relative affinities of crown ethers for alkali metal ions, and the resulting gas-phase selectivities followed the concept of "maximum contact point" for alkali metal ion complexation. The observed selectivities provide experimental evidence to support predictions of selectivities determined from theoretical studies done to account for solvent effects. Pseudo-solvation effects were examined by evaluating the selectivities of crown ether/alkali metal clusters. Dissociation of complexes of $(C_2 + M.M'.X)^+$ indicated that these pseudo-solvent effects shifted the selectivities in the direction of those observed in solution.

The structures of the complexes before dissociation may influence the product ion distribution, since it is possible that a crown ether molecule binds preferably to a metal where minimum conformational changes are required from the "preorganized" precursor ion. Currently, experiments are being designed to form these complexes from spatially separated targets by a divided-probe LSIMS experiment and also by laser desorption techniques. A comparison of CID results for complexes formed by different techniques may prove useful in understanding the effect of preorganization in CID results. Also, the structures of these complexes are presently being evaluated by application of molecular mechanics calculations.

References :

1. (a) Lehn, J.-M. *Angew. Chem. Int. Ed. Engl.* **1990**, *29*, 1304. (b) Vogtle, F.; Weber, E.; Eds.; Host Guest Complex Chemistry: Macrocycles, Springer-Verlag: New York, 1985.

2. (a) Cram, D. J. *Angew. Chem. Int. Ed. Engl.* **1986**, *25*, 1039. (b) Cram, D. J. *Science* **1988**, *240*, 760-767. (c) Reinhoudt, D. N.; Dijkstra, P. J. *Pure & Appl. Chem.* **1988**, *60*, 477.

3. Cram, D. J.; Ho, S. P. *J. Am. Chem. Soc.* **1986**, *108*, 2998.

4. Takemura, H.; Shinmyozu, T.; Inazu, T. *J. Am. Chem. Soc.* **1991**, *113*, 1323.

5. (a) Luboch, E.; Cygan, A.; Biernat, J. F. *Tetrahedron* **1991**, *47*, 4101. (b) Sakamoto, H.; Kimura, K.; Shono, T. *Anal. Chem.* **1987**, *59*, 1513.

6. (a) Izatt, R. M.; Bradshaw, J. S.; Nielsen, S. A.; Lamb, J. D.; Christensen, J. J. *Chem. Rev.* **1985**, *85*, 271. (b) Lamb, J. D.; Izatt, R. M.; Swain, C. S.; Christensen, J. J. *J. Am. Chem. Soc.* **1980**, *102*, 475. (c) Izatt, R. M.; Terry, R. E.; Nelson, D. P.; Chan, Y.; Eatough, D. J.; Bradshaw, J. S.; Hansen, L. D.; Christensen, J. J. *J. Am. Chem. Soc.* **1976**, *98*, 7626.

7. (a) Frensdorff, H. K. *J. Am. Chem. Soc.* **1971**, *93*, 600. (b) Michaux, G.; Reisse, J. *J. Am. Chem. Soc.* **1982**, *104*, 6895.

8. (a) Wu, G.; Jiang, W.; Lamb, J. D.; Bradshaw, J. S.; Izatt, R. M. *J. Am. Chem. Soc.* **1991**, *113*, 6538. (b) Schmidt, E.; Popov, A. I. *J. Am. Chem. Soc.* **1983**, *105*, 1873.

9. Liesegang, G. W.; Farrow, M. M.; Vazquez, F. A.; Purdie, N.; Eyring, E. M. *J. Am. Chem. Soc.* **1977**, *99*, 3240.

10. (a) Wipff, G.; Weiner, P.; Kollman, P. *J. Am. Chem. Soc.* **1982**, *104*, 3249. (b) Mazor, M. H.; McCammon, J. A.; Lybrand, T. P. *J. Am. Chem. Soc.* **1990**, *112*, 4411. (c) Yamabe, T.; Hori, K.; Fukui, K. *Tetrahedron*, **1979**, *35*, 1065. (d) Lybrand, T. P.; Kollman, P. A. *J. Chem. Phys.* **1985**, *83*, 2923.

11. Auffinger, P.; Wipff, G. *J. Am. Chem. Soc.* **1991**, *113*, 5976.

12. (a) Man, V. F.; Lin, J. D.; Cook, K. D. *J. Am. Chem. Soc.* **1985**, *107*, 4635. (b) Bonas, G.; Bosso, C.; Vignon, M. R. *J. Inclus. Phenomena and Mol. Recog. in Chem.* **1989**, *7*, 637.

13. (a) Johnstone, R. A. W.; Rose, M. E. *J. Chem. Soc., Chem. Commun.* **1983**,

1268. (b) Johnstone, R. A. W.; Lewis, I. A. S.; Rose, M. E. *Tetrahedron* **1983**, *39*, 1597.

14. (a) Brodbelt, J.; Maleknia, S.; Liou, C.; Lagow, R. *J. Am. Chem. Soc.* **1991**, *113*, 5913. (b) Brodbelt, J.; Maleknia, S.; Lagow, R.; Lin, T. Y. *J. Chem. Soc., Chem. Commun.*, in press.

15. Zhang, H.; Chu, I.; Leming, S.; Dearden, D. A. *J. Am. Chem. Soc.* **1991**, *113*, 7415.

16. (a) Cooks, R. G.; Kruger, T. L. *J. Am. Chem. Soc.* **1977**, *99*, 1279. (b) McLuckey, S. A.; Cameron, D.; Cooks, R. G. *J. Am. Chem. Soc.* **1981**, *103*, 1313. (c) Greco, F.; Liguori, A.; Sindona, G.; Uccella, N.; *J. Am. Chem. Soc.*, **1990**, *112*, 9092. (d) Bojesen, G.; *J. Am. Chem. Soc.* **1987**, *109*, 5557.

17. Sato, K.; Asada, T.; Ishihara, M.; Kunihiro, F.; Kammei, Y.; Kuboto, E.; Costello, C. E.; Martin, S. A.; Scoble, H. A.; Biemann, K. *Anal. Chem.* **1987**, *59*, 1652.

18. (a) Miller, J. M.; Balasanmugam, K.; Fulcher, A. *Org. Mass Spectrom.* **1989**, *24*, 497. (b) Michaud, D. P.; Kyranos, J. N.; Brennan, T. F.; Vouros, P. *Anal. Chem.* **1990**, *62*, 1069. (c) Honda, F.; Lancaster, G. M.; Fukuda, Y.; Rabalais,

J. W. *J. Chem. Phys.* **1978**, *69*, 4931.

19. Hancock, R. D.; McDougall, G. J. *J. Am. Chem. Soc.* **1980**, *102*, 6551.

20. (a) De Jong, F.; Reinhoudt, D. N. *Adv. in Phys. Org. Chem.* **1980**, *17*, 279-433. (b) Izatt, R. M.; Eatough, D. J.; Christensen, J. J. *Structure and Bonding* **1973**, *16*, 161-189.

21. Liou, C.; Brodbelt, J. *J. Am. Soc. Mass Spectrom.*, in press.

22. (a) Seiler, P.; Dobler, M.; Dunitz, J. D. *Acta Cryst.* **1974**, *B30*, 2744. (b) Dobler, M.; Phizackerley, R. P. *Acta Cryst.* **1974**, *B30*, 2746. (c) *ibid.*, 2748.

23. (a) Takeda, Y.; Yano, H.; Ishibashi, M.; Isozumi, H. *Bull. Chem. Soc. Jpn.* **1980**, *53*, 72. (b) Hopkins, H. P., Jr.; Norman, A. B.; *J. Phys. Chem.* **1980**, *84*, 309. (c) Dishong, D. M.; Gokel, G. W.; *J. Org. Chem.* **1982**, *47*, 147.

B. High Energy Fragmentation of Alkali Metal Ion Adducts of Crown Ethers

5.5 Introduction :

The results of Section A of this chapter show the gas-phase preferences of crown ethers for complexation of alkali metals. Other recent studies have shown that crown ethers exhibit size selectivity toward complexation of alkali metal ions (1). Crown ethers and their acyclic analogs bind alkali metal ions via multiple electrostatic interactions of the negatively polarized oxygen atoms with the positively charged metal ion (2). There is increasing interest in determination of the structures of these metal/crown complexes. Structural characterizations of uncomplexed crown ethers (radical molecular ions) by several different ionization and tandem mass spectrometric techniques have been reported in detail (3). Tandem mass spectrometric analyses of alkali metal adducts of several polyglycols have been reported (4), and related investigations of activation of other acyclic ethers by alternate ionization methods or under different collision conditions and instrument configurations have also been reported (5).

In this section of the chapter, the use of high energy collision induced dissociation (CID) of alkali metal ion adducts of crown ethers to evaluate the extent of skeletal cleavage of the ethers when bound to an alkali metal is described. The specific objectives of this study are to evaluate the effects of alkali metal ion binding of macrocycles on their high energy dissociation behavior, to compare the dissociation reactions of cyclic and acyclic ether complexes, and to determine if the crown ether complexes retain their cyclic nature upon high energy dissociation (as proposed in Chapter 4 for dissociation of protonated crown ethers (6)). Generally, alkali metal adducts of organic compounds form molecular ions with a localized charge, and high energy collisions are necessary to activate both electrostatic and covalent bond ruptures of these stable structures. In the specific case of macrocyclic ethers, upon low energy collisional activation in a triple quadrupole instrument, crown ether/alkali metal ion complexes dissociate by cleavage of only electrostatic bonds, resulting in bare alkali metal ions (1b). As shown by the present study, alkali metal ion adducts of ethers undergo extensive fragmentation at high collision energies, which presumably refelects that the metal ion may be sufficiently tightly bound to multiple oxygen sites that efficient internal energy redistribution within the adduct is permitted prior to dissociation. This is supported by the evidence that in many of the multi-step dissociation processes the alkali metal ion is retained by the crown ether fragment. Such behavior is not accessible under low energy (eV) collision conditions. Further

experiments with tetraethylene glycol dimethyl ether and hexaethylene glycol were performed to contrast the fragmentation behavior of acyclic ethers.

5.6 Results and Discussion :

Association with alkali metal ions dramatically alters the fragmentation behavior of cyclic and acyclic ethers compared to the simple protonated ethers (6). First, one abundant fragment ion formed from high energy collision induced dissociation of the alkali metal adducts is the bare alkali metal ion. Furthermore, as the size of the metal ion increases, the abundance of this fragment ion increases. This is rationalized based on the decreasing ionization energies of the larger alkali metals which makes them more favorable charge acceptors (7). Also, crystal structures of crown ether complexes with alkali metal ions have shown that as the size of the metal ion increases the metal-oxygen bond lengths increase and therefore the strengths of the binding interactions decrease (8). Second, fragment ions analogous to ones which predominate in the CID spectra of protonated crown ethers (i.e. $[M + H - (C_2H_4O)_n]^+$) are less abundant in the CID spectra of the alkali metal ion/crown ether adducts. This suggests that the attachment of an alkali metal ion instead of a proton results in very

different types of bond activations and binding interactions.

In general, the types of fragmentation behavior observed for the different alkali metal ion adducts are independent of the size of the alkali metal. Thus the major common features in the fragmentation patterns of the adducts will be described specifically for the potassium ion adducts, but will apply equally to the other alkali metal ion adducts. Mechanisms that are consistent with the observed data are proposed as means to rationalize the formation of many of the fragment ions; however, these mechanisms are offered only as a conceptual guide and have not been proven by labeling studies. Also, in several cases alternative fragmentation pathways are proposed to account for the products because of the absence of experimentally derived or theoretically determined thermochemical values needed to discount any mechanism. Many of the dissociation mechanisms shown result in product ions which are best rationalized as distonic radical cation structures. This is somewhat surprising considering that the initial alkali metal/ether adducts are closed-shell cations, but this is not unprecedented behavior for the high energy collisional activation of other alkali metal ion complexes (9). For example, it has been proposed for the alkali metal ion complexes of peptides that homolytic bond cleavages remote from the charge sites result in distonic radical cation structures (9).

Crown Ethers :

Collision induced dissociation results for the potassium ion adducts of 15-crown-5, 18-crown-6, and 21-crown-7 are summarized in Table 5.5. Similar fragmentation patterns are observed for the lithium, sodium, and cesium ion adducts. The CID spectrum of the potassium ion complex of 15-crown-5 is shown in Figure 5.2. The CID fragmentation behavior of this complex is representative of the other crown ether adducts. Many of the fragment ions are odd electron species (i.e. the ions at *m/z* 112, 140, 170, 200, and 228), such as acyclic, distonic radical cation structures. In order to rationalize many of the fragmentation routes observed and to develop some consistent guidelines for interpreting the CID spectra, we have designed mechanisms to account for many of the dissociations. These are shown in the Schemes. For clarity in the mechanisms, in most cases the alkali metal ion is shown attached to a single oxygen site, but it is understood that the alkali metal ion can be multiply-bound to several oxygens or localized at any of the different oxygen sites.

Scheme 5.1A shows one proposed fragmentation pathway beginning with ring opening by homolytic cleavage of the carbon-carbon bond adjacent to the charge site. The following step is transfer of a hydride to a carbon center with the loss of a CH_3-CH_2-$O(C_2H_4O)_n$-$CH_2^{\bullet}$ radical, when n = 0, 1, or 2. This mechanism may account for

Table 5.5 : CID spectra of potassium ion complexes of crown ethers[a].

	((15-crown-5)+K)$^+$ *m/z* 259		((18-crown-6)+K)$^+$ *m/z* 303		((21-crown-7)+ K)$^+$ *m/z* 347	
Neutral Loss, u	Fragment Ion *m/z*					
30		229 (3)		273 (4)		317 (5)
31		228 (16)		272 (3)		
46		213 (10)		257 (17)		301 (21)
59	A_0	200 (17)	A_0	244 (15)	A_0	288 (5)
						287 (6)
		185 (1)		229 (2)		273 (4)
76		183 (<1)		227 (4)		271 (12)
89	D	170 (9)		214 (10)		258 (13)
		169 (5)		213 (7)		257 (15)
	A_1	156 (6)	A_1	200 (7)	A_1	244 (3)
106		153 (10)		197 (18)		241 (26)
119	B_0	140 (50)	B_0	184 (56)	B_0	228 (31)
		127 (8)		169 (10)		213 (16)
		126 (2)				
	A_2	112 (23)	A_2	156 (51)	A_2	200 (39)
		111 (6)		154 (10)	B_1	184 (16)
	F	82 (4)	B_1	140 (13)	F	170 (19)
		69 (100)		127 (8)		169 (10)
			F	126 (8)	A_3	156 (27)
			A_3	112 (15)		153 (11)
				69 (100)		142 (11)
					B_2	140 (51)
						127 (18)
						126 (8)
					A_4	112 (22)
						111 (9)
						69 (100)

a The letters A to F represent fragmentation pathways shown in Scheme 5.1, and the subscripts denote the number of ethylene oxide units in conjunction with the mechanistic schemes. The numbers in parentheses represent the percent abundances.

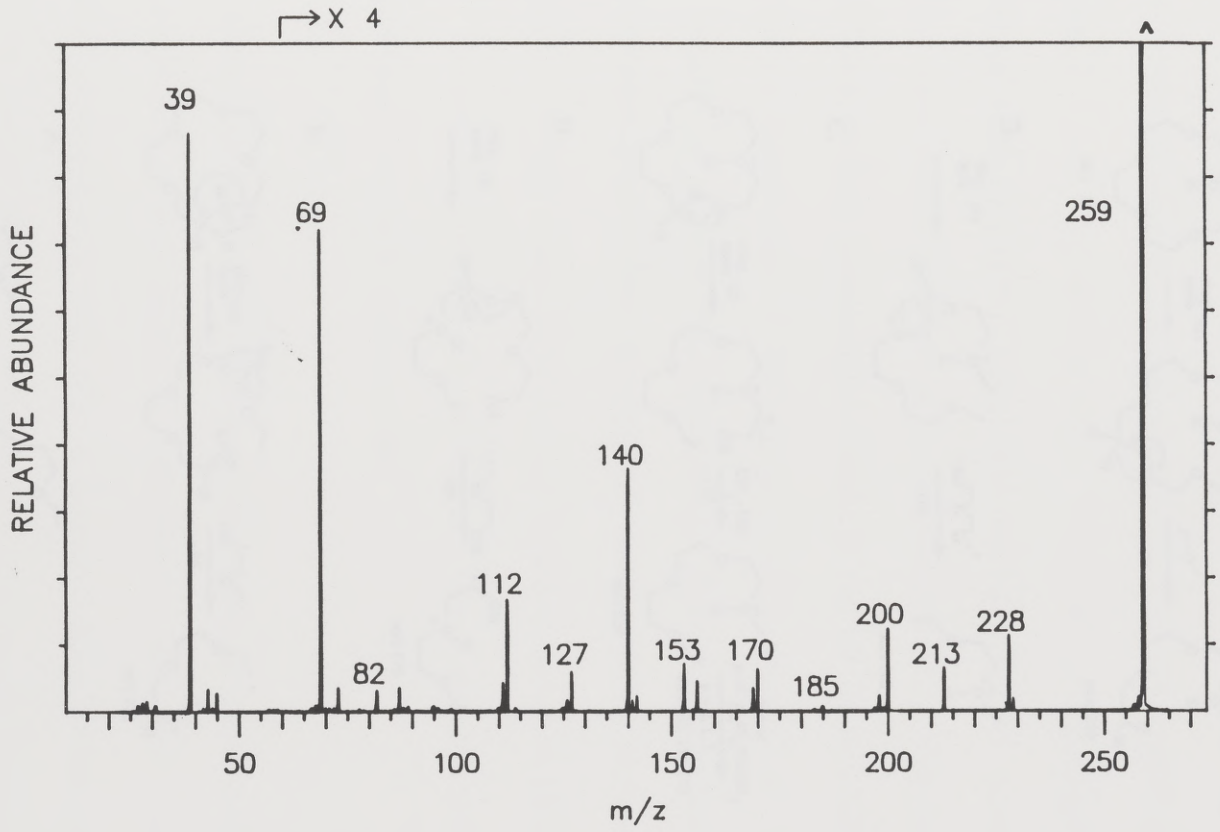

Figure 5.2 : CID mass spectrum of ((15-crown-5) + K)$^+$ ion complex at 7 keV recorded on JEOL HX110/HX110.

Scheme 5.1 : Mechanisms for dissociation pathways of alkali metal ion complexes of crown ethers.

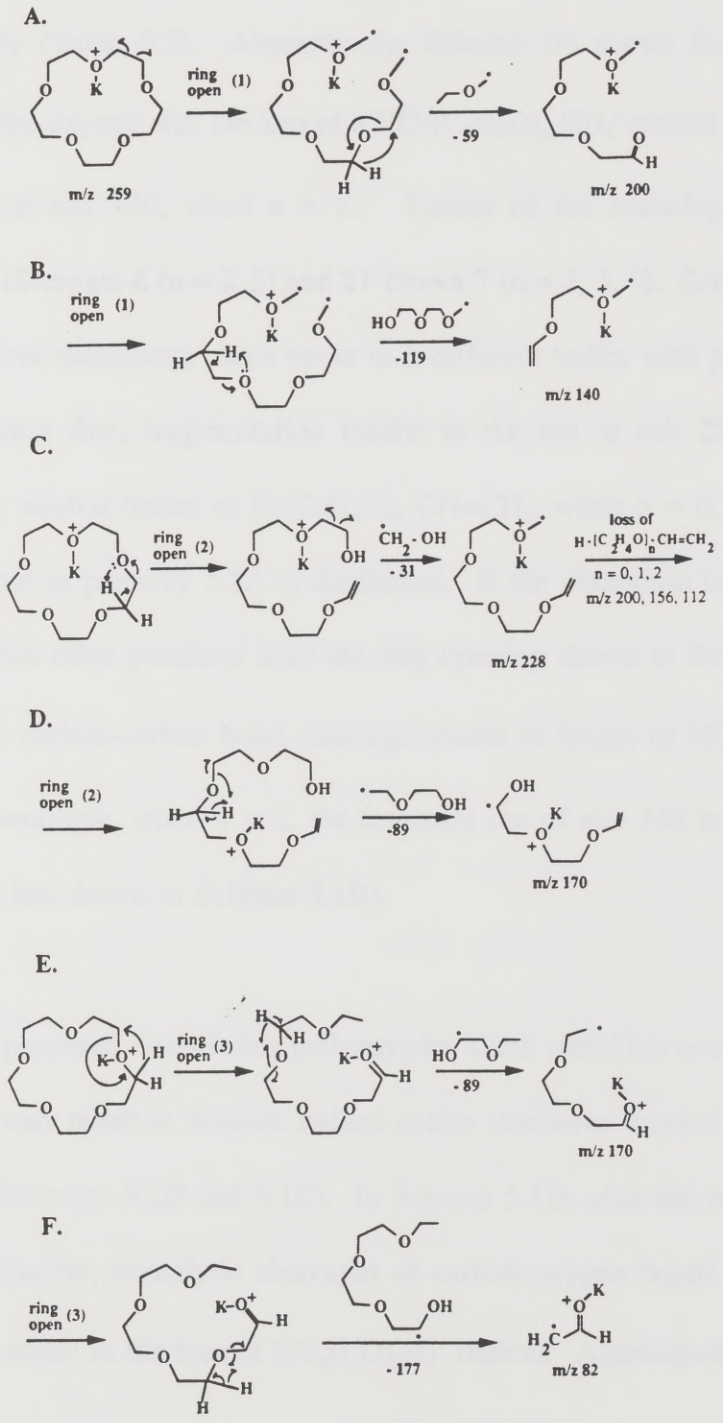

the fragment ions at *m/z* 200, 156, and 112, respectively. This pathway is also observed for 18-crown-6 and 21-crown-7 with maximum $(C_2H_4O)_n$ loss of n = 3 and 4, respectively (Table 5.5). Alternatively, Scheme 1B shows that if a proton is transfered to the oxygen site, the loss of a HO-$(C_2H_4O)_n$-$CH_2^{\bullet}$ radical results in a vinyl ether analog at *m/z* 140, when n = 2. Losses of the homologous radicals are observed for 18-crown-6 (n = 2, 3) and 21-crown-7 (n = 2, 3, 4). Scheme 5.1C shows that if the above elementary steps occur in a different order, with proton transfer to oxygen occuring first, fragmentation results in the ion at *m/z* 228. If this step isfollowed by neutral losses of H-$(C_2H_4O)_n$-$CH{=}CH_2$, when n = 0, 1, or 2, the ion series described in pathway 5.1A is duplicated. If the potassium ion is localized at any of the other ether positions after the ring opening shown in Scheme 5.1C, then the homolytic carbon-carbon bond cleavage results in losses of HO-$(C_2H_4O)_n$-$CH_2^{\bullet}$ radical. For example, when n = 2, the fragment ion of *m/z* 140 is formed (i.e. the same product ion shown in Scheme 5.1B).

Other proposed dissociation pathways for alkali metal ion complexes of crown ethers which may result in distonic radical cation structures involve the loss of 89 u as a radical (Schemes 5.1D and 5.1E). In Scheme 5.1D, after the ring opening step by a proton transfer, homolytic cleavages of carbon-oxygen bonds and a hydrogen atom transfer result in the loss of $[(C_2H_4O)_2H]^{\bullet}$ radical. Alternatively, Scheme 5.1E

shows the ring opens by a hydride transfer to a methylene carbon adjacent to the charge site, followed by a hydrogen atom transfer to an oxygen center remote from the charge site. However, if the hydrogen atom transfer step is at the oxygen adjacent to the charge site, the loss of 177 u as a radical may occur (Scheme 5.1F). Additionally, the fragment at *m/z* 82 may be formed by sequential or simultaneous cleavage of $2(C_2H_4O)$ from the final product ion (*m/z* 170) shown in Scheme 5.1E. Table 5.5 lists ions at *m/z* 82, 126, and 170 attributed to the loss of 177 u from the potassium adduct of 15-crown-5, 18-crown-6, and 21-crown-7, respectively.

The series of fragment ions attributed to neutral losses of ethanol (46 u), or di-(hydroxyethane)-ether (106 u) are rationalized by two processes which are similar in the transfer of a proton to the oxygen adjacent to the charge site. The following step occurs by the transfer of a hydride to the ethylene unit or the transfer of a proton to an oxygen, respectively. These processes lead to the formation of the fragment ions at *m/z* 213, and 153 for the ion complex of $((15\text{-crown-5}) + K)^+$. Additionally, the loss of ethanol may be accompanied by loss of ethylene oxide units, resulting in losses of $C_2H_5\text{-}(OC_2H_4)_n\text{-}OH$ species. This type of fragmentation accounts for the ion at *m/z* 169 when n = 1 for the potassium ion complex of 15-crown-5. Loss of other homologs were observed for 18-crown-6 (n = 0, 1, 2) and for 21-crown-7 (n = 0, 1, 2, 3).

The abundant fragment ion observed at *m/z* 69 in all of the crown ether spectra represents $(K + CH_2O)^+$, a species that appears in the CID spectra of every alkali metal ion/ether complex. Finally, the series of fragment ions which are observed at $(M + K - (C_2H_4O)_n)^+$ parallels the sequence of dissociation pathways observed for CID of protonated crown ethers (i.e. $[M+H-(C_2H_4O)_n]^+$). For the protonated crown ethers, the loss of two or more ethylene oxide units is more favorable than a single unit loss (6a), whereas for the metallated ethers, only the specific loss of $x(C_2H_4O)$ units occurs, where x is two less than the number of oxygens in the crown ether ring. For example, the ion of *m/z* 127 shown in Figure 5.2 for 15-crown-5 represents the elimination of three C_2H_4O units with net retention of the potassium ion.

Tetraethylene Glycol Dimethyl Ether (Tetraglyme) :

Tetraglyme is the acyclic analog of 15-crown-5, and none of the mechanisms rationalized for this ether is directly analogous to the mechanisms proposed for the crown ether adducts. Proposed fragmentation mechanisms for the potassium adduct of tetraglyme are shown in Scheme 5.2, and the CID spectrum is presented in Figure 5.3. Schemes 5.2A and 5.2B describe two possible pathways for the loss of methane combined either with sequential losses of ethylene oxide units, or as a single-step

Scheme 5.2 : Mechanisms of dissociation pathways of alkali metal ion complexes of tetraglyme.

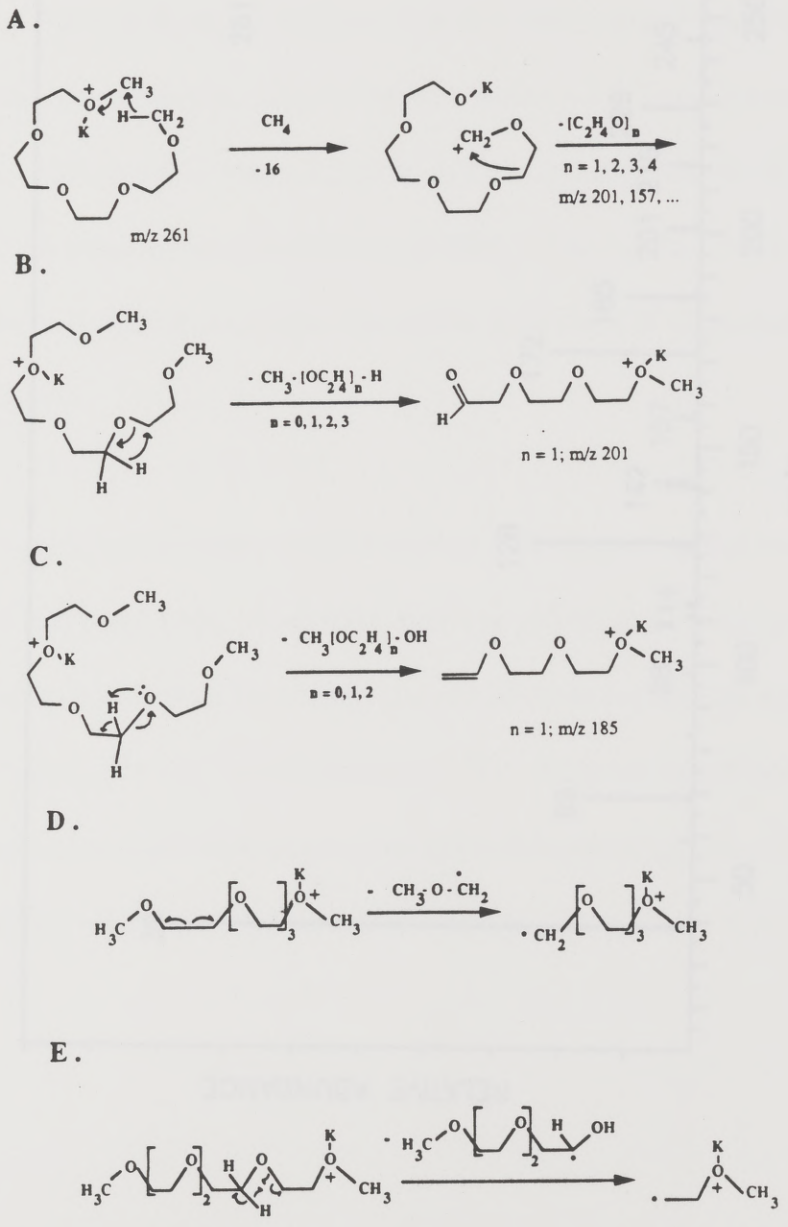

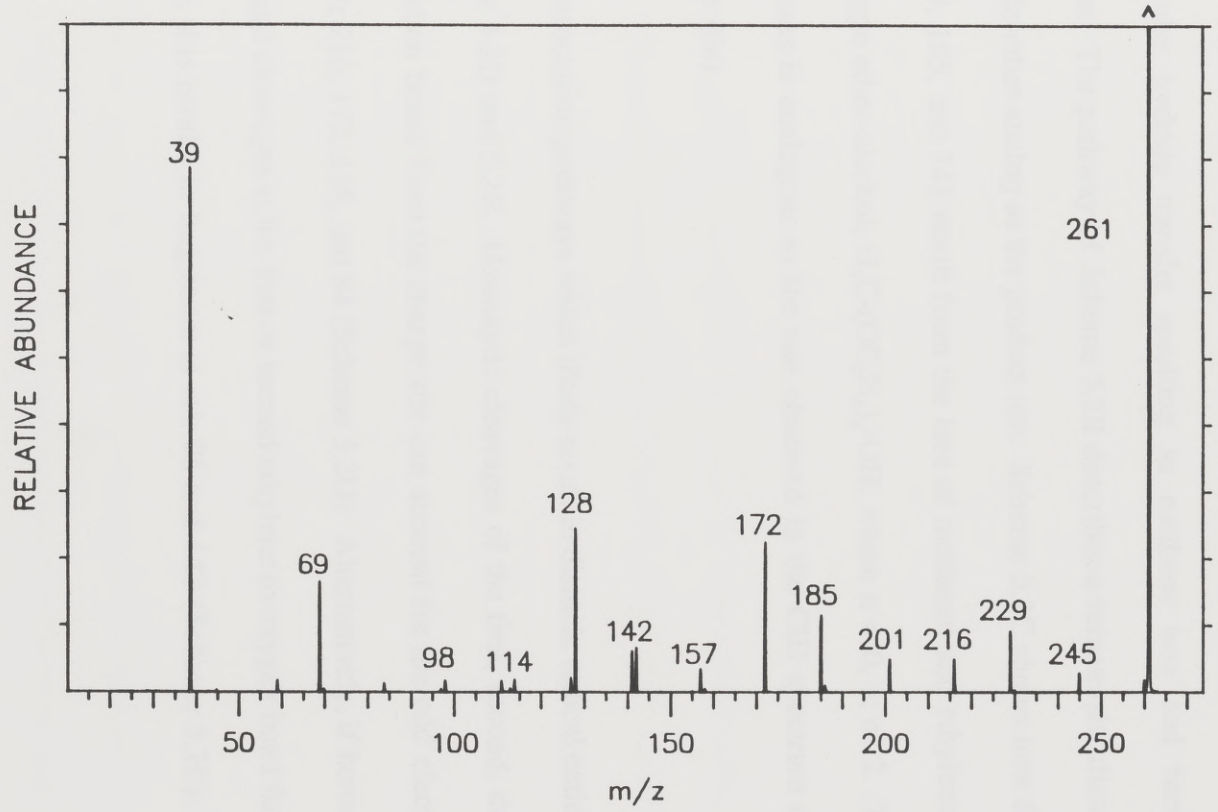

Figure 5.3 : CID mass spectrum of potassium ion adduct of tetraglyme at 7 keV recorded on JEOL HX110/HX110.

dissociation of H_3C-$(OC_2H_4)_n$-H, where n = 0, 1, 2, or 3. Both of these processes can account for the ions at *m/z* 245, 201, 157, and 113. Scheme 5.2A depicts an intramolecular hydride transfer resulting in methane loss and formation of a carbocation. The pathway of Scheme 5.2B describes a remote-site dissociation with an aldehyde-ether analog as the product ion. Scheme 5.2C shows how fragment ions at *m/z* 229, 185, and 141 result from the loss of methanol and ethylene oxide units, or as a single ether-alcohol, H_3C-$(OC_2H_4)_n$-OH, where n = 0, 1, or 2. This series of neutral losses is analogous to the one observed in the CID spectrum of protonated tetraglyme (6a).

Dissociation pathways which likely result in distonic radical cations are shown in Scheme 5.2D and 5.2E. Homolytic cleavages of the first, second, third, or fourth carbon-carbon bonds from the charge site can account for the odd electron fragment ions of *m/z* 216, 172, 128, and 84 (Scheme 5.2D). Alternatively, if homolytic carbon-oxygen bond cleavages at the first or second ethylene to oxygen bond from the charge site occur, this results in fragments at *m/z* 98 and 142 (Scheme 5.2E).

Hexaethylene Glycol :

Hexaethylene glycol is an acyclic analog of 21-crown-7. Few of the proposed mechanisms of dissociation parallel the ones suggested for the cyclic ethers. Scheme 5.3 shows proposed mechanisms of dissociation of the potassium ion adduct, and the CID spectrum is presented in Figure 5.4. Neutral losses of ethanol (Scheme 5.3A, 5.3B) or 1,2-dihydroxyethane (Scheme 5.3C) require the transfer of a hydride or a proton, respectively, in conjunction with heterolytic cleavages at the alpha bond positions of the carbon-oxygen bonds. Scheme 5.3A shows dissociation at the remote charge site where the loss of ethanol plus ethylene oxide units, C_2H_5-$(OC_2H_4)_n$-OH, where n = 0, 1, 2, 3, or 4, occurs. However, the metal ion may reside on any of the oxygen coordination sites, and then dissociation of the carbon-oxygen bonds occurs adjacent to the charge site (Scheme 5.3B). Fragmentation pathways shown in Scheme 5.3A or 5.3B account for the ion series at *m/z* 275, 231, 187, 143, and 99. The loss of 1,2-dihydroxyethane with up to three ethylene oxide units (Scheme 5.3C) produces the series at *m/z* 259, 215, 171, and 127. This series could also result from the loss of water from the potassiated molecule with successive losses of ethylene oxide units (Scheme 5.3D). Alternatively, the proton transfer may occur to any of the oxygen coordination sites, followed by heterolytic cleavages of carbon-oxygen bonds. This would also result in net loss of HO-$(C_2H_4O)_n$-H, where n = 0, 1, 2, or 3.

Scheme 5.3 : Mechanisms of dissociation pathways for alkali metal ion complexes of hexaethylene glycol.

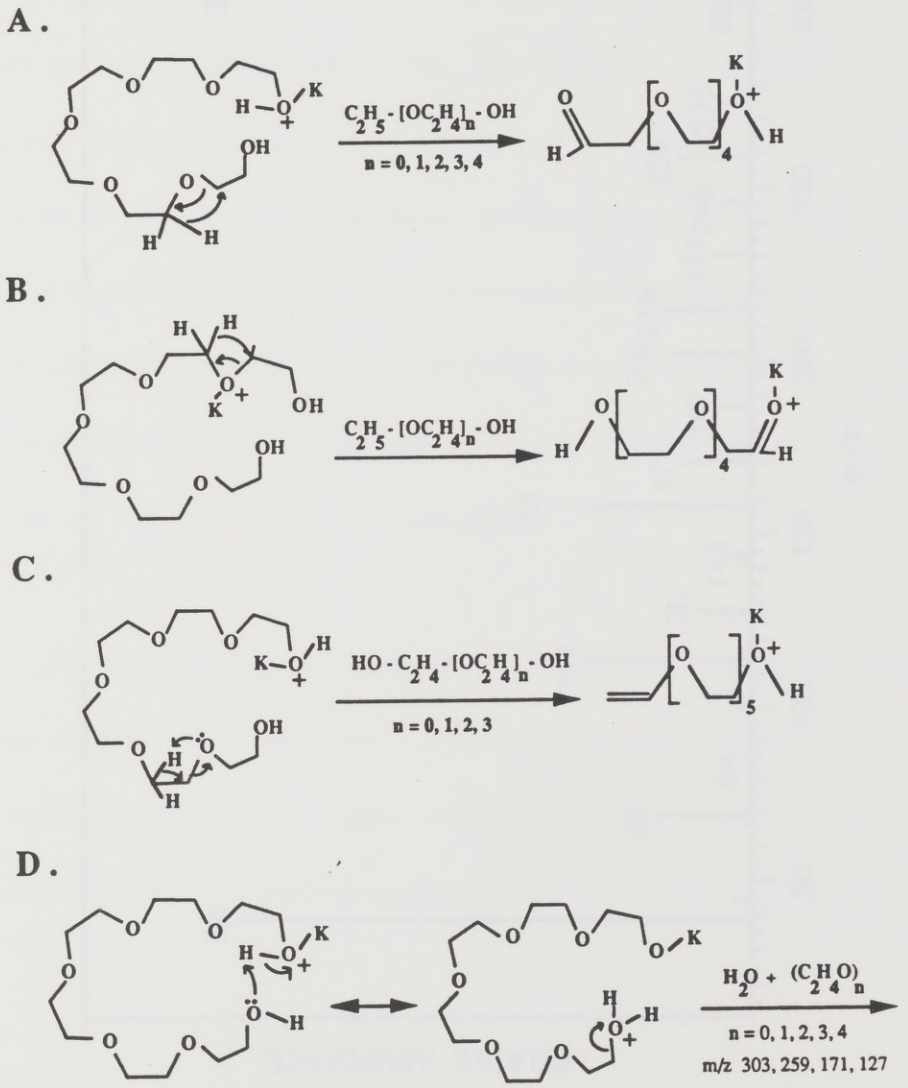

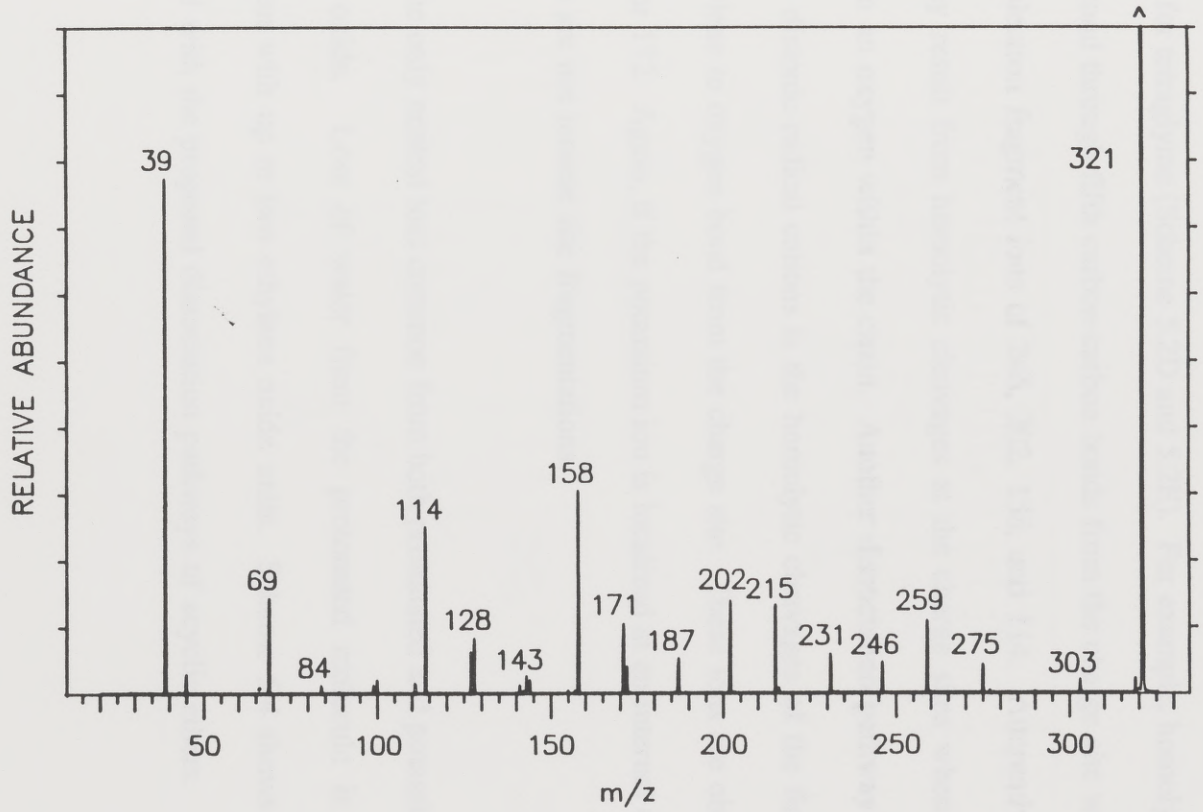

Figure 5.4 : CID mass spectrum of potassium ion adduct of hexaethylene glycol at 7 keV recorded on JEOL HX110/HX110.

Several proposed dissociation pathways which result in radical cations are assigned distonic product ion structures, and these processes are similar to the ones observed for tetraglyme (Scheme 5.2D and 5.2E). For example, homolytic cleavages of the second through fifth carbon-carbon bonds from the charge site would produce the odd electron fragment ions of 246, 202, 158, and 114. Alternatively, this ion series may result from homolytic cleavages at the charge sites when the metal is located on an oxygen within the chain. Another dissociation pathway which likely results in distonic radical cations is the homolytic cleavages of the first, second or third ethylene to oxygen bond from the charge site. These ions are observed at *m/z* 84, 128, or 172. Again, if the potassium ion is localized at an internal oxygen, these cleavages are not remote site fragmentations.

The only neutral loss common from both protonated and potassiated glycol is ethylene oxide. Loss of water from the protonated molecule is observed in conjunction with up to two ethylene oxide units. Scheme 5.4 shows product ions associated with the proposed dissociation pathways of acyclic ethers.

Scheme 5.4 : Product ion branching of acyclic ethers.[a]

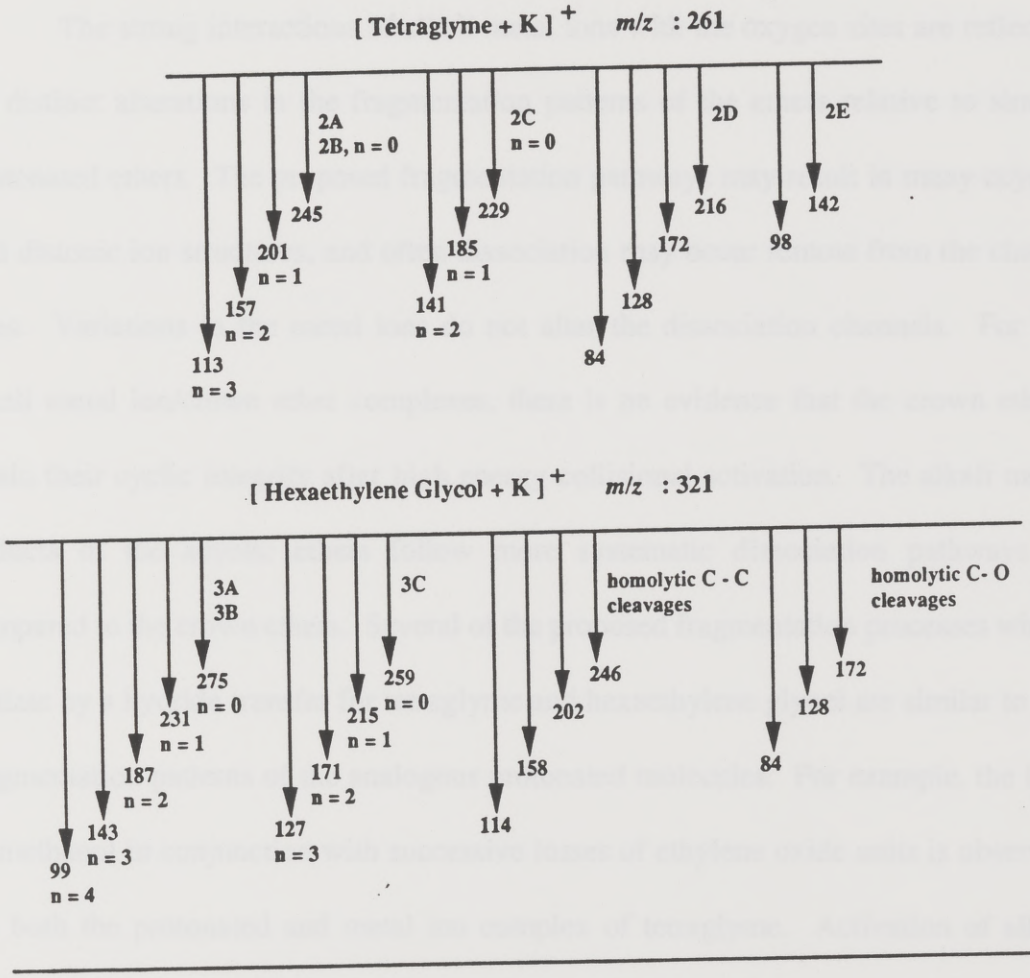

[a] Dissociation pathways of A to E are described in Schemes 5.2 and 5.3. The n = 1, 2, ... designates the number of C_2H_4O units in conjunction with the dissociation.

5.7 Conclusion :

The strong interactions of alkali metal ions with the oxygen sites are reflected by distinct alterations in the fragmentation patterns of the ethers relative to simple protonated ethers. The proposed fragmentation pathways may result in many acyclic and distonic ion structures, and often dissociation may occur remote from the charge sites. Variations in the metal ions do not alter the dissociation channels. For the alkali metal ion/crown ether complexes, there is no evidence that the crown ethers retain their cyclic integrity after high energy collisional activation. The alkali metal adducts of the acyclic ethers follow more systematic dissociation pathways as compared to the crown ethers. Several of the proposed fragmentation processes which initiate by a hydride transfer for tetraglyme and hexaethylene glycol are similar to the fragmentation patterns of the analogous protonated molecules. For example, the loss of methanol in conjunction with successive losses of ethylene oxide units is observed for both the protonated and metal ion complex of tetraglyme. Activation of alkali metal ion adducts promotes new dissociation pathways for the ethers which may resulted in odd electron, acyclic structures. These proposed processes include homolytic cleavages of the carbon-carbon and carbon-oxygen bonds for all the ethers, pathways which are not observed in the CID spectra of the corresponding protonated

molecules. The dissociation routes of crown ethers are dominated by odd electron neutral losses, whereas even electron neutral losses are more favorable processes for acyclic ethers.

For protonated ethers, both high and low energy activation predominantly result in cleavage of the carbon-oxygen ether linkages. In contrast, alkali metal ion adducts may also dissociate by pathways involving carbon-carbon bond cleavage at high collision energies.

References :

1. (a) S. Maleknia, J. Brodbelt, *J. Am. Chem. Soc.*, in press. (b) C.-C. Liou, J. Brodbelt *J. Am. Soc. Mass Spectrom.*, in press. (c) H. Zhang, I.-H. Chu, S. Leming, D. V. Dearden, *J. Am. Chem. Soc.* **113**, 7415 (1991).

2. (a) C. J. Pedersen, *J. Am. Chem. Soc.* **89**, 7017 (1967). (b) F. Vogtle, E. Weber, *Host Guest Complex Chemistry - Macrocycles*, Springer-Verlag (1985).

3. (a) B. Kiremire, R. Seraglia, P. Traldi, *Rapid Commun. Mass Spectrom.* **5**, 543 (1991). (b) Y. C. Lee, A. I. Popov, J. Allison, *Int. J. Mass Spectrom. Ion Phys.* **51**, 267 (1983). (c) D. A. Jaeger, R. R. Whitney, *J. Org. Chem.* **1**, 92 (1975).

4. (a) R. P. Lattimer, *Proc. 39th ASMS Conf. on Mass Spectrom. and Allied Topics,* Nashville, TN, May 19-24, 1991, pp. 1263-1264. (b) R. P. Lattimer, H. Münster, H. Budzikiewicz, *Int. J. Mass Spectrom. Ion Processes* **90**, 119 (1989).

5. (a) S. L. Cohen, B. T. Chait, *Proc. 39th ASMS Conf. on Mass Spectrom. and Allied Topics*, Nashville, TN, May 19-24, 1991, pp. 1269-1270. (b) J. H.

Callahan, M. M. Ross, V. H. Wysocki, F. L. King, *Proc. 39th ASMS Conf. on Mass Spectrom. and Allied Topics*, Nashville, TN, May 19-24, 1991, pp. 841-842. (c) V. F. Man, J. D. Lin, K. D. Cook, *J. Am. Chem. Soc.* **107**, 4635 (1985). (d) K. W. S. Chan, K. D. Cook, *Macromolecules* **16**, 1736 (1983).

6. (a) Partial data from Chapter 4 is published as : S. Maleknia, C.-C. Liou, J. Brodbelt, *Org. Mass Spectrom.* **26**, 997 (1991). (b) O. Curcuruto, P. Traldi, G. Moneti, L. Corda, G. Podda, *Org. Mass Spectrom.* **26**, 713 (1991).

7. F. W. Röllgen, U. Giessmann, F. Borchers, K. Levsen, *Org. Mass Spectrom.* **8**, 459 (1978).

8. M. Dobler, R. P. Phizackerley, *Acta Cryst.* B**30**, 2746 (1974).

9. (a) J. Adams, M. L. Gross, *Anal. Chem.* **59**, 1576 (1987). (b) L. M. Teesch, J. Adams, *J. Am. Chem. Soc.* **112**, 4110 (1990). (c) J. A. Leary, Z. Zhou, S. A. Ogden, T. D. Williams, *J. Am. Soc. Mass Spectrom.* **1**, 473 (1990). (d) R. P. Grese, M. L. Gross, *J. Am. Chem. Soc.* **112**, 5098 (1990). (e) L. M. Mallis, D. H. Russell, *Anal. Chem.* **58**, 1076 (1986). (f) S. Hammerum, *Mass Spectrom. Rev.* **7**, 123 (1988).

Chapter 6 - Cavity Size Dependent Dissociation of Crown Ether/Amine Ion Complexes

6.1 Introduction :

The specific site recognition and complexation between macrocycles and substrates is a complex process which requires size and conformational compatibilities of the host and guest molecules (1). Molecular recognition of amines by macrocycles has been demonstrated and is of great interest because of its similarity to important biological processes, such as transport of amino acids and drugs across membranes or enzyme/substrate interactions (1,2). Structural characterizations of several amine/macrocycle complexes have revealed the importance of multiple hydrogen bonding interactions (1,2). The chemical consequences of these interactions have been demonstrated in the case of the enhanced rates of intramolecular thiolysis when glycyl-glycine *p*-nitrophenyl ester ions form complexes to macrocycles (3). There have been few reports of the use of model compounds for formation of complexes by hydrogen-bonding in non-polar solvents, however, gas-phase reactions provide optimum conditions for the evaluation of the *intrinsic* role of hydrogen-bonding effects and other electrostatic interactions in molecular recognition processes. For

example, Section A of Chapter 5 discusses the mass spectrometric results of the selectivity of crown ethers for alkali metal ion complexation in the gas phase (4).

Crown ether macrocycles serve as simple receptor models and are well-suited as hosts because of their conformational flexibility and the presence of multiple binding sites. These characteristics provide capabilities for metal ion encapsulation (1a,5) and the formation of inclusion complexes with protonated amines (2) in solution. Structural characterizations of crown ether/amine ion complexes have been investigated by crystallographic techniques (6) and molecular modeling studies (7). These results suggest that the stability and formation of these types of host/guest complexes are greatly influenced by hydrogen bonding interactions. In the gas phase, the hydrogen bonds between the amine donors and oxygen receptor sites dominate the stability of crown/amine inclusion complexes. The capability for hydrogen-bond formation also determines the gas phase basicities (8) of polyethers, and it has been shown that primary amines form the most stable complexes with crown ethers. This higher order effect of multiple hydrogen bonding increases with the increasing cavity size of crown ethers, and an association energy of 46 kcal/mol was estimated for the ion complex of 18-crown-6 with c-$C_6H_{11}NH_3^+$ based on proton-transfer experiments in a high pressure mass spectrometer (9).

The goal of the study described in this chapter is to evaluate the extent of gas-phase intramolecular interactions of primary amines with crown ethers of different cavity sizes by tandem mass spectrometry. Three types of experiments were performed to address this question. First, the extent of multiple hydrogen bonding interactions based on increasing cavity sizes is evaluated from metastable dissociation (10) studies of the complexes. Second, collision induced dissociation (CID) (11) results of the amine ion complexes are compared to CID spectra of simple protonated crown ethers to determine new dissociation reactions which arise from intramolecular interactions of the amine sites and ethers. Third, complexes with hydrazines are examined with the aim of comparing preferential covalent bond activation of nitrogen-nitrogen or nitrogen-sulfur bonds within the guest ligand that have bond strengths similar to the association energies of the multiple hydrogen-bonding interactions which bind the hydrazine guest to the macrocyclic host. Finally, ion complexes of hexaethylene glycol, an acyclic analog of 21-crown-7, are examined to account for the differences in complexation between cyclic and acyclic ethers, a phenomenon termed the "macrocyclic effect" (2a,5).

6.2 Results and Discussion :

Two types of primary amine substrates were selected to examine their intramolecular interactions with crown ethers. First, guest molecules, such as the ammonium or hydrazinium ion (Table 6.1), that can be *completely* encapsulated by the cavity of some of the ether molecules were chosen to qualitatively evaluate differences in complexation behavior due to cavity size effects based on changes in fragmentation behavior of the complexes. The second type of guest molecules, such as methyl- and tosyl-hydrazines, can *partly* fit within the macrocycles. For these latter types of complexes, crystal structures show the geometry of the guest molecules as normal to the hosts (6). The intramolecular dissociation reactions that are promoted because of the specific site binding of crown ethers may also be related to the cavity size effect of the hosts. When the crown ether molecule anchors one portion of the guest molecule (i.e. the amine portion), the dissociation reactions from the unbound side of the guest may be altered relative to an uncomplexed guest ion. Hydrogen-bonding interactions in these types of host/guest complexes may be strong enough to withstand activation leading to covalent bond cleavages in the guest molecule. Such behavior is not unprecedented. For example, in solution, covalent bond dissociation catalyzed by intramolecular reactions of hydrogen-bonded host/guest complexes have been demonstrated in the case of thiolysis of *p*-nitrophenyl (3). In

Table 6.1 : Relative Cavity Sizes of Crown Ethers (5).

Polyether Ring	Cavity Size, Å
12-crown-4	1.2 - 1.5
15-crown-5	1.7 - 2.2
18-crown-6	2.6 - 3.2
21-crown-7	3.4 - 4.3

the gas phase, dissociation of host/guest complexes, primarily stabilized by multiple hydrogen-bonding interactions, should provide information about the hydrogen-bonding energies relative to other covalvent bonds of the complex (N-N, C-C, etc.).

Metastable Dissociation :

To determine the relative binding strengths and stabilities of polyether ion complexes of ammonium and methylammonium for this gas-phase study, the abundances of relevant metastable ions (10) were examined. For example, it was assumed that all the ammonium ion/ether complexes formed in the ion source have similar internal energy distributions, and thus the least stable complexes dissociate by elimination of ammonia (i.e. cleavage of all hydrogen bonds) to the greatest extent. This systematic examination of metastable ion abundances provides a qualitative estimate of the effects of cavity size on complexation in the gas phase.

Crown Ether / NH_4^+ Complexes : The metastable results for the ammonia from each mass-selected (ether + NH_4)$^+$ complex are expressed in Table 6.2 as the area ratio of the metastable ion for (ether + H)$^+$ from loss of NH_3 to the intact precursor ion complex of (ether + NH_4)$^+$. The metastable dissociation spectrum for

Table 6.2 : Metastable dissociation results for ammonium and methylammonium ion complexes.[a]

Polyether Hosts	% Area $\frac{(ether + H)^+}{(ether + NH_4)^+}$	% Area $\frac{(ether + H)^+}{(ether + CH_3\text{-}NH_3)^+}$
21-crown-7	0.37 ± 0.01	0.07 ± 0.01
18-crown-6	0.84 ± 0.03	0.16 ± 0.01
15-crown-5	1.40 ± 0.03	0.29 ± 0.01
Hexaethylene Glycol	4.01 ± 0.03	1.72 ± 0.03

[a] Standard deviations were calculated from three to five experiments that contained an average of 10-15 summed scans.

the ion complex of (18-crown-6 + NH_4)$^+$ is represented in Figure 6.1. In the absence of solvation effects, the binding preference of crown ethers for the ammonium ion is 21-crown-7 > 18-crown-6 > 15-crown-5 > hexaethylene glycol. As the cavity size of the cyclic ethers increases, neutral ammonia dissociation from the ion complexes decreases. This indicates that the larger cavity sizes promote formation of especially stable complexes. Also, the maximum extent of ammonia loss is observed for hexaethylene glycol, a result which suggests that preorganization of the host assists in the formation of stable complexes.

Comparison of the cavity sizes and the diameter of the ammonium ion of 2.86 Å suggests that best hydrogen-bonding interactions are possible with 18-crown-6 or 21-crown-7. Complexes of ammonium ion with 21-crown-7, 18-crown-6 or 15-crown-5 have been isolated in aqueous solution, however, under identical reaction conditions, complexes of ammonium with 12-crown-4 were not formed (12). The formation constants measured by calorimetric titration in water showed the stability of the 15-crown-5 ion complex favored over the 18-crown-6 with log K values of 1.71 and 1.23 (13), respectively. In contrast, the order of binding constants measured potentiometrically in anhydrous methanol for ammonium ion is 18-crown-6 > 21-crown-7 > 15-crown-5 > 12-crown-4 (14). These data show the importance of solvation energy effects which direct the complexation equilibrium. In addition,

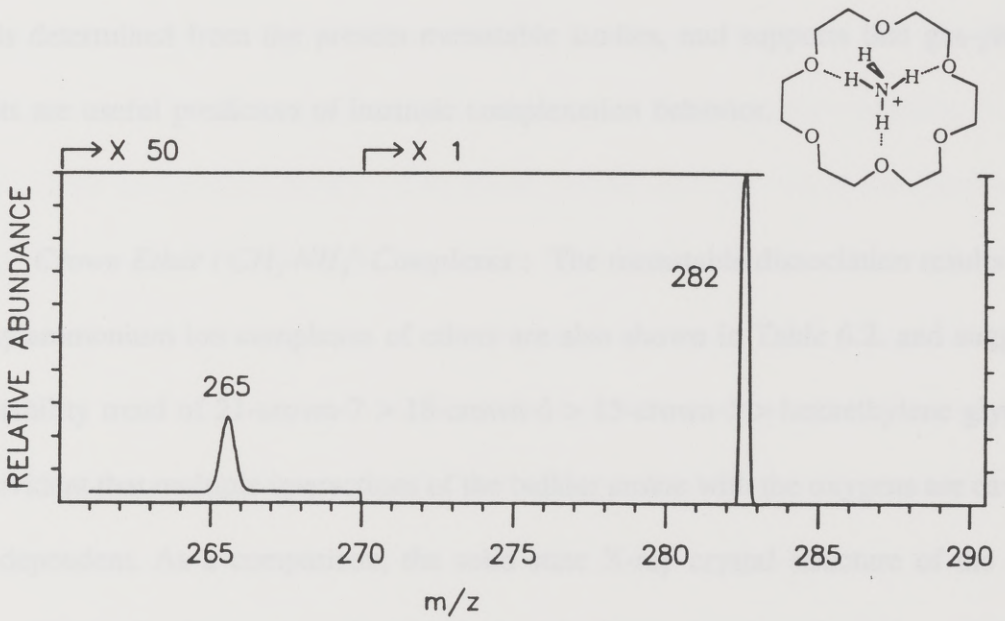

Figure 6.1 : Metastable dissociation mass spectrum of 18-crown-6/ammonium ion complex recorded on JEOL HX110/HX110.

molecular mechanics data have shown that hydrogen-bonding interactions increase with larger cavity sizes. For the 18-crown-6 complex, the possibility of three hydrogen bonds exists, whereas the cavity of 15-crown-5 accomodates only two hydrogen bonds. In the case of 12-crown-4, no favorable hydrogen-bonding interactions are predicted (7a). The latter theoretical results parallel the complexation trends determined from the present metastable studies, and supports that gas-phase results are useful predictors of intrinsic complexation behavior.

Crown Ether / CH_3-NH_3^+ Complexes : The metastable dissociation results for methylammonium ion complexes of ethers are also shown in Table 6.2, and suggest the stability trend of 21-crown-7 > 18-crown-6 > 15-crown-5 > hexaethylene glycol. It is evident that multiple interactions of the bulkier amine with the oxygens are cavity size dependent. As a comparison, the solid state X-ray crystal structure of the 18-crown-6/methylamine ion complex shows three hydrogen bonds to three ring oxygens (6a). The same degree of interaction is possible with 21-crown-7 but not with 15-crown-5 because of its smaller cavity size, as was noted for ammonium ion complexation.

The relative ion abundances for metastable dissociation of ammonium or methylammonium ion complexes, listed in Table 6.2, show that effective binding of

the ions increases with increasing cavity sizes. Moreover, the relative binding of methylammonium to ethers is significantly different from ammonium binding in the gas phase. For example, methylammonium binds more effectively to 21-crown-7 than ammonium, although the cavity of the ether provides the same number of hydrogen-bonding interactions for either amine. The difference in binding of ammonia and methylamine likely reflects differences in the thermodynamics of gas-phase complexation, as further supported by comparison of the gas-phase basicities of the crown hosts and amine guests. Gas-phase proton affinity values for ammonia, methylamine, and 18-crown-6 are 204, 214.1, and 230.0 kcal/mole, respectively (15a) Because of its higher basicity, methylamine participates in hydrogen-bonding interactions to the macrocycles which are stronger than ones possible for ammonia binding to the host. Consequently, the less basic ammonium guest is more likely to undergo intramolecular proton transfer to the more basic polyether host, rather than compete effectively for the retention of the proton and remain in a stabilized complex. Experimentally, this is supported by the more abundant metastable decay process for the ammonium ion complexes. Thus the differences in the ratios shown in Table 6.2 parallel the expected relative exothermicities of intramolecular proton transfer between the host and guest molecules.

As a comparison to solution results, in anhydrous methanol (16), 18-crown-6

shows equal binding preference for ammonium and methylammonium, whereas in chloroform (17a) or water (17b) 18-crown-6 binds more effectively to the ammonium ion than methylammonium. However, as shown from the metastable studies in the absence of solvation effects, this preference changes and the methylammonium ion shows stronger hydrogen binding interactions than the ammonium ion in the gas phase. This is not surprising because the basicities of ammonia and methylamine differ by < 2 kcal/mole in solution (15b), (as compared to the 10 kcal/mole difference in gas-phase basicities of the amines), and thus solvation plays a relatively significant role in influencing binding affinities.

Structural Characterization by Collision Induced Dissociation :

Collision induced dissociation of the amine ion complexes at high and low collision energies was used for structure elucidation and to probe the nature of the multiple interactions between the amines and polyethers. Two distinct types of fragmentation pathways are observed after high and low energy collisions. At high collision energies with the collision cell voltage floated at 3 kV (7 keV collision), the center-of-mass kinetic energy of the complexes of the polyethers with ammonium, methylammonium, or hydrazinium ion was between 40 to 60 eV. As shown in the

following section, this magnitude of kinetic energy, after partial conversion to internal energy, is sufficient to induce extensive rupture of the macrocyclic structure. At the lower collision energy (collision cell voltage of 9.6 kV, 0.4 keV collisions), less than 5 eV of internal energy is available for deposition into the ion complexes. This magnitude of energy predominantly causes the loss of a neutral amine guest after intramolecular proton transfer from the guest to the host, in combination with systematic cleavages of the resulting protonated macrocycle.

Low Energy CID :

Ion complexes incorporating ammonium, methylammonium, or hydrazinium ions show similar types of fragmentation pathways, and only dissociation reactions of ammonium ion complexes are discussed in detail.

Low energy collisions occured at the laboratory energy of 0.4 keV. As an example, Figure 6.2A shows the CID spectrum of the ammonium ion adduct of 18-crown-6. The series of fragment ions observed at *m/z* 265, 221, 177, and 133 corresponds to the losses of 0, 1, 2, or 3 ethylene oxide units in conjunction with elimination of ammonia. At this low collision energy, cleavages of carbon-oxygen

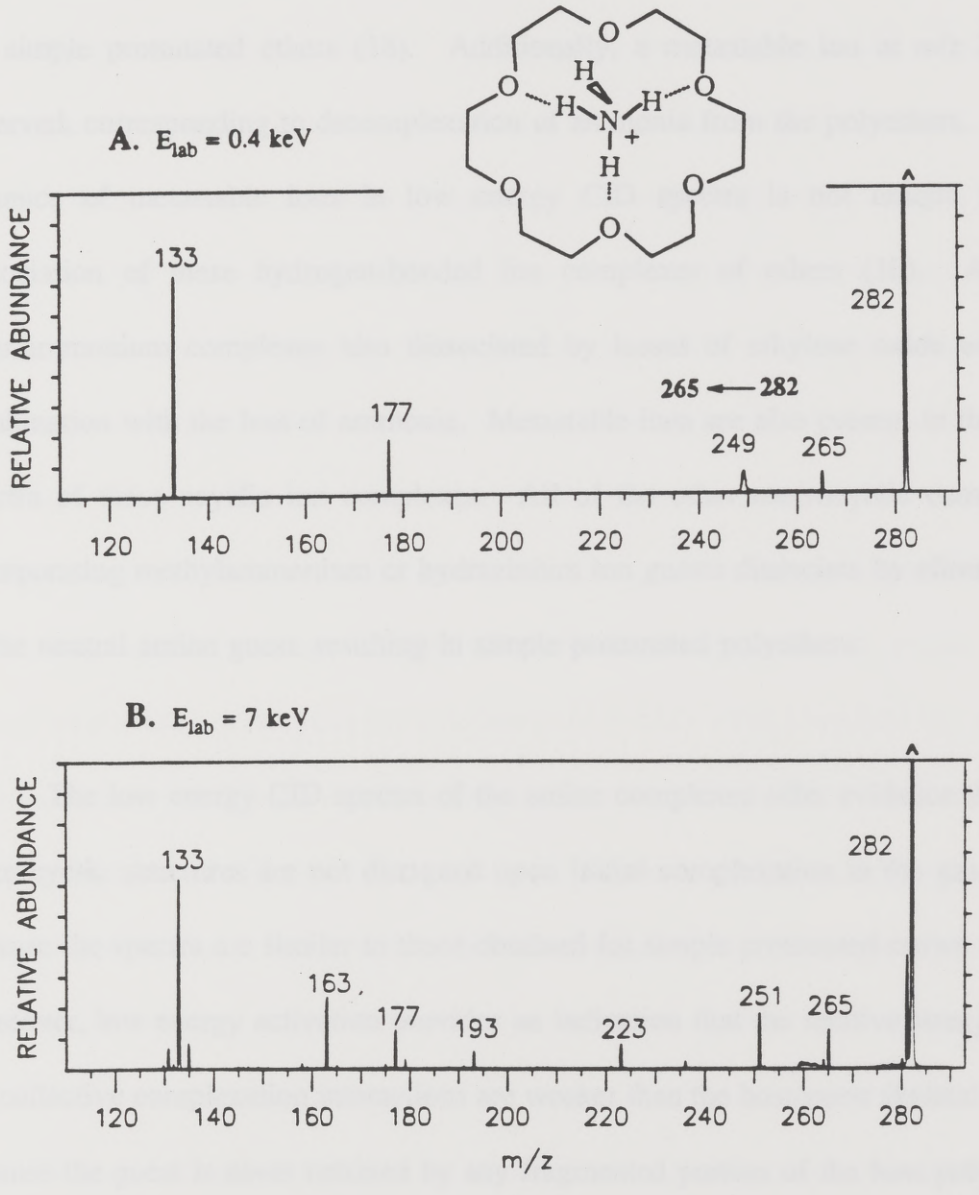

Figure 6.2 : CID mass spectra of 18-crown-6/ammonium ion complex.

bonds of the macrocyclic skeleton occur. The dissociation products of the cyclic and acyclic ether amine ion complexes are similar to the ones observed in CID spectra of the simple protonated ethers (18). Additionally, a metastable ion at *m/z* 249 is observed, corresponding to decomplexation of ammonia from the polyethers. The presence of metastable ions in low energy CID spectra is not unique to the dissociation of these hydrogen-bonded ion complexes of ethers (10). Acyclic ether/ammonium complexes also dissociated by losses of ethylene oxide units in combination with the loss of ammonia. Metastable ions are also present in the CID spectra of these acyclic ion complexes. All of the other macrocyclic complexes incorporating methylammonium or hydrazinium ion guests dissociate by elimination of the neutral amine guest, resulting in simple protonated polyethers.

The low energy CID spectra of the amine complexes offer evidence that the macrocyclic structures are not disrupted upon initial complexation in the gas phase because the spectra are similar to those obtained for simple protonated crown ethers. Moreover, low energy activation provides an indication that the relative strengths of the collective complexation interactions are weaker than the host/guest skeletal bonds because the guest is never retained by any fragmented portion of the host polyether. This comparison is evaluated more quantitatively from high energy CID experiments, as discussed in the next section.

High Energy CID :

Polyether/NH_4^+ Complexes : In general, both electronic and vibrational excitations occur after high energy collisional activation, resulting in higher energy deposition and access to different dissociation processes (19). For example, shown in Figure 6.2B is the 7 keV CID spectrum for the 18-crown-6/ammonium ion complex. The types of fragment ions produced are typical of ones observed for the other ammonium/macrocyclic ion complexes. In addition to the fragment ions seen in the low energy CID spectrum in Figure 6.2A, typical neutral losses from CID of the ion complexes of crown ethers are 31, 59, 89, or 119 u. These identical neutral losses were also observed in CID of the alkali metal ion complexes (20). Furthermore, when crown ether ion complexes with ND_4^+ were examined, the neutral losses remained unchanged which indicates that the atoms of the ND_4^+ ion are all completely retained by the ionic portion. This observation led to proposal of mechanisms (shown in Scheme 6.1) similar to fragmentation pathways of the alkali metal ion adducts (20).

Scheme 6.1 shows the proposed mechanisms of dissociation for the ammonium ion complex of 18-crown-6. After high energy activation, the crown ether complex opens. For neutral losses of 31, 89, and 119 u, the proposed ring opening process

Scheme 6.1 : Mechanisms for dissociation pathways of ammonium ion complexes of crown ethers.

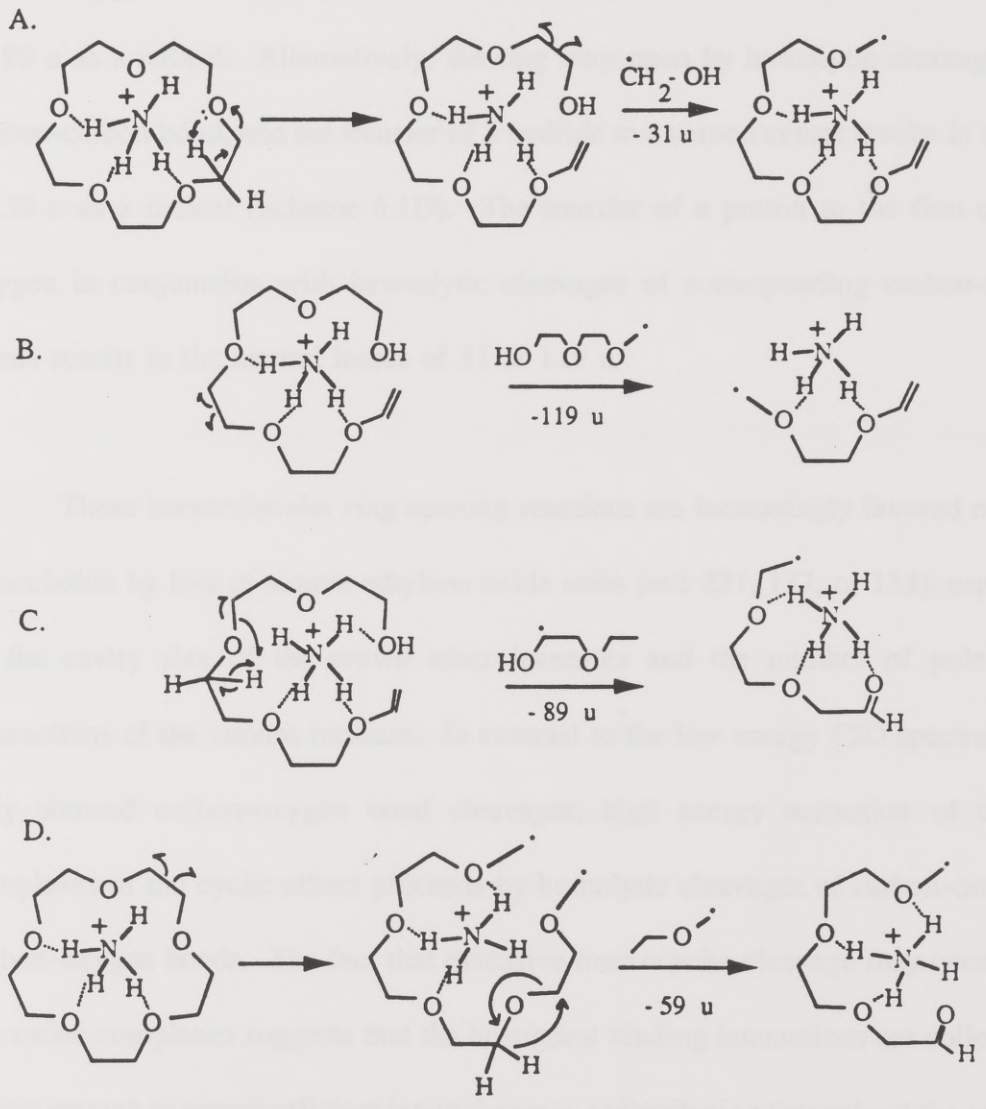

includes the transfer of a proton to an oxygen site. Homolytic cleavages of carbon-carbon bonds may result in the neutral losses of 31 and 119 u, as shown in Schemes 6.1A and B, respectively. Scheme 6.1C shows how the homolytic cleavage of a carbon-oxygen bond in conjunction with a hydrogen atom transfer results in the loss of 89 u as a radical. Alternatively, the ring may open by homolytic cleavages of a carbon-carbon bond, and the transfer of a hydride to a carbon center results in the loss of 59 u as a radical (Scheme 6.1D). The transfer of a proton to the first or third oxygen in conjunction with heterolytic cleavages of corresponding carbon-oxygen bonds results in the neutral losses of 31 or 119 u.

These intramolecular ring opening reactions are increasingly favored over the dissociation by loss of simple ethylene oxide units (*m/z* 221, 177, or 133), especially as the cavity size of the crown ether increases and the number of pole-dipole interactions of the amines increase. In contrast to the low energy CID spectra which only showed carbon-oxygen bond cleavages, high energy activation of the ion complexes of the cyclic ethers proceeds by homolytic cleavages of carbon-carbon or carbon-oxygen bonds. The fact that extensive macrocyclic cleavage may occur from the amine complexes suggests that the host/guest binding interactions are collectively strong enough to permit efficient internal energy redistribution throughout the complex after collisional activation.

As an additional comparison, collision induced activation of the ammonium ion complex of hexaethylene glycol, an acyclic analog of 21-crown-7, proceeds by homolytic cleavages of only carbon-carbon bonds. The ion series at *m/z* 225, 181, and 137 which corresponded to neutral losses of $^{\cdot}CH_2\text{-}(OC_2H_4)_n\text{-}OH$ (where n = 1, 2, or 3) is observed. These dissociation pathways occur in conjunction with the ethylene oxide unit losses which were observed in CID of the protonated molecule (18). The results from CID of ND_4^+ adducts show that the entire ammonium ion is retained by the fragment ion and may interact with the ether oxygens or the hydroxy terminus.

Crown Ether/$CH_3\text{-}NH_3^+$ Complexes : Figure 6.3 shows the high energy CID spectrum of 18-crown-6 ion complex with methylammonium. Dissociation pathways for this ion complex are similar to the ones occuring from the ammonium ion complex; for example neutral losses of 31, 59, and 89 u are observed. These similarities support mechanisms which do not intimately involve the participation of the guest. The extent of the ring opening intramolecular dissociation reactions of crown ether/methylammonium ion complexes increases with increasing cavity sizes.

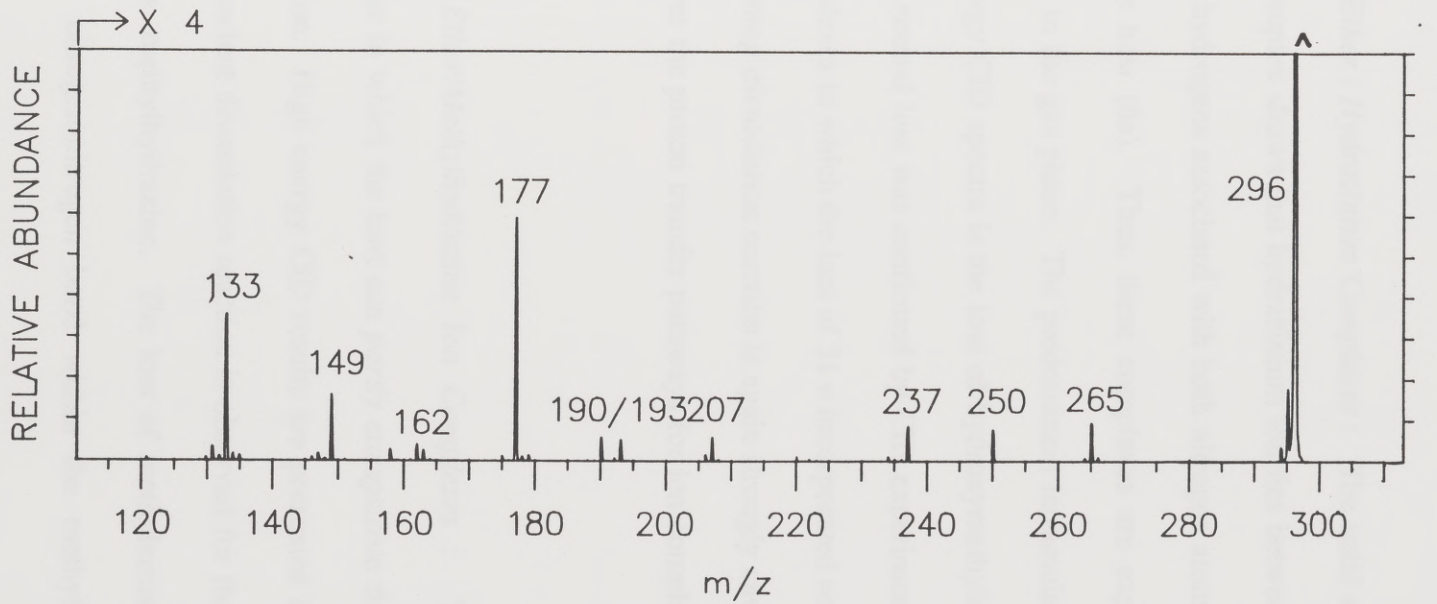

Figure 6.3 : CID mass spectrum of 18-crown-6/methylammonium ion complex at 7 keV recorded on JEOL HX110/HX110.

Crown Ether / Hydrazinium Complexes : The solid state structure of the 18-crown-6 ion complex shows that hydrazinium ion lies between two upper and lower O_3 planes, and hydrogens associated with both nitrogen atoms bond to five different oxygens of the host (6a). Thus, these complexes are expected to be especially strongly bound in the gas phase. The predominant intramolecular reaction observed in the high energy CID spectra is the loss of hydroxymethylene radical (31 u). The identity of this neutral loss was confirmed by CID experiments of the corresponding $N_2D_5^+$ ion complexes in which the loss of 31 u incorporated no deuterium. The extent of this ring opening dissociation reaction is again strongly cavity size dependent, and it dominates over the proton transfer pathways for ion complexes of 18-crown-6 and 21-crown-7.

Crown Ether/Methylhydrazine Ion Complexes : This type of complex represents a case in which the host can *partly* encapsulate the guest and binds only the amine portion. High energy CID results are presented in Table 6.3. Again, a cavity size dependent dissociation reaction is observed for the elimination of neutral methylamine vs. methylhydrazine. The loss of methylamine specifically involves cleavage of the nitrogen-nitrogen bond within the methylhydrazine guest. For

Table 6.3 : Product ion ratios from dissociation of crown ether ion complexes with hydrazines[a].

Polyether Ring	Hyrdazine Substrates	
	CH_3 - NH - NH_3^+	Tosyl - NH - NH_3^+
	$(C + H)^+ : (C + NH_2)^{+\cdot}$	$(C + H)^+ : (C + N_2H_4)^{+\cdot}$
15-crown-5	100 : 10	100 : 10
18-crown-6	60 : 100	100 : 25
21-crown-7	10 : 100	100 : 25

[a] C denotes the crown ether molecule. Spectra were recorded at 7 keV.

quantitative comparison, the dissociation energy of the nitrogen-nitrogen bond is estimated as 67 kcal/mol (21). As the cavity size of the ether increases, dissociation of the complex by nitrogen-nitrogen bond cleavage increases relative to the loss of the neutral methylhydrazine guest by intramolecular proton transfer. This result supports the proposal that multiple pole-dipole interactions occur with the larger cavity sizes, and the total multiple hydrogen-bonding interaction energy is at least on the order of the nitrogen-nitrogen bond strength. Other fragment ions observed in the high energy CID spectra include those formed by losses of ethylene oxide units from the decomplexed protonated polyether.

Crown Ether/Tosylhydrazine Ion Complexes : High energy collisional activation of tosylhydrazine ion complexes of crown ethers results in the cleavage of the nitrogen-sulfur bond in the guest which is estimated as 59 kcal/mol (22). The results in Table 6.3 which show the relative abundance of tosylhydrazine elimination vs. loss of the tosyl unit suggest a less pronounced cavity size dependence for dissociation of these complexes relative to the effects observed for the methyl-hydrazine complexes. This observation may be related to the increased bulk and number of vibrational modes of the tosylhydrazine guest which would tend to disfavor the cleavage of the strong sulfur-nitrogen bond relative to the weaker hydrogen bonds. Other less abundant fragment ions in the high energy CID spectra include ions

attributed to cleavages within the tosylhydrazine guest, and ions due to elimination of ethylene oxide units from the decomplexed protonated polyether.

To provide a comparison of the dissociation routes of a non-complexed guest ion, the high energy CID spectra of protonated tosylhydrazine was examined. After collisional activation, protonated tosylhydrazine dissociates by elimination of N_2H_2 or N_2H_4, two routes which involve sulfur-nitrogen bond cleavage. The loss of N_2H_2 suggests facile transfers of hydrogens to the oxygen sites. However, the predominant dissociation pathway of each crown ether ion complex is the cleavage of the nitrogen-sulfur bond which results in the ion of (crown ether + N_2H_4)$^+$. The dissociation pathway for elimination of N_2H_2 for the crown ether/tosylhydrazine complexes is disfavored due to hydrogen-bonding interactions.

6.3 Conclusion :

Tandem mass spectrometric results suggest that the gas phase hydrogen-bonding interactions of crown ethers with primary amines are cavity size dependent. Metastable dissociation results show that the binding strength of polyethers with ammonium and methylammonium increases in the order of : 21-crown-7 > 18-crown-6 > 15-crown-5 > hexaethylene glycol. Also, the relative gas phase basicities of the

host and guest determined the binding preference of polyethers for the methylammonium ion over the ammonium ion.

Intramolecular dissociation reactions of the ion complexes are energy dependent. Low energy CID activation promoted decomplexation of the amine guests from the polyethers by intramolecular proton transfer to the hosts. Additionally, sequential cleavages of carbon-oxygen bonds of the polyether hosts were observed. High energy fragmentation pathways proceeded by homolytic bond cleavages of the host or guest depending on the size of the amine molecules. For ion complexes of the ammonium, methylammonium, or hydrazinium ion, homolytic carbon-carbon or carbon-oxygen bonds of the polyether host occured. In contrast, ion complexes of crown ethers with methyl- and tosyl-hydrazine dissociated by the nitrogen-nitrogen or nitrogen-sulfur bonds found in the guests. Although the bond energy of nitrogen-nitrogen in hydrazine is estimated to be on the same order as the substituted hydrazines, dissociation of the nitrogen-nitrogen bond in the hydrazinium ion complex did not occur. These results suggest stronger electrostatic interactions within the host/guest complexes that adopt a nesting conformation. In addition, covalent bond activation of nitrogen-nitrogen and nitrogen-sulfur bonds of the guest molecules provided an estimation for the association energy of the multiple hydrogen-bonding complexation process.

References :

1. (a) Vogtle, F.; Weber, E.; Eds.; *Host Guest Complex Chemistry : Macrocycles*, Springer-Verlag : New York, 1985. (b) Atwood, J. L.; Ed. *Inclusion Phenomena and Molecular Recognition*, Plenum Press : New York, 1988.

2. (a) Cram, D. J., in *Applications of Biochemical Systems in Organic Chemistry*, Techniques of Chemistry, Vol. 10, Part II, Jones, J. B.; Sih, C. J.; Perlman, D.; Eds. John Wiley & Sons, 1976 (b) Reinhoudt, D. N. *J. Coord. Chem.* **1988**, *18*, 21-43.

3. Lehn, J.-M.; Sirlin, C. *J. Chem. Soc., Chem. Commun.* **1978**, 949-951.

4. (a) Maleknia, S.; Brodbelt, J. *J. Am. Chem. Soc.* in press. (b) Liou, C.-C.; Brodbelt, J. *J. Am. Soc. Mass Spectrom.* in press. (c) Zhang, H.; Chu, I.-H.; Leming, S.; Dearden, D. V. *J. Am. Chem. Soc.* **1991**, *113*, 7415-7417.

5. Izatt, R. M.; Christensen, J. J.; Eds.; *Synthetic Multidentate Macrocyclic Compounds*; Academic Press : New York, 1978.

6. (a) Trueblood, K. N.; Knobler, C. B.; Lawrence, D. S.; Stevens, R. V. *J. Am. Chem. Soc.* **1982**, *104*, 1355-1362 (b) Nagano, O.; Kobayashi, A.; Yukiyoshi, S. *Bull. Chem. Soc. Jpn*, **1978**, *51*, 790-793.

7. (a) Howard, A. E.; Singh, U. C.; Billeter, M.; Kollman, P. A. *J. Am. Chem. Soc.* **1988**, *110*, 6984-6991 (b) Gehin, D.; Kollman, P. A.; Wipff, G. *J. Am. Chem. Soc.* **1989**, *111*, 3011-3023.

8. (a) Moet-Ner, M. *J. Am. Chem. Soc.* **1983**, *105*, 4906-4911 (b) Aue, D. H.; Bowers, M. T. in *Gas Phase Ion Chemistry*, Vol. 2, M. T. Bowers; Ed. Academic Press : New York, 1979.

9. Meot-Ner, M. *J. Am. Chem. Soc.* **1983**, *105*, 4912-4195.

10. Cooks, R. G.; Beynon, J. H.; Caprioli, R. M.; Lester, G. R. *Metastable Ions*, Elsevier : New York, 1973.

11. Sato, K.; Asada, T.; Ishihara, M.; Kunihiro, F.; Kammei, Y.; Kubota, E.; Costello, C. E.; Martin, S. A.; Scoble, H. A.; Biemann, K. *Anal. Chem.* **1987**, *59*, 1652-1659.

12. Wang, W. J.; Chantooni, M. K.; Kolthoff, I. M. *J. Coord. Chem.* **1990**, *22*, 43-52.

13. Izatt, R. M.; Terry, R. E.; Haymore, B. L.; Hanson, L. D.; Dalley, N. K.; Avondet, A. G.; Christensen, J. J. *J. Am. Chem. Soc.* **1976**, *98*, 7620-7626.

14. Gokel, G. W.; Goli, D. M.; Minganti, C.; Echegoyen, L. *J. Am. Chem. Soc.* **1983**, *105*, 6786-6788.

15. (a) Lias, S. G.; Bartmess, J. E.; Liebman, J. F.; Levin, R. D.; Mallard, W. G. *J. Phys. Chem. Ref. Data* **1988**, Vol. 17, supplement No. 1. (b) Smith, J. W. in *Chemistry of the Amino Group*, Patai, S.; Ed. Interscience: New York, 1968.

16. Izatt, R. M.; Izatt, N. E.; Rossiter, B. E.; Christensen, J. J.; Haymore, B. L. *Science*, **1978**, *199*, 994-996.

17. (a) Beresford, G. D.; Stoddart, J. F. *Tetrahedron Letters*, **1980**, *21*, 867-870. (b) Naguchi, H.; Nagamatsu, M.; Yoshio, M. *Bull. Chem. Soc. Jpn.*, **1985**, *58*, 1855-1856.

18. Data from Chapter 4 is in press : Maleknia, S.; Liou, C.-C.; Brodbelt, J. *Org. Mass Spectrom.* **1991**, *26*, 997-1002.

19. Bush, K. L.; Glish, G. L.; Mc Luckey, S. A. *Mass Spectrometry/Mass Spectrometry*, VCH publishers : New York, 1988.

20. The results of Section A of Chapter 5 is in press : Maleknia, S.; Brodbelt, J. *Rapid Commun. in Mass Spectrometry*, accepted for publication.

21. Schmidt, E. W. *Hydrazine and its Derivatives*, John Wiley & Sons : New York, 1984.

22. Fleig, V. H.; Becke-Goehring, M. *Zeit. Anorg. Chemie*, **1970**, *375*, 8-14.

Chapter 7 - Host-Guest Selectivity in Biological Systems

A. Reactions of Perfluorinated Crown Ethers

7.1 Introduction :

The abilities of crown ethers to form complexes with alkali cations and organic molecules has generated long-term interest (1-4), and more recently because of the developments in molecular recognition and host-guest chemistry (5). Likewise this interest has extended to the coordination abilities of perfluorinated macrocylic analogs which exhibit decreased basicities and presumably have different pocket size dimensions due to the fluorine substitution. Some biocompatible perfluorinated compounds have high oxygen carrying capacity (6) and have demonstrated great potential as artificial blood components (7). From a physiological standpoint, the mechanism of oxygen binding to the fluoroethers is particularly intriguing but poorly understood.

In this chapter the results for selective formation and structural characterization of oxygen/perfluoro crown ether negatively charged complexes in the gas-phase are presented. Three points of interest are examined: 1) the capability of the fluorinated

crown ethers to form complexes with O_2 as compared to the abilities of the non-fluorinated ethers and acyclic perfluorinated ethers to form complexes, 2) the propensity to form adducts with CO, CO_2, Ar, as compared to O_2, and 3) the nature of the structure of the complexes.

7.2 Results and Discussion :

Figure 7.1 shows the negative ionization mass spectrum for the reaction products of perfluoro 18-crown-6 (molecular weight 696) with oxygen. An abundant adduct ion is observed at m/z 728 due to $(M+32)^{-\cdot}$. This ion is not observed in the absence of oxygen in the source. The $(M+O_2)^{-\cdot}$ adduct ion is also observed for the other perfluorinated crown ethers with an abundance of 20-60% relative to the molecular ion. The capability for oxygen adduct formation was also examined for the non-fluorinated crown ethers. Adducts with O_2 were *never* observed, either in the positive or negative ionization modes.

Additionally, the abilities of the perfluoro crown ethers to form complexes with CO, CO_2, and Ar, species with similar sizes and some similar chemical and physical properties as O_2, were examined. Adducts with these species were *never*

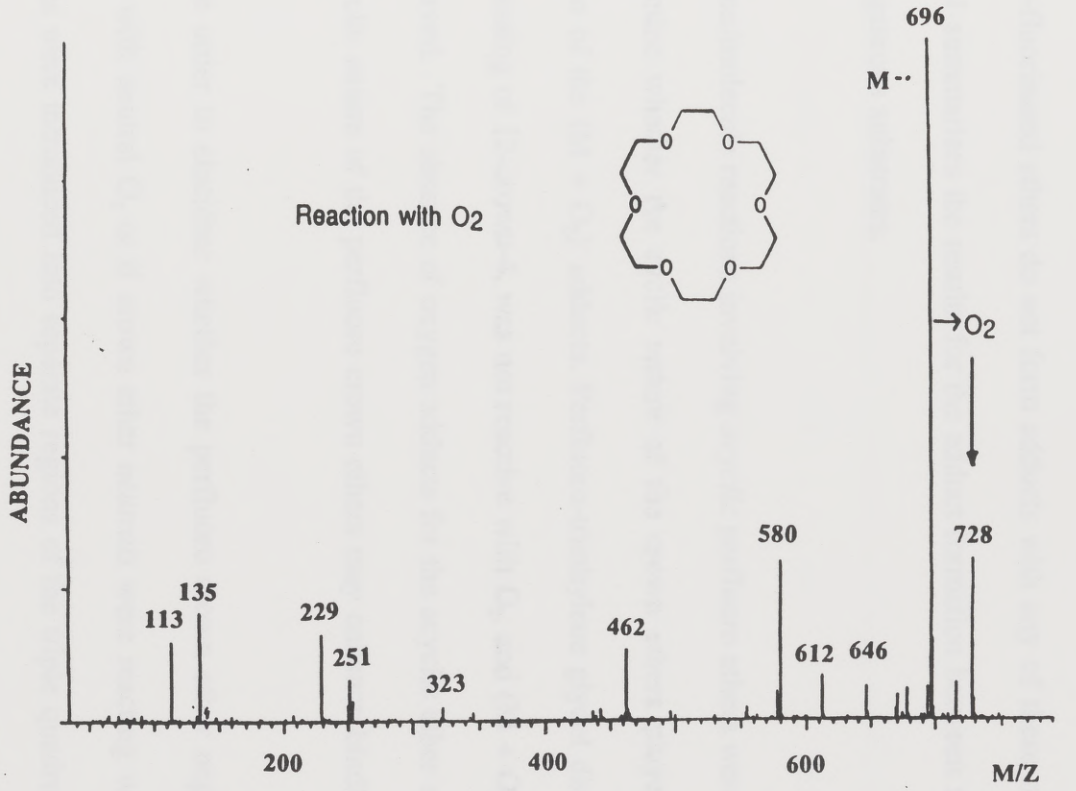

Figure 7.1 : Mass Spectrum of Perfluoro 18-crown-6 and oxygen in the negative mode recorded on Finnigan TSQ-70.

observed in either the positive or negative ionization modes. Thus, the tendencies of the perfluoro crown ethers to form adducts exhibits striking selectivity for O_2 only. The non-fluorinated ethers do not form adducts with any of these molecules either. Table 7.1 summarizes the results for the adduct formation between the cyclic ethers and the gaseous substrates.

Ion/molecule reactions involving *acyclic* perfluoro ethers were also examined to determine whether the cyclic nature of the crown ethers played a role in the formation of the $(M + O_2)^-$ adducts. Perfluoro-triethylene glycol dimethyl ether, an acyclic analog of 12-crown-4, was not reactive with O_2, and $(M + O_2)^-$ adducts were not observed. The absence of oxygen adducts for the acyclic ether suggests that the macrocyclic nature of the perfluoro crown ethers may enhance binding to O_2.

In order to elucidate whether the perfluoro crown ether negative *ions* were reacting with neutral O_2 or if crown ether *neutrals* were reacting with O_2^-, the two substrates were introduced into separate regions of the triple quadrupole instrument so that selective ion/molecule reactions could be performed. For these experiments, 5 mtorr O_2 was admitted into the second quadrupole region which also may serve as a reactive collision chamber. The perfluoro crown ether was ionized in the source, then the molecular ion, $M^{-\cdot}$, was mass-analyzed and isolated with the first quadrupole.

Table 7.1 : Adduct Formation

Compound	O_2	CO	CO_2	Ar
perfluoro 12-crown-4	**YES**	no	no	no
perfluoro 15-crown-5	**YES**	no	no	no
perfluoro 18-crown-6	**YES**	no	no	no
12-crown-4	no	no	no	no
15-crown-5	no	no	no	no
18-crown-6	no	no	no	no

These ions were passed through the reaction quadrupole at a kinetic energy of 6 eV. Abundant $(M + O_2)^-$ adducts were observed in the resulting mass spectrum, indicating that crown ether negative *ions* may attach to *neutrals* O_2. The alternative route, O_2^- attachment to crown ether neutrals, could not be confirmed due to restrictions on introducing the less volatile crown ethers into the collision quadrupole.

Structural details of the perfluoroether ions, $M^{-\cdot}$, and their O_2 adduct ions, $(M + O_2)^-$, were probed via collisionally induced dissociation (CID) of the mass-selected precursor ions. Figure 7.2 shows the CID spectra of the molecular ion (M^-) of the perfluoro 18-crown-6 (m/z 696) and its $(M+O_2)^-$ adduct (m/z 728). Although experimental conditions were similar, the non-dissociated product ion abundances are not the same for the $M^{-\cdot}$ and $(M + O_2)^-$ CID spectra. This does not necessarily indicate that the stabilities of these precursor ions are dramatically different, however, because even small variations in experimental conditions can alter the efficiency of precursor ion dissociation.

The molecular ion, $M^{-\cdot}$, dissociates primarily via a series of losses of $(C_2F_4O)_n$ units (116 amu). The CID spectrum of the (perfluoro 18-crown-6 + $O_2)^-$ adduct ion shows two series of fragment ions. One is a series of losses of $(C_2F_4O)_n$, analogous to the series of losses observed from the M^- ion, resulting in fragment ions at m/z

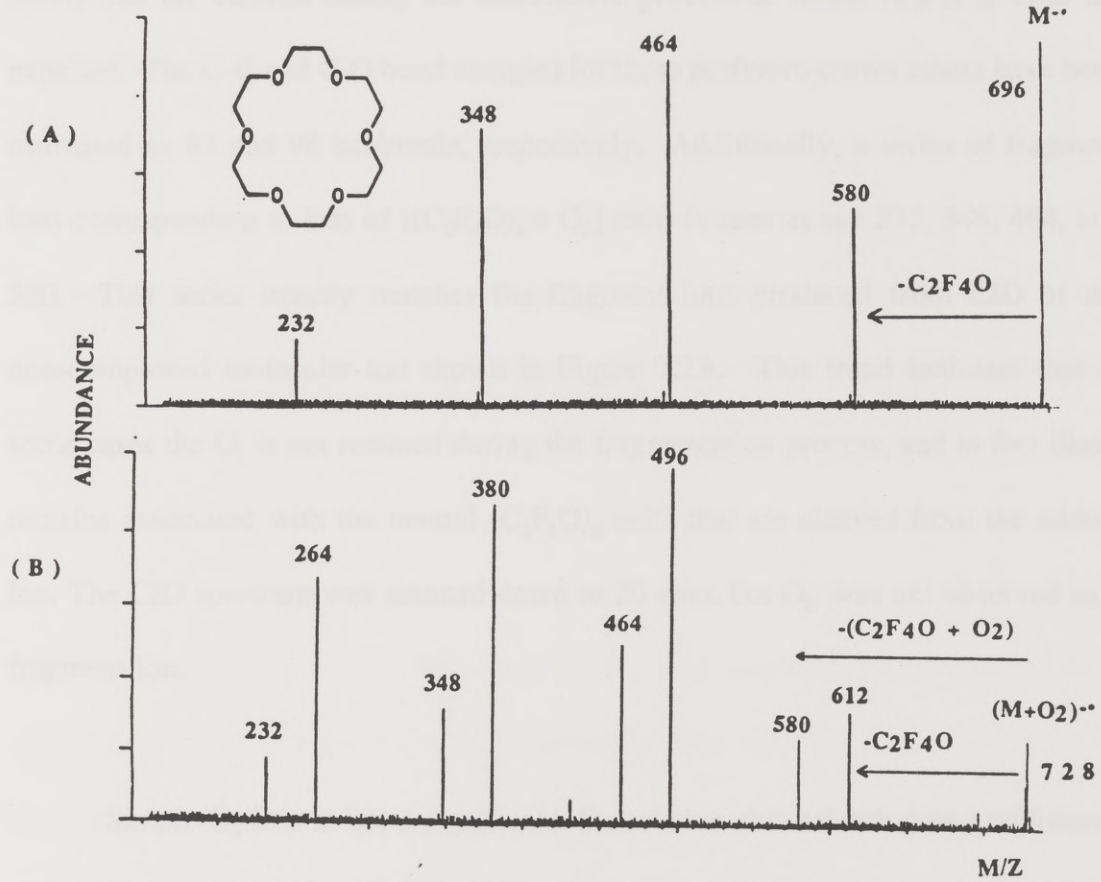

Figure 7.2: CID mass spectra at 30 eV recorded on Finnigan TSQ-70.

A) perfluoro 18-crown-6; B) (perfluoro 18-crown-6 + O_2)$^-$ adduct ion.

264, 380, 446, and 612. This trend indicates that the O_2 is bound to the perfluoro crown ether strongly enough to be retained after the adduct ion is activated, and that this binding interaction presumably must be at least as strong as the C-C and C-O bonds that are cleaved during the dissociative process in which $(C_2F_4O)_n$ units are expelled. The C-C and C-O bond energies for these perfluoro crown ethers have been estimated as 84 and 98 kcal/mole, respectively. Additionally, a series of fragment ions corresponding to loss of $[(C_2F_4O)_n + O_2]$ units is seen at *m/z* 232, 348, 464, and 580. This series exactly matches the fragment ions produced from CID of the non-complexed molecular ion shown in Figure 7.2A. This trend indicates that in some cases the O_2 is not retained during the fragmentation process, and in fact likely remains associated with the neutral $(C_2F_4O)_n$ units that are cleaved from the adduct ion. The CID spectrum was scanned down to 20 amu, but O_2^- was not observed as a fragment ion.

Simple O_2 loss is not a significant dissociative channel using any collisional activation conditions (for 10-120 eV kinetic energy collisions, the percentage of the total fragment ion abundance due to O_2 loss is 0-5%). This suggests that the O_2-crown ether complex is not a loosely bound adduct, but instead a species in which stronger bonding forces are involved than those associated with weak ion/dipole electrostatic interactions. An adduct species in which O_2 fits in the pocket of the

crown ether is possible (enhancing multiple bonding interactions), or a structure in which the O_2 is cradled by four electronegative fluorine atoms is feasible. In general, O-F bonds are not expected to be stronger than 50 kcal/mole, so a complex containing a single F-O_2 binding interaction is not likely. In any case, the inability of the nonfluorinated analogs or the perfluoro acyclic analogs to form $(M + O_2)^-$ adducts clearly underscores the dramatic impact of fluorine substitution and the cyclic nature of the substrate on complexation behavior. Finally, the selectivity of adduct formation between the perfluoro macrocyclic anions and only molecular oxygen (not CO or CO_2) suggests that there may be underlying chemical reasons for this selectivity, not solely topological ones.

Additionally, reactions were performed with a number of reactive *ionic* species, including F^-, Cl^-, OH^-, NH_2^-, and $^-OCH_3$. Only perfluoro crown ether adducts with F^- and $^-OCH_3$ attachment were observed. In these cases, neutral counterparts of these ionic species are not present in the source because these ions are generated by dissociative ionization of CH_2F_2, CH_2Cl_2, H_2O, NH_3, and CH_3ONO respectively. The selectivity of adduct formation with other small ionic substrates is under further examination.

References :

1. Dang, L.; Kollman, P. *J. Am. Chem. Soc.* **1990**, *112*, 5716.

2. Dietrich, B.; Lehn, J.; Sauvage, *J. Tetrahedron Lett.* **1969**, 2885.

3. De Boer, J.; Reinhoudt, D.; Harkema, S.; van Hummel, G.; de Jong, F. *J. Am. Chem. Soc.* **1982**, *104*, 4073.

4. De Jong, F.; Reinhoudt, D. *Adv. Phys. Org. Chem.* **1980**, *17*, 279.

5. Cram, D, *Science* **1988**, *240*, 760.

6. Reiss, J.; LeBlanc, *M. Ang Chemie Int. Ed. Eng.* **1978**, *17*, 621.

7. Weiss, R. *Science News* **1987**, *132*, 200.

8. Huang, H.; Lagow, R. *Bull. de la Soc. Chem. de France* **1986**, *6*, 993.

9. Lin, W.; Bailey, W.; Lagow, R. *J. Chem. Soc., Chem. Commun.* **1985**, 1350.

B. Reactions of Perfluorinated Bicyclic Ethers

7.3 Introduction :

Cryptands are macrobicyclic compounds (1) that form stable complexes with metal cations and may act as host for specific guests via molecular recognition (2). Perfluorinated cryptands (3) are particularly interesting derivatives because they are physiologically compatible and may possess important biological properties, such as the ability to carry oxygen and transport ions through membranes. Recently, the unusual ability of fluorinated macrocycles to bind fluoride ion via four C-H hydrogen bonds in solution was reported (4). Additionally, the complexation chemistry of molecular oxygen and fluoride with several binuclear copper azo-cryptands (5) and azo-oxo-crown ethers (6) were examined in solution. The formation and characterization of gas-phase ion complexes of perfluorinated macrocycles demonstrates that intrinsic host/guest chemistry may be examined in the solvent-free environment of a mass spectrometer.

The first section of this chapter discussed the results for complexation of molecular oxygen by perfluorinated crown ethers in the gas-phase (7). In this section

the reactions of a perfluorinated cryptand with substrates of fluoride and molecular oxygen are discussed to investigate the factors of geometry and size of the cavity in host/guest complexation processes.

7.4 Results and Discussion :

Ion complexes of the cryptand, perfluoro 4, 7, 13, 16, 21, 24-hexaoxo-1, 10-diazabicyclo [8.8.8] hexacosane, $(M + O_2)^{-\cdot}$ and $(M + F)^-$, were formed in the chemical ionization (CI) or liquid secondary ionization (LSIMS) modes utilizing a triple quadrupole or a four sector JEOL HX110/HX110 mass spectrometer, respectively. For chemical ionization experiments methane was used to aid in the production of thermal eletrons for negative ionization, and oxygen or 1,1-difluoroethylene (as a source of F^-) were admitted into the source as reagent gases. For LSIMS experiments the fluoride ion complexes were generated from a mixture of sodium fluoride with the perfluorinated cryptand.

The high energy CID spectrum of the molecular anion, $M^{-\cdot}$, of the perfluorocryptand, in Figure 7.3A, shows similar fragmentation patterns to the low energy CID spectrum (8). This spectrum serves as a comparison to the CID spectrum

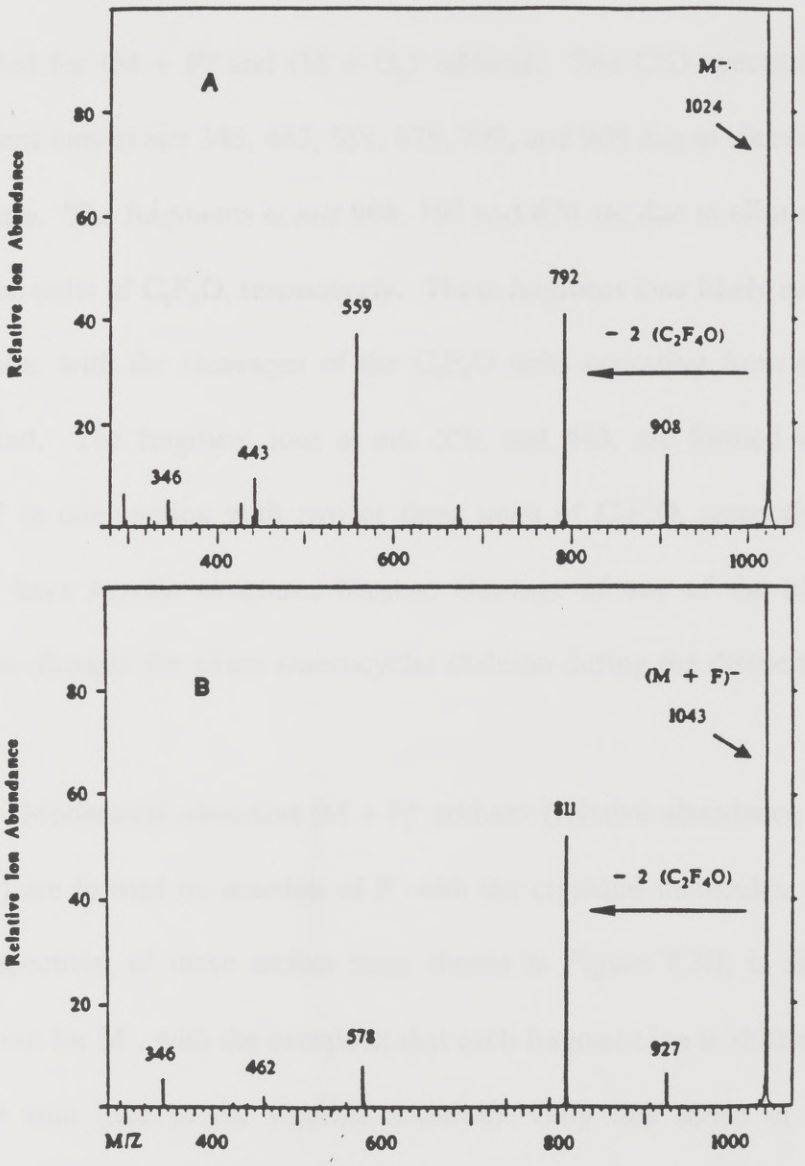

Figure 7.3 : CID mass spectra at 2 keV recorded on the JEOL HX110/HX110.

A) the molecular anion, $M^{-\cdot}$, of perfluorocryptand; B) fluoride adduct of perfluorocryptand.

recorded for $(M + F)^-$ and $(M + O_2)^-$ adducts. The CID spectrum of $M^{-\cdot}$ contains fragment ions at *m/z* 346, 443, 559, 676, 792, and 908 due to cleavage of the bicyclic structure. The fragments at *m/z* 908, 792 and 676 are due to elimination of one, two or three units of C_2F_4O, respectively. These fragment ions likely retain a monocyclic structure, with the cleavages of the C_2F_4O units occurring from one branch of the cryptand. The fragment ions at *m/z* 559, and 443, are formed via elimination of C_4F_9N in conjunction with two or three units of C_2F_4O, respectively. These ions likely have acyclic structures because cleavage of one of the nitrogen-containing bridges disrupts the entire macrocyclic skeleton during the dissociation process.

Moderately abundant $(M + F)^-$ adducts (relative abundance = 10% compared to $M^{-\cdot}$) are formed by reaction of F^- with the cryptand molecules. The high energy CID spectrum of these adduct ions, shown in Figure 7.3B, is similar to the CID spectrum for $M^{-\cdot}$, with the exception that each fragment ion is shifted to a higher mass by 19 amu (due to the fluorine addition). Only this series of fragment ions at $(Fragment + F)^-$ is observed, indicating that the fluorine is *always* retained by the ionic portion during dissociation. The most abundant dissociative process is loss of two C_2F_4O units. The simple loss of $F^\cdot$ or F_2 is not observed. This suggests a very strong cryptand-fluoride binding interaction. A possible mechanism for formation and dissociation of $(M + F)^-$ is shown in Scheme 7.1. Upon activation, the fluoride

Scheme 7.1 : Proposed mechanism for dissociation of fluoride adduct of the perfluorocryptand.

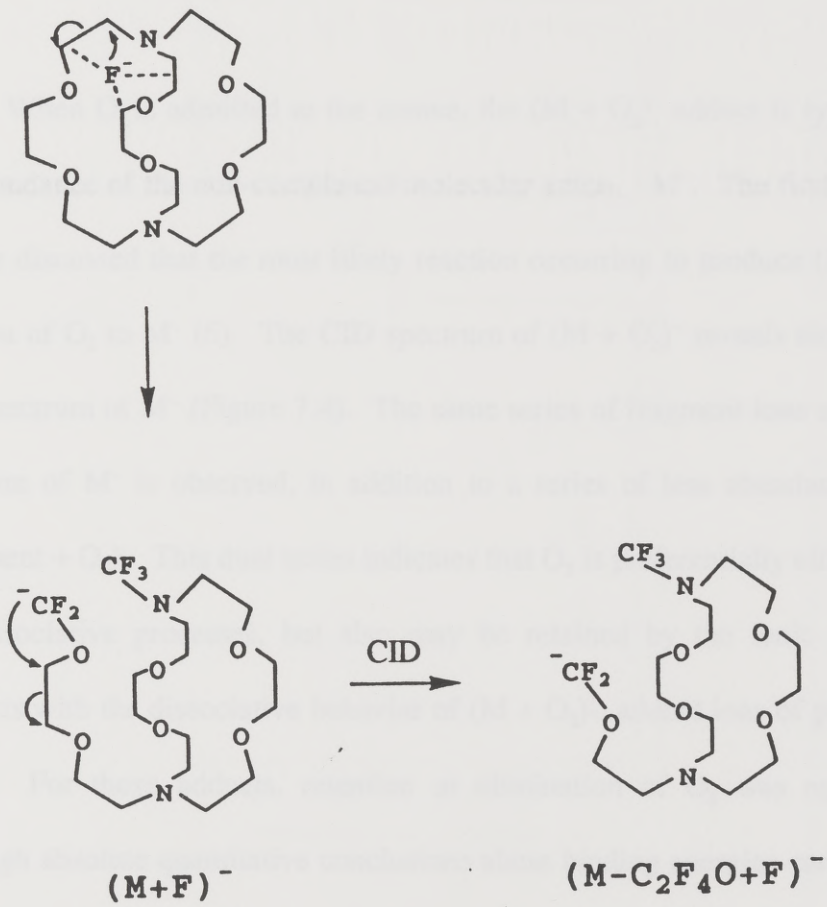

attacks the least nucleophilic carbon position which promotes ring opening, resulting in a branched monocyclic structure. This could then undergo facile elimination of one or two C_2F_4O units. The initial adduct structure may be a ring-opened monocyclic structure or an anion/molecule complex with the fluoride ion stabilized through ion-dipole attractions within the cavity of the cryptand (as shown).

When O_2 is admitted to the source, the $(M + O_2)^{-\cdot}$ adduct is typically 50% of the abundance of the non-complexed molecular anion, $M^{-\cdot}$. The first section of this chapter discussed that the most likely reaction occurring to produce $(M + O_2)^{-\cdot}$ is the addition of O_2 to $M^{-\cdot}$ (6). The CID spectrum of $(M + O_2)^{-\cdot}$ reveals similarities to the CID spectrum of $M^{-\cdot}$ (Figure 7.4). The same series of fragment ions seen in the CID spectrum of $M^{-\cdot}$ is observed, in addition to a series of less abundant fragments at $(Fragment + O_2)^{-}$. This dual series indicates that O_2 is preferentially eliminated during the dissociative processes, but also may be retained by the ionic portion. This contrasts with the dissociative behavior of $(M + O_2)$-. adduct ions of perfluoro crown ethers. For those adducts, retention or elimination of O_2 was equally favored. Although absolute quantitative conclusions about binding energies can not be drawn, it appears that O_2 is bound less strongly to the cryptand than to the crown ethers. Additionally, the loss of simple O_2 occurs to a great extent, resulting in $M^{-\cdot}$ at *m/z* 1024. This loss was never a predominant process for the crown ether/O_2 adducts.

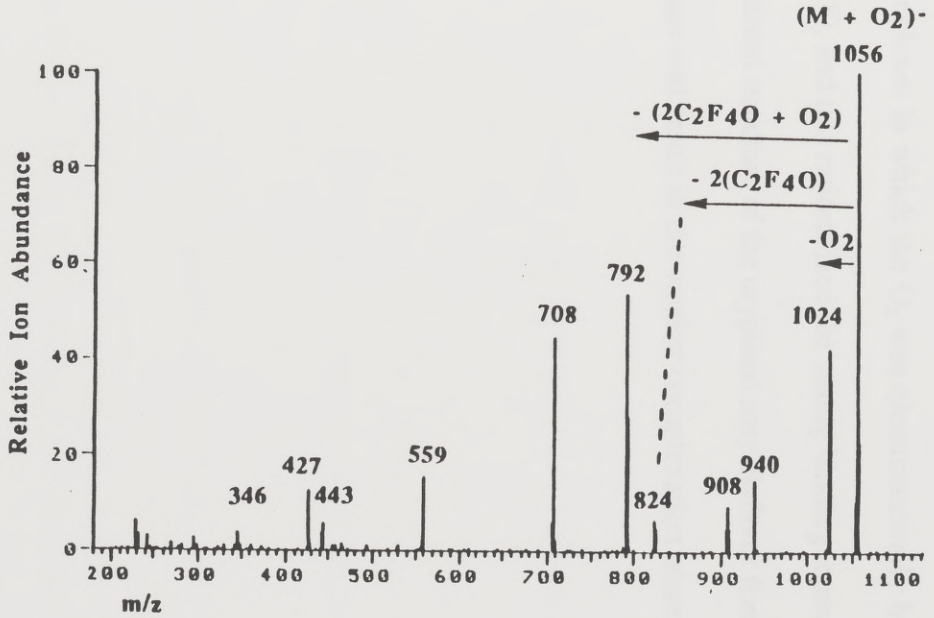

Figure 7.4 : CID mass spectrum of the oxygen adduct of the perfluorocryptand at 25 eV recorded on Finnigan TSQ-70.

This adds support to the proposal that the cryptand/O_2 adducts are more loosely-bound than the crown/O_2 complexes.

It was proposed that the gas-phase crown ether/O_2 adduct ions were perhaps inclusion complexes in which the O_2 was electrostatically bound in the cavity of the crown ether (8), and this rationalized the strong binding interactions. The increasingly sterically hindered structure of the cryptand may disfavor formation of such a complex in the gas-phase and result in the weaker complexation observed in the present study.

References :

1. B. Dietrich, J.M. Lehn, J.P. Sauvage, *Tetrahedron Lett.* **1969**, *34*, 2885.

2. "Host Guest Complex Chemistry", eds. F. Vogtle, E. Wever, Springer-Verlag, 1985.

3. W.D. Clark, T.Y. Lin, S.D. Maleknia, R.J. Lagow, *J. Org. Chemistry.*, **1990**, *55*, 5933.

4. W. B. Farnham, C. C. Roe, D.A. Dixon, J.C. Calabrese, R.L. Harlow, *J. Am. Chem. Soc.* **1990**, *112*, 7707.

5. A. E. Martell, *J. Inclus. Phenomena and Mol. Recog. in Chem.*, **1989**, *7*, 99.

6. R. J. Motekaitis, A. E. Martell, *Inorg. Chem.*, **1991**, *30*, 694.

7. The results of section A of Chapter V and publication of J. Brodbelt, S. Maleknia, C.-C. Liou, R. Lagow, *J. Am. Chem. Soc.*, **1991**, 113, 5913.

8. The results from Chapter IV and publication of S. Maleknia, J. Liou, J. Brodbelt, *Org. Mass Spectrom.*, **1991**, 26, 997.

Chapter 8 - Conclusions and Prospects

Noncovalent interactions determine the informational exchange processes at the intermolecular bond level between two or more molecular units. These interactions are important in the functions of the living systems and also direct the assembly of molecular units for the formation of new materials. This investigation examined two kinds of molecular association reactions directed by noncovalent interactions in the absence of solvation effects by tandem mass spectrometric techniques. First, cluster ions of transition metal oxides were investigated because of the interest in their catalytic properties. Secondly, reactions of crown ethers were investigated to model host-guest interactions in the gas phase.

A simple thermal desorption method was developed for formation of molybdenum and tungsten trioxide clusters. Collision induced dissociation results of the clusters showed distinctive size-selective fragmentation pathways. These metal oxide clusters formed stable complexes with several chalcogenide atom donor ligands. Upon collisional activation, covalent bond cleavages within the ligands were favored over the dissociation of the metal trioxide units. For example, activation of the cluster complex of $[(WO_3)_4$ + ethylene oxide$]^-$ showed a more abundant fragment ion for the

elimination of ethylene than for the loss of ethylene oxide. This type of fragmentation pathway suggested that the interactions of ligands were site specific and could be used to distinguish structural variations of the clusters due to their geometric or electronic differences.

The chemical and topological aspects of association reactions of crown ethers parallel biological host-guest complexation interactions, and these macrocyclic molecules are used as models for molecular recognition processes. The complexation properties of crown ethers in the gas phase were evaluated by the analysis of ion complexes of alkali metals and several amine substrates. The cyclic ethers showed a cavity size dependent complexation behavior which was best described by the concept of maximum contact point. For example, collision induced dissociation of the ion complex of [18-crown-6 + Na.K.Cl]$^+$ showed a more abundant fragment ion for the sodium ion complex than potassium ion complex. This preference in the gas phase duplicated the trends estimated by modeling techniques and demonstrated that the intrinsic host-guest complexation selectivity could be examined.

Hydrogen-bonded complexes of crown ethers with primary amine substrates also showed a cavity size dependent dissociation behavior. In this case, collisional activation results showed covalent bond dissociations of the *host* molecule when the

guest substrate was encapsulated by the cyclic host. However, preferential covalent bond dissociation of the *guest* molecule resulted when the guest molecule was only partially encapsulated, exemplified by cleavages of the nitrogen-nitrogen or nitrogen-sulfur bonds for ion complexes of polyethers with methyl- and tosyl-hydrazines.

These simple and well-documented reactions with alkali metals and primary amines were selected to provide a basic understanding for the complexation properties of the cyclic hosts in the gas phase. However, mass spectrometric techniques are currently being used to reveal the noncovalent interactions of a variety of macromolecular biological complexes, and collisional activation experiments can also provide qualitative information about their binding interactions. For example, perfluorinated compounds are used as blood substituents for their oxygen transport ability, but the mechanism of their binding is not known. Selective complexes of perfluorinated cyclic and bicyclic ethers with oxygen were formed in the gas phase, and collisional activation of these ion complexes proceeded by covalent bond dissociation of the cyclic hosts while the oxygen was retained by the fragment ions. Results of the covalent bond dissociation from the ligand complexes of transition metal oxide clusters, amine complexes of crown ethers, or the macrocyclic host have shown that tandem mass spectrometric techniques are useful in evaluating the strengths of the interactions of associative complexes held by noncovalent bonding.

The vita has been removed from the digitized version of this document.